REGULATION AND DYSREGULATION VIA DOCKING INTERACTIONS IN WNK AND ERK1/2 MAPK SIGNALING

APPROVED BY SUPERVISORY COMMITTEE

Melanie H. Cobb, Ph.D.

Joseph P. Albanesi, Ph.D.

Elizabeth J. Goldsmith, Ph.D.

Kenneth D. Westover, M.D. Ph.D.

DEDICATION

I dedicate this work to all those who supported me during times of difficulty in my life.

Without their help I would not have made it where I am today.

REGULATION AND DYSREGULATION VIA DOCKING INTERACTIONS IN WNK AND ERK1/2 MAPK SIGNALING

by

CLINTON A. TAYLOR IV

DISSERTATION / THESIS

Presented to the Faculty of the Graduate School of Biomedical Sciences

The University of Texas Southwestern Medical Center at Dallas

In Partial Fulfillment of the Requirements

For the Degree of

DOCTOR OF PHILOSOPHY
The University of Texas Southwestern Medical Center at Dallas

Dallas, Texas

December, 2016

REGULATION AND DYSREGULATION VIA DOCKING INTERACTIONS IN WNK AND ERK1/2 MAPK SIGNALING

CLINTON A. TAYLOR IV, Ph.D.

The University of Texas Southwestern Medical Center at Dallas, 2016

Supervising Professor: MELANIE H.COBB, Ph.D.

Protein-protein interactions are essential for nearly every cellular process. Within signaling pathways, such interactions carry out numerous functions such as defining substrate specificity, inhibition of both other interactions and enzyme activity, localizing signaling partners, acting in a switch-like manner depending on post-translational modifications, etc… My work has focused primarily on protein-protein interactions, and in particular protein-peptide docking interactions, within two independent cellular signaling pathways, the WNK, and ERK1/2 MAPK pathways.

The WNK pathway is an essential regulator of cellular ionic composition and volume. Initially discovered due to the genetic link between mutations in some of the WNK kinases and an inherited form of hypertension, the pathway is now well defined and known to regulate the activity of multiple SLC12 cation chloride coupled cotransporters. WNK kinases activate SPAK and OSR1 kinases, which then regulate the activity of cotransporters. My initial work within this pathway was focused on understanding the role of SPAK and OSR1 activation loop domain-swapping. I solved the structure of the inactive SPAK kinase domain, and utilized a previously identified dimerization blocking mutation to probe the role of SPAK dimerization on activation and activity. I determined that SPAK has multiple activation states and that the monomeric form is both active and can be activated by WNK1. I next shifted focus to the SPAK and OSR1 CCT domains, which mediate protein-peptide interactions with motifs found in WNKs, cotransporters, and other interaction partners. I further defined the specificity of the CCT domains for the motifs, and discovered a new motif variant. I used this information to predict new interaction partners. Although validation of the predictions is still in the early stages, my initial choice for validation was a group of inward rectifier potassium channels. Through collaboration, we now have evidence that OSR1 kinase activity regulates flux through one of the eight channels, and testing of more of the channels is underway.

The ERK1/2 MAPK pathway is involved in numerous cellular processes, and is well known for its role in responding to extracellular signals that regulate cell growth and differentiation. As such, aberrant signaling within the pathway is found within approximately thirty percent of all cancers. The terminal kinases of the cascade, ERK1 and ERK2, phosphorylate hundreds of cytosolic and nuclear substrates, and in many cases protein-peptide docking interactions between ERK1/2 and substrates are required. One of the docking sites on

ERK2 has been shown to be the site of a mutation, E322K, that is the most enriched ERK2 missense mutation in human cancers. Using a previously determined dataset, I was able to refine the structure of the mutant ERK2. As expected the site of the mutation was structurally disrupted, but the mutation also caused structural changes throughout the entire kinase domain, including solvent exposure of the activation loop. Docking induced solvent exposure of the activation loop had already been suggested to be important for MAPK activation and inactivation by presenting the sites of phosphorylation to modifying enzymes. Therefore, the structural data fit well with previous findings indicating that the mutant was able to be activated by upstream kinase MEK1, but could not be inactivated by phosphatase DUSP6. I also found that the mutation affected a distal docking site and disrupted interactions with at least some interaction partners at that site. The combined results of this project have shown that this mutation has multiple effects on ERK2 structure and function, and implies that this mutation is enriched primarily because it allows ERK2 to be activated similar to wild type, while having a diminished capacity to be deactivated.

TABLE OF CONTENTS

PRIOR PUBLICATIONS

Karra AS, **Taylor CA 4th**, Thorne CA, Cobb MH. A Kinase Divided. *Cancer Cell*. **2015** Aug 10;**28**(2):145-7.

Taylor CA 4th, Juang YC, Earnest S, Sengupta S, Goldsmith EJ, Cobb MH. Domain-Swapping Switch Point in Ste20 Protein Kinase SPAK. *Biochemistry*. **2015** Aug 18;**54**(32):5063-71.

Byers CE, Barylko B, Ross JA, Southworth DR, James NG, **Taylor CA 4th**, Wang L, Collins KA, Estrada A, Waung M, Tassin TC, Huber KM, Jameson DM, Albanesi JP. Enhancement of dynamin polymerization and GTPase activity by Arc/Arg3.1. *Biochim Biophys Acta*. **2015** Jun;**1850**(6):1310-8.

Huang N, Chelliah Y, Shan Y, **Taylor CA**, Yoo SH, Partch C, Green CB, Zhang H, Takahashi JS. Crystal structure of the heterodimeric CLOCK:BMAL1 transcriptional activator complex. *Science*. **2012** Jul 13;**337**(6091):189-94.

Piasecki SK, **Taylor CA**, Detelich JF, Liu J, Zheng J, Komsoukaniants A, Siegel DR, Keatinge-Clay AT. Employing modular polyketide synthase ketoreductases as biocatalysts in the preparative chemoenzymatic syntheses of diketide chiral building blocks. *Chem Biol*. **2011** Oct 28;**18(**10):1331-40.

Zheng J, **Taylor CA**, Piasecki SK, Keatinge-Clay AT. Structural and functional analysis of A-type ketoreductases from the amphotericin modular polyketide synthase. *Structure*. **2010** Aug 11;**18**(8):913-22.

LIST OF FIGURES

LIST OF TABLES

LIST OF ABBREVIATIONS

AI	autoinhibitory domain
AMP-PNP	adenylyl imidodiphosphate
AP-MS	affinity purification-mass spectrometry
ATP	adenosine triphosphate
BME	β-mercaptoethanol
Cab39	calcium binding protein 39
CC	coiled-coil
CCT	conserved C-terminal
CD	common docking
CHK2	checkpoint kinase 2
DAPK3	death-associated protein kinase 3
DTT	dithiothreitol
DUSP	dual specificity protein phosphatase
EDTA	ethylenediaminetetraacetic acid
EGFR	epidermal growth factor receptor
ELK1	ETS domain-containing protein Elk-1
ERF	Ets2 repressor factor
ERK	extracellular signal-regulated kinase
FAM	carboxyfluorescein
FBS	fetal bovine serum
FCS	fluorescence correlation spectroscopy
FITC	fluorescein isothiocyanate
GCK	germinal center kinase
GDP	guanosine diphosphate
GEF	guanine nucleotide exchange factor
GST	glutathione S-transferase
GTP	guanosine triphosphate
HEK	human embryonic kidney
HePTP	hematopoietic protein-tyrosine phosphatase
IPTG	isopropyl β-D-1-thiogalactopyranoside
IRK	inward rectifier potassium channel
KCC	K^+-Cl^- cotransporter
KIM	kinase interaction motif
LB	Luria broth
LOK	lymphocyte-originated kinase
MAPK	mitogen-activated protein kinase

MBP	myelin basic protein
MEK	MAPK/ERK kinase 1
MKP	MAP kinase phosphatase
MO25	mouse protein 25
MST	mammalian STE20-like protein kinase
NCC	Na^+-Cl^- cotransporter
NKCC	Na^+-K^+-$2Cl^-$ cotransporter
NMR	nuclear magnetic resonance
OSR1	oxidative stress-responsive kinase 1
PAK6	p21-activated kinase 6
PEA-15	15 kDa phosphoprotein enriched in astrocytes
PF1/2	PASK and Fray
PKA	proetin kinase A
PMSF	phenylmethane sulfonyl fluoride
PP1	protein phosphatase 1
PSSM	position-specific scoring matrix
RMSD	root mean square deviation
RSK	ribosomal protein S6 kinase
RTK	receptor tyrosine kinase
SH3	SRC homology 3
SLK	Ste20-like kinase
SPAK	Ste20-related proline-alanine-rich kinase
SPOC	SPAK/OSR1 C-terminus
SPR	surface plasmon resonance
TAO2	thousand and one amino acid protein kinase 2
TBST	TBS with 0.1% Tween
TEV	tobacco etch virus
WNK	with no lysine (K^+)
Y2H	yeast two-hybrid

CHAPTER ONE

INTRODUCTION

Protein-Protein Interactions

Eukaryotic cells contain tens of thousands of different types of proteins, and the overall concentration of these proteins is remarkably high, whether they are confined to membranes or soluble. Therefore, the fact that many different proteins are able to specifically interact with either one or a subset of proteins in this environment illustrates how they have evolved unique, complementary interfaces that energetically favor selection of their cognate interacting partner(s).

Quantitative Description of Binary Protein-Protein Interactions

In order to physically describe the stability of protein-protein interactions Gibbs free energy change upon binding or (ΔG) is used. ΔG describes the spontaneity of a reversible process at constant temperature and pressure, with a negative value indicating that energy is lost to the surroundings, and thus is energetically favorable. Gibbs free energy consists of an enthalpic term (ΔH) that describes the total heat content of a system (assuming no work), and a temperature-dependent entropic term ($T\Delta S$) that describes the disorder of the system, or in other words the number of possible configurations. The second law of thermodynamics states that for an isolated system entropy is always increasing when spontaneous change is occurring.

Therefore, heat lost to the environment (decreased ΔH)), or increased disorder (increased $T\Delta S$); both enhance the stability of a protein-protein interaction. Therefore when examining the equation for ΔG (1.1), it becomes clear why a decrease in free energy is favorable for a protein-protein interaction or any other reaction.

$$\Delta G_{bind} = \Delta H_{bind} - T\Delta S_{bind} \qquad (1.1)$$

Another useful way of expressing Gibbs free energy of binding is in terms of the equilibrium dissociation constant (K_D), which describes the affinity of an interaction.

$$\Delta G_{bind} = RT\ln(K_D) \qquad (1.2)$$

From equation 1.2 it becomes evident that a lower value for the dissociation constant is associated with a more energetically favorable protein-protein interaction. The dissociation constant, in this case for a simple, bimolecular interaction describes the concentration of product, [AB], for any given concentrations of reactants, [A] and [B]. At equilibrium the concentration of reactants and products no longer changes and thus the forward and reverse reactions are equal on average.

$$d[AB]/dt = [A][B]k_{on} - [AB]k_{off} = 0 \qquad (1.3)$$

$$[A][B]k_{on} = [AB]k_{off} \qquad (1.4)$$

Since K_D describes the on and off rates for a reaction at equilibrium, then by rearranging equation 1.4 it becomes clear why K_D describes the amount of reactants and products in a binding reaction.

$$K_D = k_{off} / k_{on} = [A][B] / [AB] \qquad (1.5)$$

Typically, experimental determination of binding affinity (K_D) is done *in vitro*. However, as already stated, cells are extremely crowded. As a result, the concentrations of [A] and [B] required to elicit binding in the cytosol, for example, will typically be much lower than the concentrations required to achieve the same amount of complex formation determined in an *in vitro* experiment due to exclusion of water in the crowded cellular environment.

Non-covalent Interactions

Various non-covalent interactions participate in both intra- and intermolecular protein-protein interactions. At one end of the spectrum are hydrophobic interactions. Hydrophobic amino acid side chains, such as leucine, for example, do not contain polarized bonds, and therefore cannot hydrogen bond with water. As a result, water molecules must form an ordered hydrogen bonding network around hydrophobic moieties, which results in decreased entropy. Therefore, it is energetically favorable for hydrophobic sidechains and surfaces to interact with one another in order to exclude water. Unlike other types of interactions, such as hydrogen bonds, the decrease in free energy from hydrophobic interactions is variable, and the orientation of the interaction is dictated primarily by packing such that the maximum amount of solvent is excluded.

Van der Waals interactions are the result of transiently induced or permanent dipoles causing an unequal distribution of the electron clouds around atoms leading to partial charges interacting with one another. In the case of transient dipoles, as two atoms approach one another they induce fluctuations in their electron clouds leading to a weak interaction. Certain chemical groups where one atom is more electronegative than the other, such as carbonyl groups in the

peptide backbone, generate permanent dipoles. In either case the opposite partial charges attract one another. Van der Waals interaction strength falls off quickly with distance, and electron cloud charge repulsion also prevents interacting atoms from coming into too close of contact. The most energetically favorable distance is knowns as the Van der Waals radii and is dependent on the radius of the atoms electron cloud. The distance for a carbon-carbon interaction is 3.4 Å, for example. However, the energy associated with Van der Waals interactions is typically very weak, around 1-2 kcal/mol, but interactions between large complementary surfaces can significantly contribute to the energetics of protein-protein interactions.

Hydrogen bonds are most notable for their specific directionality. Hydrogen bonds form when two electronegative atoms, a donor and an acceptor partially share a hydrogen atom. For example, a serine hydroxyl electron lone pair would serve as the acceptor for a lysine amino hydrogen. Since both the O and N atoms are sp^3 hybridized certain geometric constraints are placed on the directionality of the hydrogen bond and any other hydrogen bonds the atoms have formed, such that the most energetically favorable configurations would result in the most linear arrangement between the donor and acceptor atoms and the shared hydrogens. In addition, since the two atoms share the hydrogen, the typical distance for a hydrogen bond is around 2.5 Å owing to the partial covalent nature of the bond.

Directionality helps define the specific orientations between atoms in protein-protein interactions, and is in large part responsible for the formation of ordered structures in macromolecules, such as alpha helices and beta sheets. A single hydrogen bond between chemical groups on a protein may contribute as little as 1-2 kcal/mol since most side chains are already hydrated and the interaction only displaces bound water, but multiple hydrogen bonds acting together can contribute significantly to the decrease in free energy upon binding.

At the opposite end of the spectrum from hydrophobic interactions lie ionic interactions. Some amino acid sidechains such as lysine or aspartate carry a formal charge at neutral pH. Ions generate a uniform electric field in all directions, and as a result ionic interactions do not have directionality. Ionic interactions can significantly contribute to the overall change in free energy provided they are in close proximity. However, unlike the other types of interactions they can contribute to the binding energy at greater distances owing to the electric fields created by the ion point charges.

Protein-Protein and Protein-Peptide Interaction Interfaces

Although a single noncovalent interaction is not likely to mediate a protein-protein interaction, a combination of multiple types of interactions provides both the necessary binding energy, as well as specificity. As a general rule of thumb the approximate lower limit for a bona fide protein-protein interaction interface is 600 $Å^2$, with an average interface of approximately 1200 $Å^2$ and most interfaces between two globular domains are relatively flat, although protein-peptide interfaces can often achieve a higher degree of concavity with a smaller contact area (Jones and Thornton 1996, London, Movshovitz-Attias et al. 2010). Most protein-protein interaction interfaces are found to contain a central region enriched in hydrophobic amino acids surrounded by polar residues. In the majority of cases, hydrophobic interactions tend to be less-specific but contribute more of the binding energy, whereas electrostatic and hydrogen bonding interactions contribute less to overall binding free energy change, but are essential to determining specificity (Li, Huang et al. 2005). Within these interfaces it is common to find only one or a few residues, termed ‘hot spots’ by Clackson and Wells, contributing most of the binding free energy

(Clackson and Wells 1995). Based off of known complex crystal structures, a large-scale analysis of individual residue contributions to binding free energy by alanine scanning mutagenesis has shown that arginine, tryptophan, and tyrosine residues are enriched hot spot residues, followed by charged residues (Bogan and Thorn 1998). This same study also found that hot spots were generally clustered near the center of interfaces, and the "O-ring" hypothesis, in which inert, polar residues surround hot spots in order to occlude water, was put forward to explain this observation.

Protein-peptide interactions share many common characteristics with their larger interface counterparts, but also have unique characteristics. This type of interaction occurs between a globular domain and a sequence motif on an interacting protein that consists of a short contiguous stretch of residues that may or may not adopt secondary structure. As expected, the average interface size is much smaller than for protein-protein interactions at approximately 500 $Å^2$ (London, Movshovitz-Attias et al. 2010). However, packing tends to be more complementary in protein-peptide interactions, and the interfaces tend to utilize more hydrogen bonds per equivalent amount of surface area. In order to obtain additional binding energy from smaller available surface areas, protein-peptide interactions have a propensity for using more peptide backbone hydrogen bonds (Remaut and Waksman 2006, London, Movshovitz-Attias et al. 2010). As a result of the overall efficiency with which protein-peptide interactions derive binding energy, these interactions can have dissociation constants anywhere from low nanomolar to high micromolar, making them suitable to carry out a variety of cellular functions.

Protein-Peptide Interactions in Cellular Signaling

Protein-peptide interactions are also integral to cellular signaling. For example, eukaryotic protein kinases phosphorylate serine, threonine, and tyrosine residues on substrate proteins. There are over 500 protein kinases in the human proteome (Manning, Whyte et al. 2002). However, each kinase has unique substrate specificity. The first ever structure of a protein kinase in complex with a substrate was that of PKA bound to a 20 residue peptide substrate inhibitor where the normal phosphorylation site was mutated (Knighton, Zheng et al. 1991). The structure revealed that the substrate peptide around the phosphoacceptor site assumed a linear conformation upon binding and made extensive interactions with the C-terminal domain of the kinase. This and subsequent studies have shown that the substrate binding surface of the kinase confers specificity for substrates with particular sequences (Goldsmith, Akella et al. 2007). In addition, these interactions are often regulated by post-translational modification. For example, many protein kinases are activated by activation loop phosphorylation. One feature common to many active protein kinases is formation of the P+1 specificity pocket that is complementary to one or a subset of residue sidechains that are adjacent to the substrate phosphoacceptor site (Goldsmith, Akella et al. 2007). In the case of MAP kinases, activation loop phosphorylation leads to the formation of a shallow hydrophobic groove that is complementary to the proline adjacent to the phosphoacceptor serine or threonine in MAPK substrates (Canagarajah, Khokhlatchev et al. 1997).

Another common feature of protein-peptide interactions in signaling is the use of modular protein interaction domains to bind specific motifs in interacting proteins. Combinations of protein interaction domains and interaction motifs provide a means to confer specificity, modulate interactions based on regulatory inputs and outputs (i.e. post-translation modification),

and bring multiple signaling components in close proximity (Pawson and Nash 2003). In the proceeding sections and chapters protein-protein and protein-peptide interactions within the WNK and ERK1/2 MAPK pathway will be examined, which will further highlight their essential role in cellular signaling.

SPAK and OSR1 Kinases of the WNK Signaling Pathway

Background

In animals, ion concentrations and cell volume are controlled to maintain blood pressure, hearing, neurotransmission, fluid secretion, and to preserve cell viability for all other physiological functions (Xie, Craig et al. 2006, Welling, Chang et al. 2010, McCormick and Ellison 2011). The Ste20-related proline-alanine-rich kinase (SPAK; also called PASK and STK39) and its close relative oxidative stress-responsive kinase 1 (OSR1) directly contribute to regulation of ion balance through phosphorylation of the cytoplasmic tails of the SLC12 family of Na^+-Cl^-, Na^+-K^+-$2Cl^-$, and K^+-Cl^- ion cotransporters (NCC, NKCCs 1 and 2, and KCCs 1-4) (Darman and Forbush 2002, Liu, Xie et al. 2011, Gagnon and Delpire 2012, Alessi, Zhang et al. 2014, Markadieu and Delpire 2014). Reflecting the close connection between salt flux and blood pressure, mutations in the gene encoding SPAK have been linked to increased susceptibility to hypertension (Wang, O'Connell et al. 2009). Additionally, kinase-dead SPAK knock-in mice are hypotensive, and show reduced activation and expression of NKCC2 and NCC in the kidney, whereas OSR1 knock-outs die during embryonic development with blood vessel defects (Xie, Wu et al. 2009, Rafiqi, Zuber et al. 2010, Liu, Xie et al. 2011, Xie, Yoon et al. 2013). These results suggest that therapies specifically targeting SPAK or OSR1 have the potential to treat

hypertension, which is estimated to cost over $130 billion annually worldwide (Castaneda-Bueno and Gamba 2010, Heidenreich, Trogdon et al. 2011, Alessi, Zhang et al. 2014).

SPAK and OSR1 Kinases

SPAK and OSR1 are members of the Ste20 germinal center kinase (GCK)-VI subfamily of protein kinases (Dan, Watanabe et al. 2001, Gagnon and Delpire 2012). They share a common structural organization with the kinase domain near the N-terminus (Figure 1-1). The C-terminus contains two conserved domains only found in this subfamily, initially referred to as PF1 and PF2 (PF stands for PASK and Fray, the Drosophila homolog) (Leiserson, Harkins et al. 2000). The PF1 domain is required for kinase activity and may fold with the kinase domain. The PF2 domain, also referred to as the conserved C-terminal (CCT) domain, is involved in protein-protein interactions, and binds a short consensus motif [RFX(V/I)] found in SCL12 family cotransporter substrates, as well as in upstream regulators, the WNK (with no lysine (K)) kinases (Moriguchi, Urushiyama et al. 2005, Vitari, Deak et al. 2005, Anselmo, Earnest et al. 2006, Gagnon, England et al. 2006, Delpire and Gagnon 2007). Structural studies illuminated the basis for this interaction, which will be discussed in depth in the proceeding section (Villa, Goebel et al. 2007).

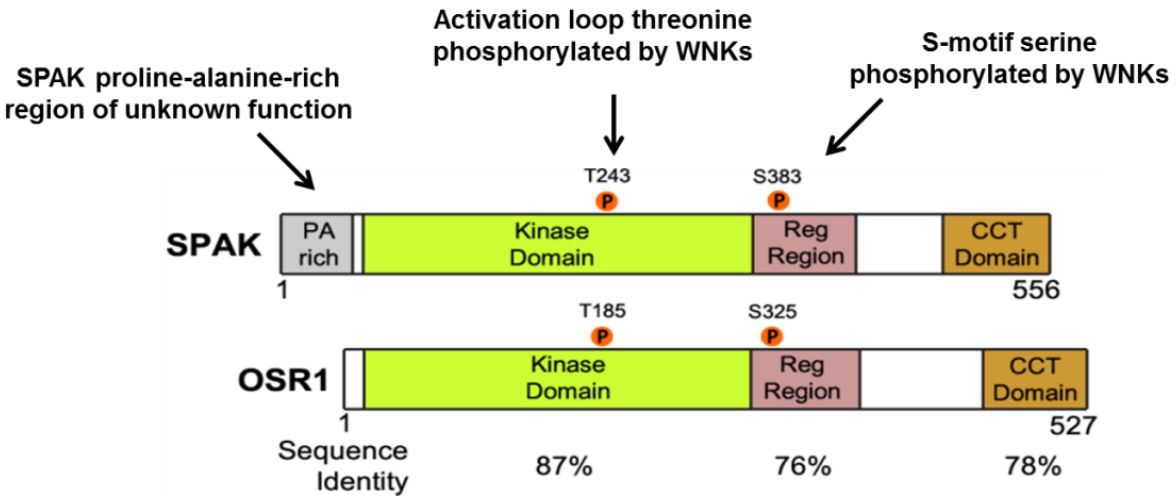

Figure 1-1. SPAK and OSR1 Domain Organization.

SPAK and OSR1 share a similar domain organization with an N-terminal kinase domain and C-terminal extension containing a regulatory region (PF1) and CCT protein interaction domain (PF2). Both kinases are activated by dual-phosphorylation of the activation loop and S-motif within the regulatory region. SPAK and OSR1 share high sequence identity, and thus have similar function.

Mutations in the upstream WNK1 and WNK4 kinases were shown by positional cloning to be responsible for single gene forms of inherited hypertension, pseudohypoaldosteronism type II (Wilson, Disse-Nicodeme et al. 2001). WNKs are activated by hypotonic, low Cl-, and hyperosmotic conditions, due at least in part to a direct Cl- sensing mechanism involving the WNK1 kinase domain (Piala, Moon et al. 2014). SPAK and OSR1 are activated by all four WNK kinases by phosphorylation (Figure 1-1, 1-2) at two conserved sites, T243 and S383 (mouse SPAK numbering) (Vitari, Deak et al. 2005, Anselmo, Earnest et al. 2006, Gagnon, England et al. 2006). Threonine 243 is located within the activation loop of the kinase domain and serine 383 is located in the PF1 domain and has been suggested to be part of an auto-inhibitory element, but its precise function remains unclear (Gagnon and Delpire 2010).

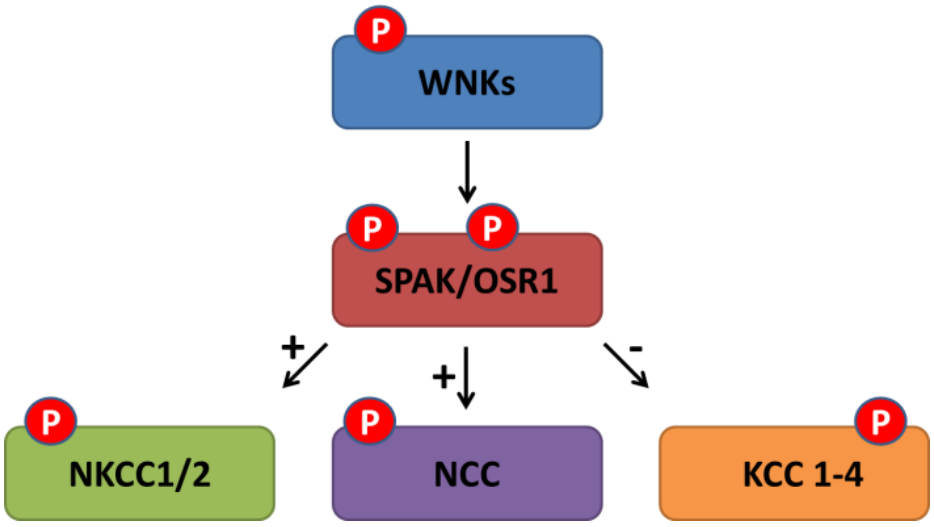

Figure 1-2. The canonical WNK pathway.

WNK kinases are activated by osmotic stress and low chloride through autophosphorylation of the activation loop. WNK kinases then activate SPAK and OSR1 by phosphorylation of the activation loop and S-motif. Active SPAK and OSR1 then activate NKCC1/2 and NCC and inhibit KCC 1-4 by phosphorylation of the cytoplasmic tails of the cotransporters.

SPAK/OSR1 Activation Loop Domain-Swapping

Previous crystal structures of the unphosphorylated OSR1 kinase domain (Villa, Deak et al. 2008, Lee, Cobb et al. 2009), and activating phosphorylation phosphomimetic mutant mouse SPAK 63-390 (T243D) have been solved (Taylor, Juang et al. 2015). The structures revealed OSR1 and SPAK activation loop domain-swapped dimers (Figure 1-3A,B), where the active sites of both kinases in the dimer are formed with residues from both monomers (Figure 1-3C) (Rousseau, Schymkowitz et al. 2003). Previous work on several other domain-swapped kinases, such as CHK2, DAPK3, SLK, and LOK had revealed that the dimers observed in the crystal structures were in active configurations and that dimerization enhanced autoactivation (Oliver, Paul et al. 2006, Oliver, Knapp et al. 2007, Pike, Rellos et al. 2008). However, the structures of

SPAK (T243D) and OSR1 kinase domain, although domain-swapped, were not observed to be in active configurations in the crystal structures.

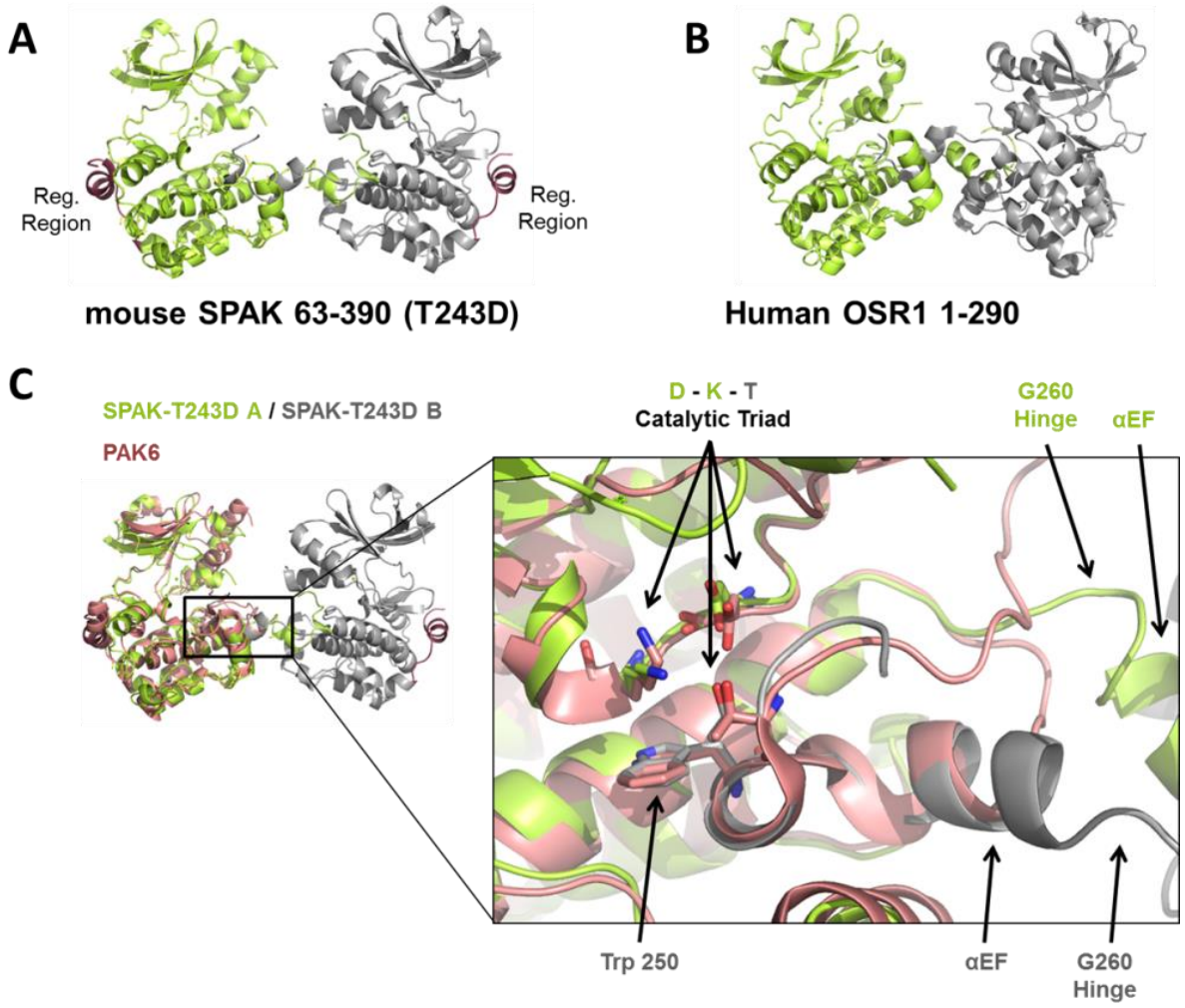

Figure 1-3. SPAK and OSR1 activation loop domain-swapping.

(A, B) Crystal structures of the activation loop domain-swapped homodimers of the SPAK and OSR1kinase domains (PDB: 5DBX and 3DAK). (C) Overlay of the SPAK dimer and monomeric PAK6 (PDB: 2C30). Close up view indicating the structural elements of the SPAK active site that are made up of parts of both kinases in the dimer. In particular the D-K-T catalytic triad that is important for formation of the P+1 pocket and position of residues in the catalytic loop is in part made up of interaction from the threonine of the other molecule of the dimer.

SPAK and OSR1 Docking Interactions Are Essential to WNK Pathway Signaling

The identity of the kinases involved in regulating NKCC1 and other SLC12 co-transporters was first gained from yeast two-hybrid experiments. Piechotta and colleagues identified SPAK and OSR1 as proteins that interact with multiple SLC12 ion cotransporter family members (Figure 1-4). The study found that a C-terminal fragment of both kinases, containing the CCT domain, was sufficient for interaction with co-transporters. The minimal requirement for interaction was a nine residue fragment containing the consensus sequence 'xRFxVxxxx' (Piechotta, Lu et al. 2002). The link between SPAK activity and the regulation of NKCC1 in humans was shown in HEK cells using a dominant negative form of SPAK. Overexpression of inactive SPAK significantly reduced NKCC1 phosphorylation at previously characterized regulatory sites (Dowd and Forbush 2003). The similarity between SPAK and OSR1, and NKCC1 with NKCC2 and NCC suggested that SPAK and OSR1 regulate multiple SLC12 co-transporters, potentially through similar interactions.

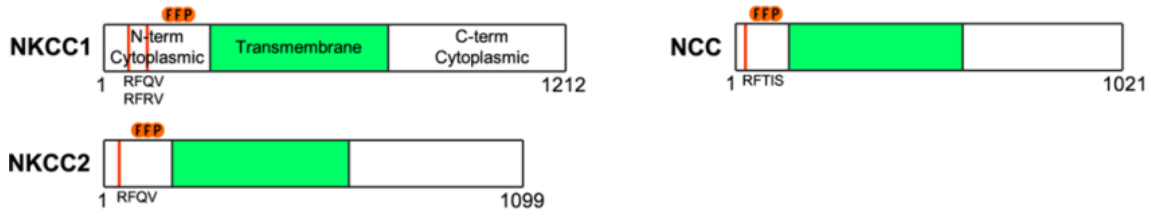

Figure 1-4. Domain organization and RFxV motifs within SLC12 cotransporters NKCC1/2 and NCC.

Schematic indicating the location of the RFxV motifs and activating SPAK/OSR1 phosphorylation sites in the N-terminal tails of SLC12 cotransporters NKCC1/2 and NCC.

Prior to being linked to hypertension and subsequently shown to interact with SPAK/OSR1 through CCT-mediated docking interactions, our lab first identified and characterized WNK1 (Xu, English et al. 2000). WNK 1-4 are large, primarily unstructured scaffolds containing an N-terminal kinase domain (Figure 1-5) (Xu, Min et al. 2002, Richardson and Alessi 2008). Later, our lab determined hypertonic and hypotonic stress activates WNK1 in cells (Lenertz, Lee et al. 2005). Several studies then showed that WNK1 and WNK4 activate SPAK/OSR1 by phosphorylation at the conserved residue T243/T185 on the activation loop (Moriguchi, Urushiyama et al. 2005, Vitari, Deak et al. 2005, Anselmo, Earnest et al. 2006). S383/S325 in the regulatory domain is also phosphorylated by WNKs, and to a greater extent, but the function of this phosphorylation is unknown (Moriguchi, Urushiyama et al. 2005, Vitari, Deak et al. 2005). These same studies found that SPAK/OSR1 activation was required for phosphorylation of NKCC1/2 and NCC. Later work demonstrated that WNK2 and WNK3 also activate SPAK/OSR1 in response to osmotic stress. SPAK/OSR1 in turn, activates NKCC1/2 and NCC, and inhibits KCCs by phosphorylation (Ponce-Coria, San-Cristobal et al. 2008, Rinehart, Vazquez et al. 2011, Pacheco-Alvarez, Vazquez et al. 2012, de Los Heros, Alessi et al. 2014).

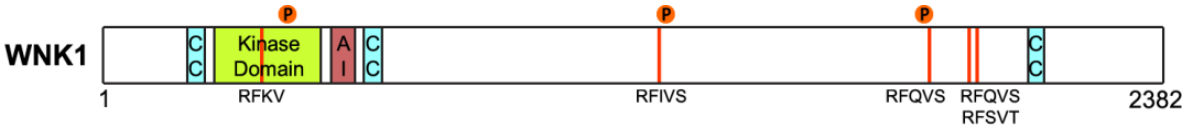

Figure 1-5. Domain organization and RFxV motifs within WNK1.

WNK1 is a large, relatively unstructured scaffold with an N-terminal kinase domain. Several RFxV motifs are scattered throughout the protein, but primarily clustered at the C-terminus. Also depicted are several coiled-coils (CC) that are implicated in oligomerization, and an autoinhibitory domain (AI) directly following the kinase domain. The activating phosphorylation site within the kinase domain and two MS identified phosphorylation sites of unknown function near RFxV motifs are indicated. WNKs 2-4 share a similar organization, containing kinase, AI, and CC regions and multiple RFxV motifs.

A common finding in several of these studies and others is that SPAK/OSR1 RFxV-mediated docking interactions with WNKs and cotransporters are essential for SPAK/OSR1 activation by WNKs (Vitari, Thastrup et al. 2006, Ponce-Coria, San-Cristobal et al. 2008, Pacheco-Alvarez, Vazquez et al. 2012), deactivation by PP1 (protein phosphatase 1) (Gagnon, England et al. 2007, Gagnon and Delpire 2010), and phosphorylation of co-transporter substrates (Figure 1-6) (Vitari, Thastrup et al. 2006, Gagnon, England et al. 2007, Richardson, Rafiqi et al. 2008, Richardson, Sakamoto et al. 2011, de Los Heros, Alessi et al. 2014).

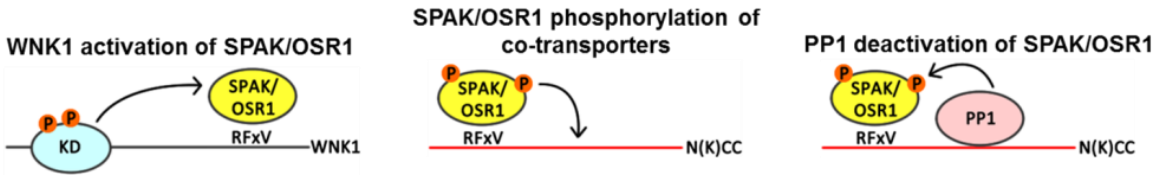

Figure 1-6. Roles of CCT domain docking interactions in the canonical WNK pathway.

SPAK and OSR1 CCT domain interactions with RFxV motifs have been shown to be required for SPAK/OSR1 activation by WNK kinases, SPAK/OSR1 phosphorylation of cotransporters, and SPAK/OSR1 deactivation by phosphatases.

SPAK/OSR1 CCT Domains

The SPAK and OSR1 CCT domain sequence and function are conserved from humans to at least *C. elegans* (Denton, Nehrke et al. 2005). The 1.7 Å crystal structure of the OSR1 CCT domain bound to a small peptide bearing an RFxV motif from WNK4 (GRFQVT) was determined nearly a decade ago and shed light on the structural basis for the interaction. Although the apo OSR1 CCT structure was also solved and refined, the authors did not deposit

the coordinates, or discuss the structure on the basis that it was too disordered in the absence of peptide (Villa, Goebel et al. 2007). The 94 residue domain adopts a fold, unique at the time of publication; that the authors refer to as the SPOC (SPAK/OSR1 C-terminus) fold. The domain is composed of four antiparallel β-strands packed against two alpha helices that span the length of the domain and an additional helix located in a loop (Figure 1-8A). The sequence of 2^0 structure elements are β1-L1 - β2 - L2 - α1 - L3 - α2 - L4 - β3 - L5 - α3 - L6 - β4. Helix α2 spans the entire length of the β-sheet forming the hydrophobic core of the domain through interactions with the interior face of the β-sheet. Helix α3 makes few interactions with the rest of the domain and sits within a large loop composed of L5 and L6.

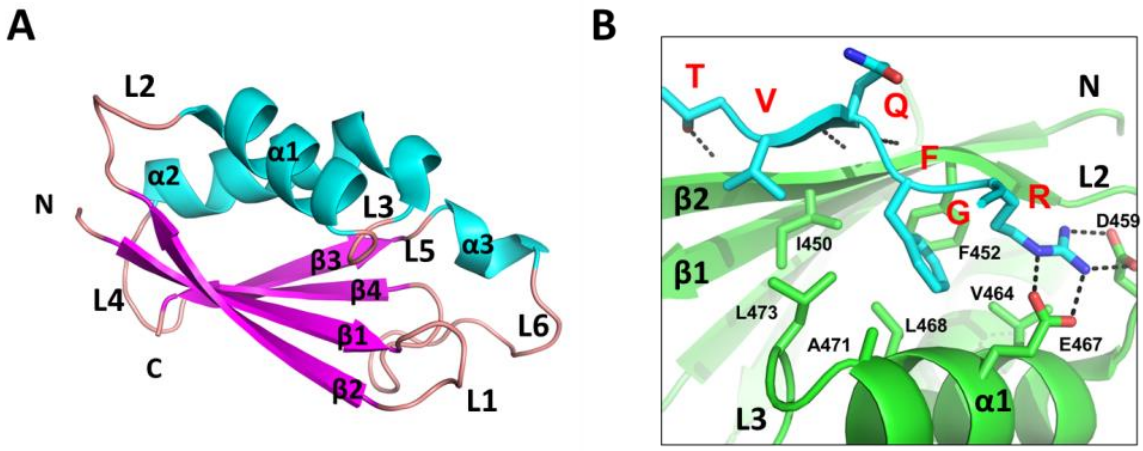

Figure 1-8. Structure of the OSR1 CCT domain bound to a WNK4 GRFQVT hexapeptide.

(A) SPOC fold and secondary structure elements of the OSR1 CCT domain from the OSR1:GRFQVT peptide complex structure (PDB 2V3S). (B) Core RFxV binding pocket. The peptide binds in part through β-strand addition.

The GRFQVT hexapeptide makes multiple interactions with residues from α1, L2, β2, and L3 (Figure 1-8B). Arginine and phenylalanine from the peptide sit in shallow pocket where arginine makes dual electrostatic interactions and four hydrogen bonds with D459 and E467, and phenylalanine makes multiple hydrophobic contacts with F452, L468, A471, and L473. The peptide valine stacks against L450, while glutamine points directly away from the CCT domain. As seen in other protein-peptide interactions, backbone hydrogen bonding is utilized to enhance the energetic favorability of the interactions ((London, Movshovitz-Attias et al. 2010). In this case β-strand addition is utilized ((Remaut and Waksman 2006), with peptide glutamine and valine backbone atoms hydrogen bonding to strand β2, as is the peptide threonine side chain.

Although the CCT domain – peptide complex structure revealed the structural basis for the interaction, it only partially addressed the question of specificity. It was evident that due to the number of hydrogen bonds and electrostatic interactions that arginine in the motif was most likely required, but whether additional hydrophobic residues could be used in place of the phenylalanine and valine were less clear. Only a handful of experimentally verified CCT domain interactions are available. Alignment of these known interaction motifs provides some insight into CCT domain specificity determinants (Figure 1-9). From this alignment it is evident that R and F at the 1 and 2 positions are almost certainly required, and that V/I is likely required at the 4 position. Additionally there is a preference for G at the -1, S/T at +1, and V/I/T at +3. However, since these motifs are primarily found within the pathway, only a small number of available motifs can be compared, and methods such as pull-downs may not be able to capture more transient interactions so the results are potentially biased.

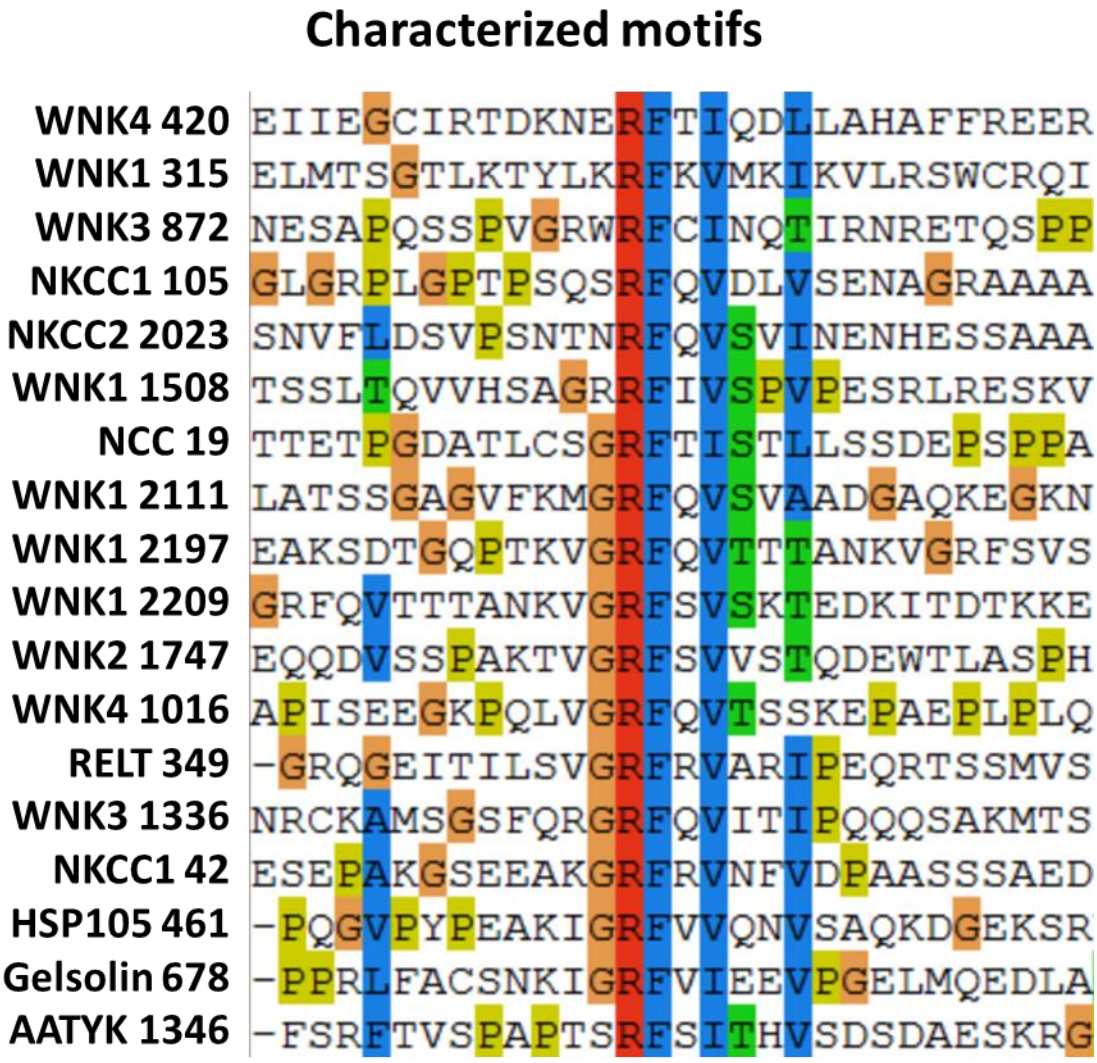

Figure 1-9. Known RFxV motif alignments.

Alignment of RFxV motifs experimentally verified to interact with CCT domains (except WNK4 420). Numbering is from arginine in core motif.

Some limited quantitative data on the affinity of the interactions also exists (Table 1-1). Surface plasmon resonance measurements using the OSR1 CCT domain suggest that the domain binds stably to a WNK4 RFxV motif, whereas several fluorescence correlation spectroscopy measurements imply that the interactions with the SPAK CCT domain with a WNK1, WNK4,

and NCC motif are approximately two to three orders of magnitude lower affinity. However, since the measurements were taken with alternative techniques, and GST-tagged, the reliability of the measurements is questionable.

CCT Domain (GST tag)	Peptide Source	Peptide Sequence	K_D (μM)	Technique	Reference
OSR1	WNK4	biotin-SEEGKPQLVGRFQVTSSK	0.008	SPR	(Vitari, Thastrup et al. 2006)
OSR1	WNK4	biotin-SEEGKPQLVGRFQVpTSSK	---	SPR	(Villa, Goebel et al. 2007)
OSR1	WNK4	biotin-SEEGKPQLVGRFAVTSSK	~0.008	SPR	(Vitari, Thastrup et al. 2006)
OSR1	WNK4	biotin-SEEGKPQLVGAFQVTSSK	---	SPR	(Vitari, Thastrup et al. 2006)
OSR1	WNK4	biotin-SEEGKPQLVGRAQVTSSK	---	SPR	(Vitari, Thastrup et al. 2006)
OSR1	WNK4	biotin-SEEGKPQLVGRFQATSSK	---	SPR	(Vitari, Thastrup et al. 2006)
OSR1	WNK1	biotin-AGRRFIVSPVPESRL	0.038	SPR	(Zagorska, Pozo-Guisado et al. 2007)
OSR1	WNK1	biotin-AGRRFIVpSPVPESRL	---	SPR	(Zagorska, Pozo-Guisado et al. 2007)
SPAK	WNK1	TAMRA-SDTGQPTKVGRFQVTTTA	1.3	FCS	(Mori, Kikuchi et al. 2013)
SPAK	WNK4	TAMRA-SEEGKPQLVGRFQVTSSK	1.3	FCS	(Mori, Kikuchi et al. 2013)
SPAK	NCC	TAMRA-TPGDATLCSGRFTISTLL	11.2	FCS	(Mori, Kikuchi et al. 2013)

Table 1-1. Review of quantitative data regarding CCT domain – RFxV motif interaction affinities.

SPR and FCS are surface plasmon resonance and fluorescence correlation spectroscopy, respectively.

ERK MAPK Pathway in Cancer

Extracellular signal-regulated kinase 1/2 (ERK1/2) are the terminal kinases of the core ERK MAPK cascade (Boulton, Yancopoulos et al. 1990), which consists of a series of three kinases: Raf → MEK1/2 → ERK1/2 (Figure 1-10). A variety of stimuli lead to activation of the

pathway (Roskoski 2012). The canonical route to pathway activation begins with extracellular ligand binding to receptor tyrosine kinases (RTKs), such as epidermal growth factor receptor EGFR. Ligand binding induces RTK dimerization which facilitates transphosphorylation of the cytoplasmic tails of the receptors (Yarden and Schlessinger 1987, Zhang, Gureasko et al. 2006, Lemmon and Schlessinger 2010). RTK phosphorylation recruits multiple signaling molecules including the guanine nucleotide exchange factors (GEF), Sos1/2, which in turn activate the small Ras GTPases by enhancing the exchange of GDP for GTP ((Roskoski 2012). Active Ras-GTP facilitates the activation of the Raf kinases. Raf kinases then activate MEK1/2, which in turn activate ERK1/2. ERK1/2 have hundreds of substrates within the cytosol and nucleus that are important in a variety of cellular functions such as proliferation, homeostasis, differentiation, transcriptional and translational regulation, and cell motility (Keshet and Seger 2010)

Due to the pathway's centrality in a variety of cellular functions, the ERK MAPK is often activated in cancers, either by mutation, amplification, or other means. It is estimated that ~30% of all human cancers contain Ras mutations, while Raf mutations are found in ~7% of cancers (Vakiani and Solit 2011, Roskoski 2012). Although, the upstream components of the pathway, such as Ras and Raf have been shown to be oncogenes, mutations in ERK1/2 have yet to shown to be oncogenic, and have been rarely described in the literature.

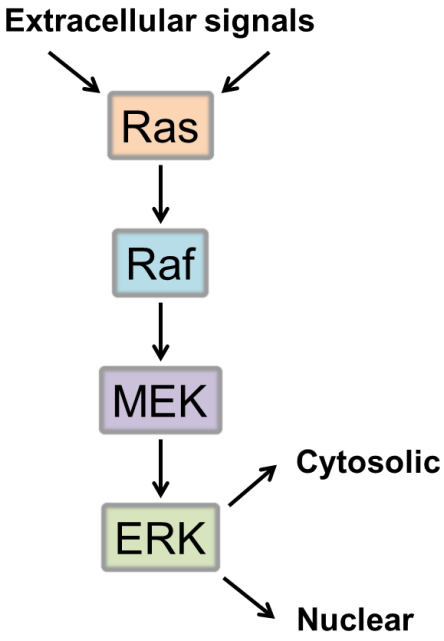

Figure 1-10. Overview of the ERK MAPK cascade.

The canonical ERK MAPK pathway. Extracellular stimuli lead to activation of the Ras small GTPase. Ras-GTP activates Raf kinases. Raf kinases then activate MEK1/2. MEK1/2 then activate ERK1/2 leading to the phosphorylation of a large number of cytosolic and nuclear substrates.

ERK2 E322K: A Potential Oncogenic ERK2 Mutant

The human MAPK1 gene missense mutation that results in expression of ERK2 E322K was originally discovered in the oral squamous cell carcinoma line, HSC6, because it migrated faster on denaturing gels, and led to constitutive activation of the ERK1/2 MAPK pathway (Arvind, Shimamoto et al. 2005). More recently, the E322K mutation was found to occur in ~5% of cervical carcinomas, and was recently classified as a cancer mutational hotspot by Chang and collegues (Ojesina, Lichtenstein et al. 2013, Chang, Asthana et al. 2016). Searching a publicly available database containing the combined results of 147 cancer genomics studies we found that the relative abundance of the missense somatic mutation, E322K was over 7-fold more abundant

than the next most abundant somatic missense mutations N257S and D321N in the MAPK1 gene (Figure 1-11) (Cerami, Gao et al. 2012, Gao, Aksoy et al. 2013). The mutation is concentrated in cancers with a squamous cell lineage but has also been found in other cancer types such as T cell lymphomas.

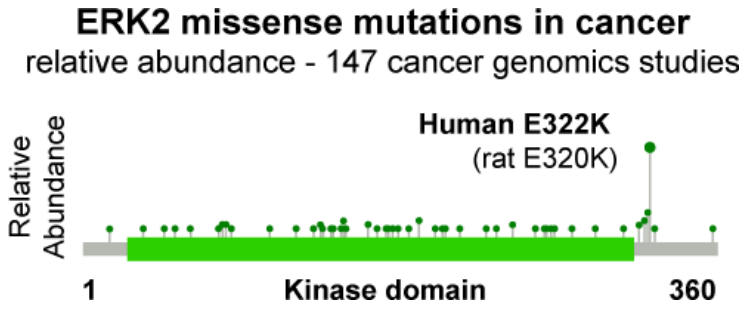

Figure 1-11. Relative abundance of ERK2 E322K mutation in cancers.

Schematic of human ERK2 with identified missense mutations in the MAPK1 gene shown as green dots. Dots represent combined results of 147 large-scale cancer genomics studies found at CBioPortal. Dot height represents the relative abundance of the given mutation. Human E322K (rat E320K) is the most abundant mutation by at least 7-fold. All subsequent structures and data utilize rat ERK2 numbering.

Human E322K, or rat E320K (rat numbering used for remainder of text) is found in the ERK2 L16 loop acidic motif (D316-X-X-D319-E320) of the common docking (CD) site (Zhang, Strand et al. 1994). The L16 loop runs along the entire backside of the kinase contacting both the N and C-terminal domains (Figure 1-12) . The CD site is present in most MAPK family members, lies on the opposite side of the kinase from the catalytic site, and interacts with basic/hydrophobic kinase interaction motifs (KIMs) often of the form K/R-K/R-X_{4-6}-Φ-X-Φ in substrates, regulators, and other interaction partners (Figure 1-13A,B) (Tanoue, Adachi et al. 2000).

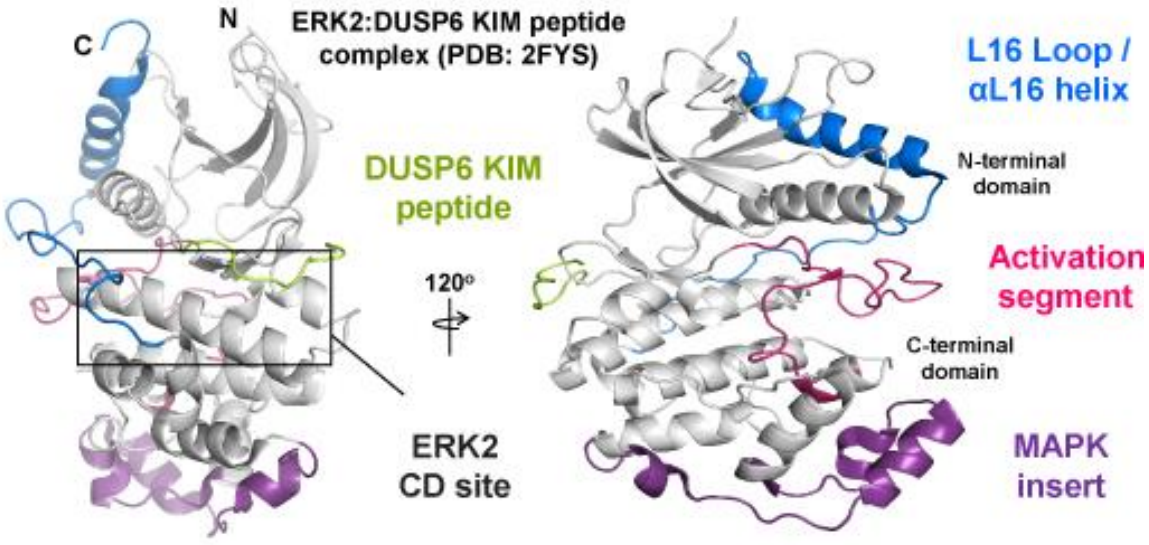

Figure 1-12. Structure of ERK2 bound to DUSP6 KIM.

Structure of rat ERK2 bound to a KIM peptide from DUSP6 (PDB: 2FYS). ERK2 common docking (CD) site (black box) is bound to DUSP6 peptide (lime). ERK2 activation segment (magenta) regulates kinase activity based on phosphorylation of T183/Y185; MAPK insert (purple) is a C-terminal domain insertion found only in MAPKs and is required for certain protein interactions; L16 loop/αL16 helix (blue) begins as a loop at the end of the ERK2 C-terminal domain and wraps around the back of the kinase domain where it is part of the CD site and ends as a helix that packs onto the N-terminal domain.

The importance of the multipurpose CD site for ERK2 function was first revealed through a genetic screen in Drosophila to overcome loss of activation of the sevenless tyrosine kinase, essential for development of the normal fly eye. That screen uncovered the mutation D334N, which in ERK2 corresponds to D319N, as a gain-of-function mutant in sevenless-dependent eye development and other tyrosine kinase pathways (Brunner, Oellers et al. 1994). D319 is required for direct interaction with basic residues in KIMs (Figure 1-13A,B). These and subsequent studies of mammalian ERK2 showed that ERK2 D319 is important for interaction with numerous ERK2 substrates including the ribosomal protein S6 kinases (RSKs) and many transcription factors, as well as the activating kinases MEK1 and MEK2 and the MAPK

phosphatases/dual specificity protein phosphatases (MKPs/DUSPs) (Figure 1-13B) (Tanoue, Adachi et al. 2000). Increased function in these pathways was attributed to reduced sensitivity of ERK2 D319N to DUSPs (Figure 1-13D), DUSP nomenclature used for clarity (Zhou, Wu et al. 2001) . Some DUSPs, such as DUSP6 used in this study, are also activated allosterically through interaction with ERK1/2, and KIMs are required for this activation (Camps, Nichols et al. 1998, Zhou, Wu et al. 2001). Initially shown for MAPK p38α, and later for ERK2, KIM interactions at the CD site can also allosterically regulate the conformation of MAPK activation loops, and the kinases generally have three known activation loop conformations (Figure 1-13C): inactive, active (ERK2 pT183/pY185), and solvent-exposed (KIM-bound) (Chang, Xu et al. 2002, Liu, Sun et al. 2006, Zhou, Sun et al. 2006). Presumably, solvent-exposure presents the activating phosphorylation sites to modifying enzymes to insulate the pathway from erroneous inputs (Verissimo and Jordan 2001, Zhou, Sun et al. 2006, Goldsmith, Akella et al. 2007, Akella, Min et al. 2010).

In contrast to ERK2 D319, which is a surface residue that directly contacts docking sequences, E320 does not directly interact with docking motifs, but instead points into the core structure making hydrogen-bonds and electrostatic interactions with helix αG residues K136 and Y129 (Figure 1-13A). Therefore, it is likely to disrupt CD site function, but why it is enriched in cancer (Figure 1-11) compared to other mutations that disrupt the CD site is unclear.

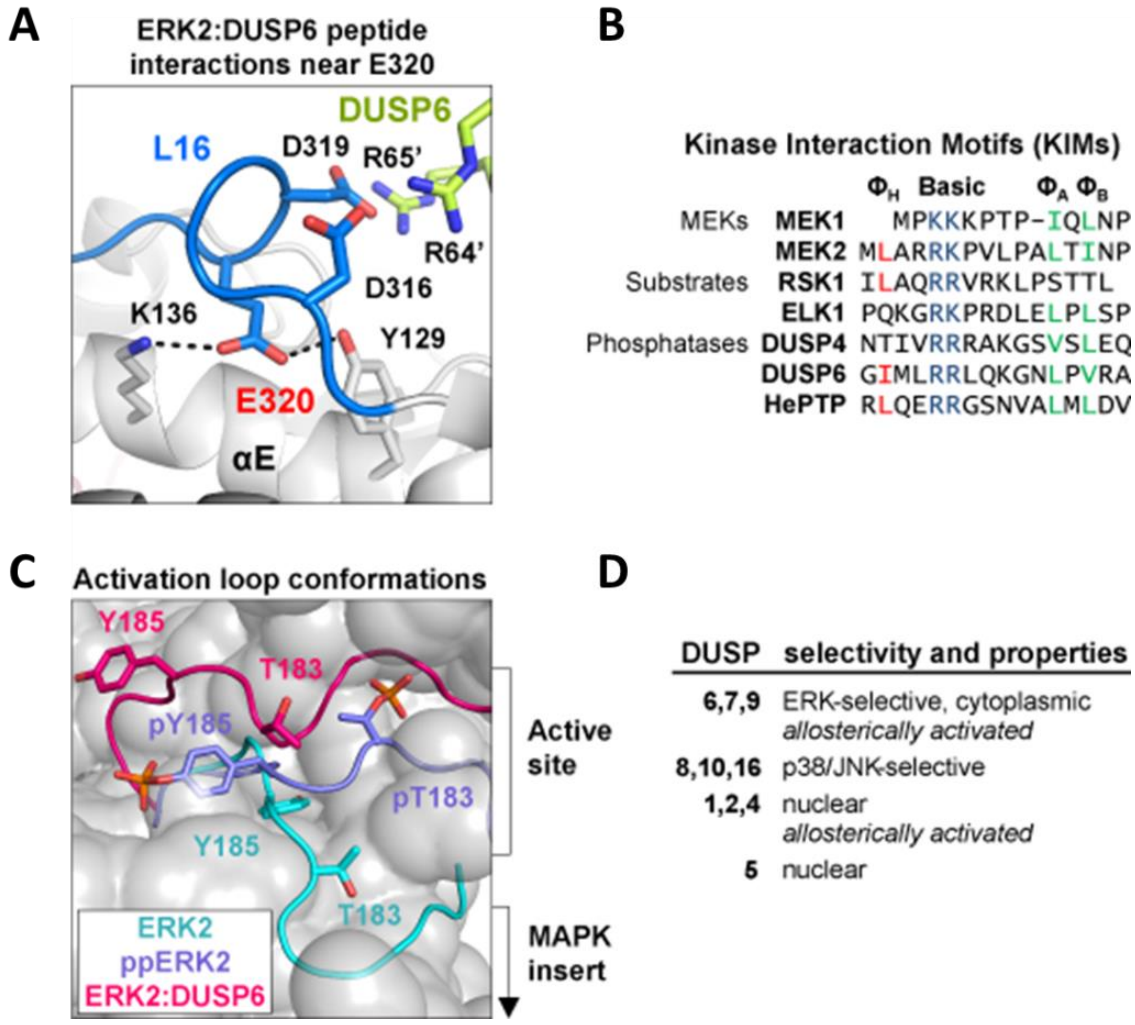

Figure 1-13. KIMs bind the ERK2 CD site and allosterically regulate the activation loop conformation.

(A) Close-up view of the interactions between the dual arginine residues in the DUSP6 KIM peptide (lime) and the acidic residues, D316/D319 in the rat ERK2 L16 loop (blue) that makes up part of the CD site. E320 (red label) is a buried charge that points inward toward the kinase domain. (B) Sequence alignment of relevant ERK1/2 kinase interaction motifs. (C) The three known conformations of the rat ERK2 activation loop around the activating phosphorylation sites T183 and Y185: inactive ERK2 (PDB: 1ERK, cyan), active ppERK2 (PDB: 2ERK, light purple), and ERK2:DUSP6 KIM (magenta). (D) Summary of MAPK DUSPs selectivity and ability to be allosterically activated by MAPK interaction.

Description of the Thesis

This dissertation focuses on how protein-protein and protein-peptide interactions contribute to the overall regulation, and in the case of mutation, misregulation, of the WNK and ERK MAPK signaling pathways. Although technically three separate projects, the work contained herein all relates to interactions within the two pathways.

The aim of the SPAK dimerization project was to investigate: how the domain-swapped SPAK and OSR1 dimers observed in the crystal structures related to their function; what were the functional differences between SPAK and OSR1 monomers and dimers, and whether dimerization was a prerequisite for kinase transactivation as had been observed with several other domain-swapped dimers.

The purpose of the SPAK/OSR1 CCT RFxV motif interaction project was two-fold: The first goal was to further characterize the specificity determinants of the SPAK and OSR1 CCT domains for RFxV motifs since other residues outside of the core motif were likely to participate in the interactions, but this characterization had yet to be undertaken. The second goal was to use the binding specificity data to predict potentially new interactions, and validate whether these predicted interactions were physiologically relevant.

The objective of the ERK2 E320K project was to fully characterize, both structurally and functionally, the effects of the E320K CD site charge reversal mutation on ERK2. Previous work had shown that it was present in cancers, particularly those of squamous cell origin, but other than its relative abundance compared to other ERK2 mutants and enhanced activation in the absence of stimuli, little else was known ((Arvind, Shimamoto et al. 2005, Ojesina, Lichtenstein

et al. 2013, Goetz, Ghandi et al. 2014, Van Allen, Lui et al. 2015, Brenan, Andreev et al. 2016, Chang, Asthana et al. 2016).

The dissertation contains the following chapters:

Chapter One, Introduction; includes background information relevant to all four projects.

Chapter Two, Structural and Functional Characterization of SPAK Dimerization; structural characterization of the inactive mouse SPAK 63-403 dimer and comparison to the active mouse SPAK 63-390 (T243D) and inactive human OSR1 1-295 dimers; functional characterization of dimerization using a dimerization blocking mutation.

Chapter Three, Binding Specificity-based Prediction of SPAK/OSR1 Docking Interactions; peptide arrays and fluorescence polarization were used to further define SPAK and OSR1 CCT domain (mouse SPAK 459-556, human OSR1 433-527) binding specificity beyond the general RFxV/I core motif; the results were used to develop a methodology for predicting SPAK/OSR1 CCT domain docking interactions.

Chapter Four, Structural and Functional Characterization of the ERK2 E322K Mutation; structural characterization of rat ERK2 E320K; functional characterization of the effect of the mutation of ERK2 E320K on docking interactions, kinase activity, and activity of activating kinases and deactivating phosphatases.

Chapter Five, Future Directions.

CHAPTER TWO

STRUCTURAL AND FUNCTIONAL CHARACTERIZATION OF SPAK DIMERIZATION

Abstract

The related protein kinases SPAK and OSR1 regulate ion homeostasis in part by phosphorylating cation cotransporter family members. The structure of the kinase domain of OSR1 was solved in the unphosphorylated inactive form, and like some other Ste20 kinases, exhibited a domain-swapped activation loop. To further probe the role of domain swapping in SPAK/OSR1, I determined the crystal structure of SPAK 63-403 at 3.1 Å, and Yu-Chi Juang determined the structure of SPAK 63-390 T243D at 2.5 Å resolutions. These structures encompass the kinase domain and different portions of the C-terminal tail, the longer without, and the shorter with an activating point mutation T243D. The structure of the T243D protein reveals significant conformational differences relative to unphosphorylated SPAK and OSR1, but also has some features of an inactive kinase. Both structures are domain-swapped dimers. Sequences involved in domain swapping were identified and mutated by Yu-Chi Juang to create a SPAK monomeric mutant with kinase activity, indicating that monomeric forms are active. I determined the monomeric mutant is activated by WNK1, but has reduced activity toward its substrate NKCC2, suggesting regulatory roles for domain swapping. The structure of the partially active SPAK T243D is consistent with a multi-stage activation process in which phosphorylation induces a SPAK conformation that requires further remodeling to build the active structure.

Experimental Procedures

Protein expression and purification. SPAK 63-390 T243D was expressed in Rosetta (DE3) *E.coli* (Novagen). Cells were grown at 37 °C until OD_{600} reached 0.4-0.6, and then induced with 0.5 mM IPTG overnight at 16 °C. Cells were lysed in 1 mg/ml lysozyme in 50 mM HEPES, pH 8.0, 0.3 M NaCl, 10% glycerol, and protease inhibitors (1 mM phenylmethanesulfonyl fluoride, 10 mM benzamidine, 0.2 μg/ml leupeptin, 2 μg/ml aprotinin), on ice for 30 min followed by sonication. Soluble proteins were applied to nickel-nitrilotriacetic acid-agarose (Ni^{2+}-NTA) and SPAK was eluted with 250 mM imidazole. Fractions with SPAK were identified by polyacrylamide gel electrophoresis in sodium dodecyl sulfate (SDS-PAGE), and dialyzed against 50 mM HEPES, pH 7.5, and 50 mM NaCl at 4^{o}C overnight. The tag was cleaved with His_6-TEV protease at a ratio of 50:1 (protein: protease), and removed by re-chromatography on Ni^{2+}-NTA agarose. SPAK was further purified on Mono S using a 0.05-1 M NaCl gradient in 50 mM HEPES, pH 7.5, 1 mM dithiothreitol (DTT), and 1 mM EDTA and on Superdex75 equilibrated in 50 mM HEPES, pH 7.0, 50 mM NaCl, 1 mM DTT, and 1 mM EDTA. Similar procedures were effective for all SPAK 63-390 mutants evaluated.

SPAK 63-403 was purified similarly (Figure 2-1). The lysis buffer was as above except that glycerol was increased to 15% and included 2.5 mM β-mercaptoethanol. The dialysis buffer contained 20 mM HEPES, pH 7.5, 0.1 M NaCl and 5% glycerol. Before gel filtration, the protein was further purified on Mono Q eluted with a gradient of 0.1-0.5 M NaCl in dialysis buffer also containing 1 mM DTT.

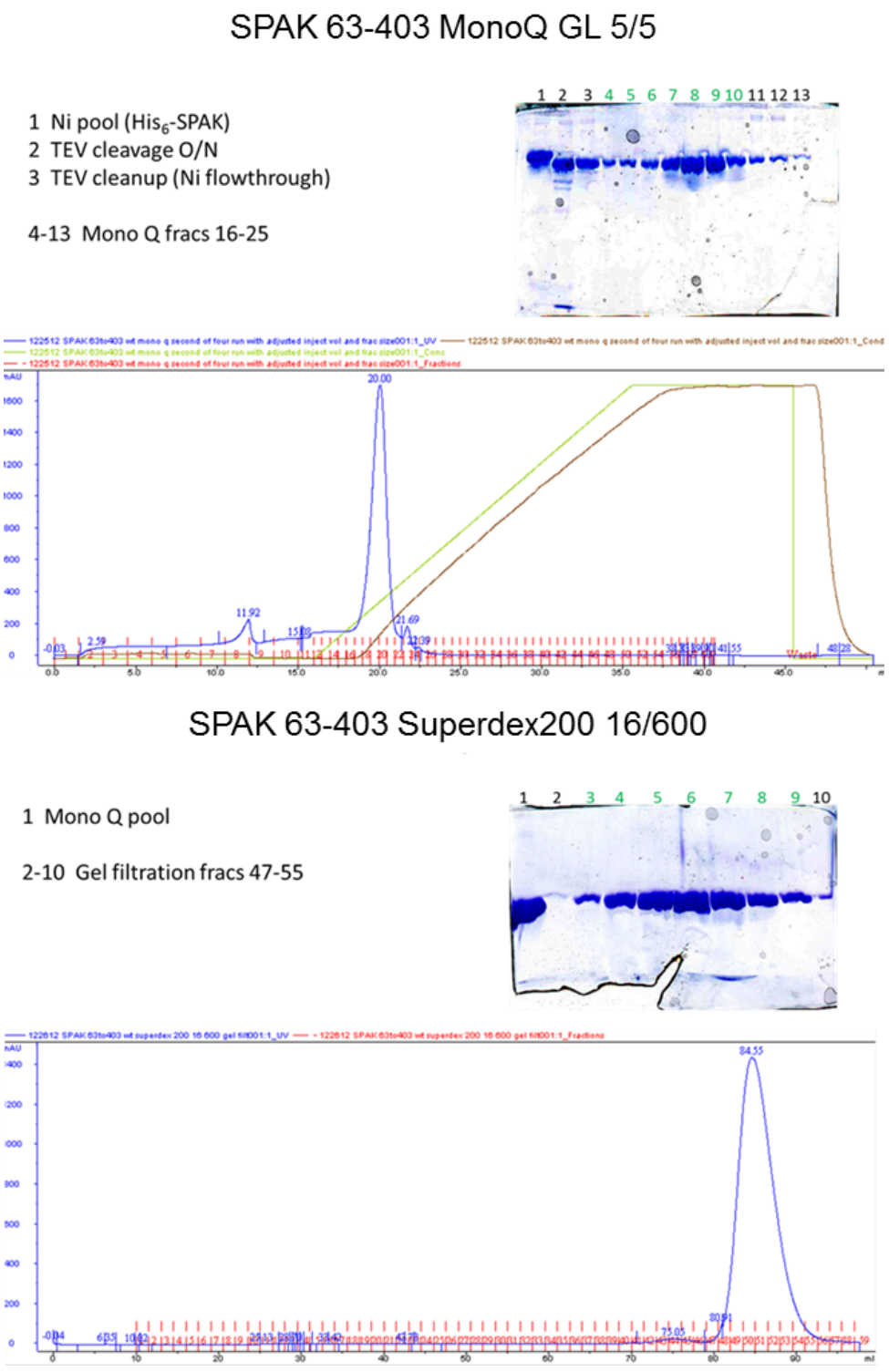

Figure 2-1. Purification of SPAK 63-403.

Purification scheme to produce high purity SPAK 63-403 that was suitable for crystallization. The scheme was Ni-NTA → mono Q → gel filtration. Pooled fractions are indicated by green lettering.

Crystallization. SPAK 63-390 T243D was crystallized by Yu-Chi Juang. SPAK 63-403 at 15 mg/ml was pre-incubated with 5 mM ATP, 5 mM $MgCl_2$ for 30 min on ice. Crystallization was carried out at 20^o C in hanging drops by mixing protein with an equal volume of well solution, 100 mM MES, pH 5.5, 150 mM ammonium sulfate, and 18% PEG4000 (Figure 2-2A). Rectangular plates 0.2 x 0.1 mm long with a maximum cross-section of 10-15 µm were flash frozen in liquid nitrogen after soaking in cryoprotectant, 20% ethylene glycol, 22% PEG4000, 100 mM MES, pH 5.5, 150 mM ammonium sulfate, 100 mM NaCl, 5 mM $MgCl_2$, 20 mM HEPES, pH 7.5, 5% glycerol.

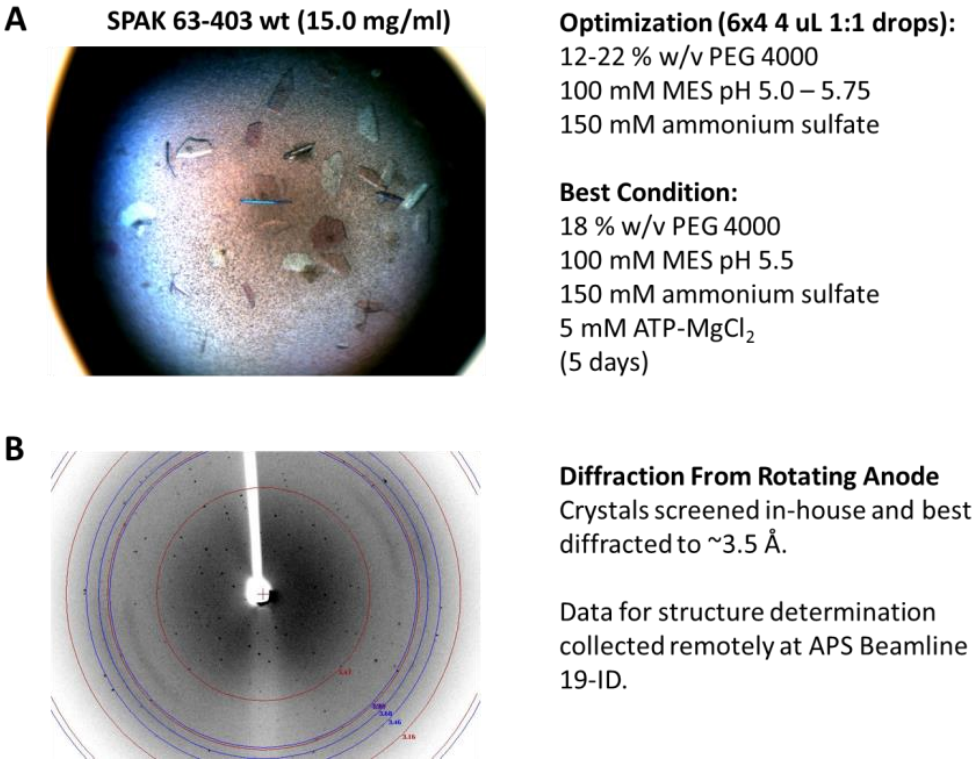

Figure 2-2. Crystallization and diffraction of SPAK 63-403.

(A) Crystals used for data collection and crystallization conditions. (B) Rotating anode diffraction image of screened crystal that was subsequently used for synchrotron data collection.

Data collection and structure determination. Diffraction data (Figure 2-2B) were collected at beamline 19-ID at the Advanced Photon Source (Argonne National Laboratory, Argonne, IL). Data were indexed, integrated, and scaled in HKL2000 (Otwinowski and Minor 1997). The structure of SPAK 63-390 T243D was determined by molecular replacement in PHASER in the CCP4 suite (McCoy, Grosse-Kunstleve et al. 2005, McCoy, Grosse-Kunstleve et al. 2007). The p21-activated kinase PAK6 (PDB 23C0) provided the best search model. The structure contains two molecules in the asymmetric unit (the solvent content was about 50% and V_M=2.51 $Å^3$/Da). Model building was carried out in Coot and refinement was performed with REFMAC5 in the CCP4 suite (Murshudov, Vagin et al. 1997, Emsley and Cowtan 2004). $As(CH_3)_2$ was covalently linked to a subpopulation of SPAK T243D cysteine residues, as a result of the crystallization conditions. TLS (translation/libration/screw) refinement was carried out in TLSMD (Painter and Merritt 2006). The structure was checked on the MolProbity web server (Davis, Murray et al. 2004);

The structure of SPAK 63-403 was solved using molecular replacement in PHASER in Phenix (McCoy, Grosse-Kunstleve et al. 2005, McCoy, Grosse-Kunstleve et al. 2007, Adams, Afonine et al. 2010). The refined structure of SPAK 63-390 T243D chain A N-terminal domain excluding helix αC and C-terminal domain excluding the activation loop were used as search models. The structure contains two SPAK molecules per asymmetric unit. Manual rigid body docking of the SPAK 63-390 T243D chain A activation loop and helix αC excluded from the molecular replacement search models was followed by iterative rounds of refinement (TLS, rigid body, and individual ADPs) in phenix.refine and model building in Coot (Emsley and Cowtan 2004, Adams, Afonine et al. 2010, Afonine, Grosse-Kunstleve et al. 2012). Secondary structure restraints were used until the final rounds of refinement. Model validation was carried out in

phenix.refine, which uses analyses derived, in part, from the MolProbity web server (Davis, Murray et al. 2004, Adams, Afonine et al. 2010, Afonine, Grosse-Kunstleve et al. 2012). Dimer interface surface areas were calculated by directly inputting the structures into the PISA server (http://http://www.ebi.ac.uk/pdbe/pisa), and using the A to B ranges with symmetry operator x,y,z (Krissinel and Henrick 2007). Figures were made in PyMOL (The PyMOL Molecular Graphics System, Schrödinger, LLC).

Kinase assays. 0.5-1 µg of SPAK proteins were added to a 30 µl kinase reaction containing 20 mM HEPES, pH 7.6, 50 µM ATP (10 µCi [γ-^{32}P]ATP), 10 mM $MgCl_2$, 10 mM β-glycerophosphate, 1 mM DTT, and 1 mM benzamidine, with 5 µg of either GST-PAK1 1-230 or GST-NKCC2 1-175 as substrate for a 30-min reaction at 30°C. For the coupled assays using WNK1 pre-activated SPAK, SPAK was first phosphorylated by WNK1 kinase domain (residues 132-483) by incubation of 1 µg of SPAK with 2.5 µg of WNK1 in a 20 µl kinase reaction containing 1 mM DTT, 20 mM HEPES pH 7.6, 50 µM ATP, 75 mM NaCl, 5% w/v glycerol, 15 mM $MgCl_2$ for 30 min at 25^{o}C. Then 5 µl of a substrate mixture containing 2 µg GST-NKCC2 (residues 1-175), 250 µM ATP (10µCi [γ-^{32}P]ATP), and 75 mM $MgCl_2$ was added to the reaction and incubated for 5 min at 25^{o}C. Samples were analyzed by SDS-PAGE. Gels were stained with Coomassie blue, dried, and exposed to film.

Gel filtration chromatography. Gel filtration chromatography of 250 µM SPAK mutants was on a Superdex 75 10/300 GL column in 50 mM HEPES (pH 7.0), 50 mM NaCl, 1 mM DTT, and 1 mM EDTA.

Results

SPAK Crystallization and Structure Determination

Extensive bacterial expression and crystallization screening of the SPAK kinase domain together with both N and C-terminal extensions led to crystals of SPAK 63-403 and SPAK 63-390 T243D (SPAK 63-390 T243D structure determined by Yu-Chi Juang). The constructs crystallized encompass the kinase domain (residues 75-350), an N-terminal extension (residues 63-74), and residues 351-390 or 351-403 from the PF1 homology box (residues 351-403) (Figure 2-3A) (Leiserson, Harkins et al. 2000, Chen, Yazicioglu et al. 2004). SPAK 63-403 will be referred to throughout as SPAK WT and SPAK 63-390 T243D will be referred to as SPAK T243D. The previously reported structure of wild type OSR1, residues 1-295, used for comparison in this study (PDB code 3DAK) will be referred to as OSR1 WT (Lee, Cobb et al. 2009).

SPAK WT and SPAK T243D crystallized in different conditions and space groups. SPAK WT crystallized in the presence of ATP and was solved at 3.1 Å resolution with a final R_{work} = 23.7% and R_{free} = 26.9%. SPAK T243D crystallized in the presence of AMP-PNP at 2.5Å resolution and was refined with a final R_{work} = 20.6% and R_{free} = 24.6% by Yu-Chi Juang. The refined models display reasonable geometry and Ramachandran statistics (Table 2-1). Two SPAK molecules are in each asymmetric unit in both structures (Figure 2-3B). The conformations of the two monomers in SPAK WT and SPAK T243D are similar, with average root mean square deviations (RMSD) in Cα positions of 0.31 Å and 0.45 Å, respectively.

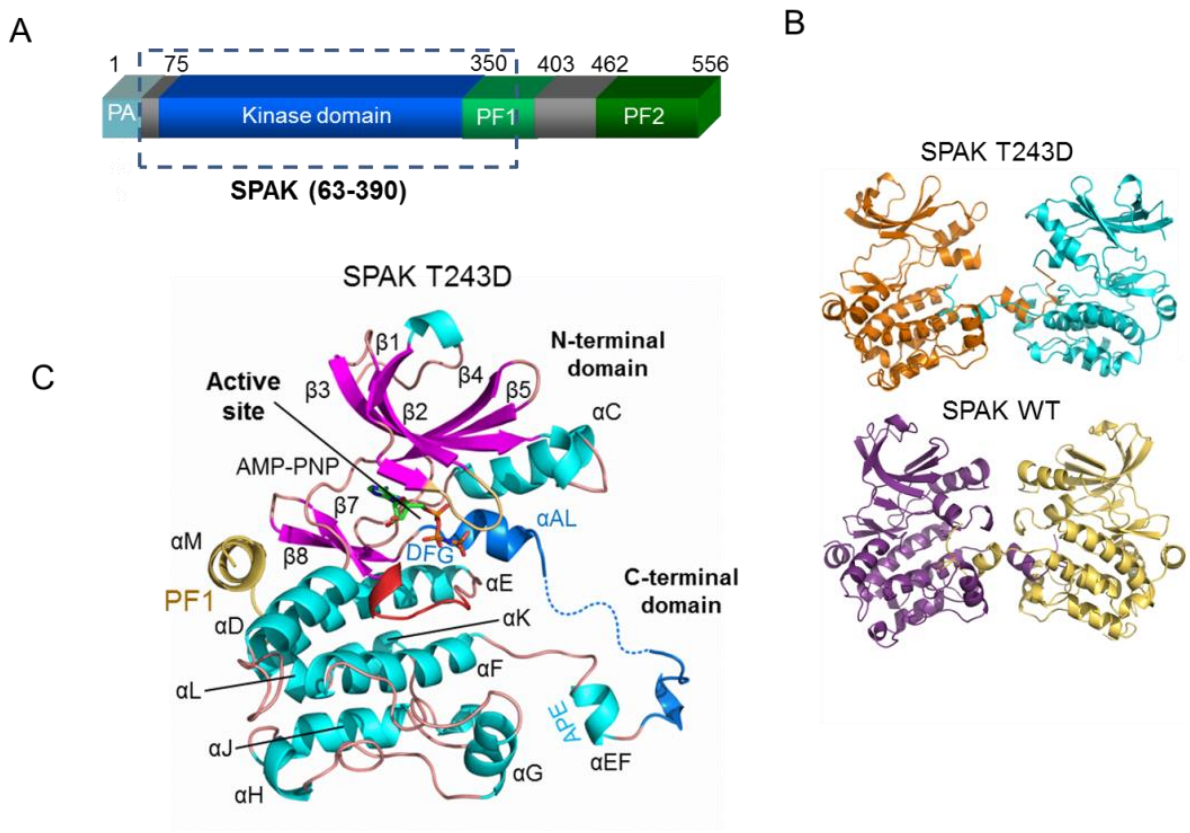

Figure 2-3. Domain organization and structure of SPAK WT and T243D.

(A) Domain organization of mouse SPAK. The kinase domain (residue 75-350) is shown in blue, the PF1 domain (residues 350-403) in green, and the PF2 domain (residue 462-556) in darker green. The SPAK T243D fragment crystallized is boxed. (B) Activation loop domain-swapped dimers of SPAK T243D and SPAK WT. The two SPAK T243D dimer subunits are colored orange and blue, and the two SPAK WT subunits are colored purple and yellow. (C) Ribbon diagram of a SPAK T243D subunit (or monomer) as observed in the domain-swapped dimer structure determined by Yu-Chi Juang. α-helices-cyan; β-strands-magenta; glycine-rich loop- brown; catalytic loop- red; activation loop- blue; PF1 domain- yellow. AMP-PNP is shown in a stick representation.

Data	SPAK 63-403	SPAK 63-390 (T243D)
Spacegroup	P 2_1	P 2_1 2_1 2_1
Cell dimensions (Å)	*a*= 72.4, *b*= 56.1, *c*= 100.0	*a*= 66.4, *b*= 101.7, *c*= 104.1
α, β, γ	90˚ , 108.3˚ , 90˚	90˚ , 90˚ , 90˚
Resolution (Å)	42.9-3.10 (3.20-3.10)	50-2.45 (2.54-2.45)
Observed reflection	38612	308327
Unique reflection	13658	27322
Completeness	85.6 (44.3)	93 (80.7)
R_{merge} (outer shell)[1]	0.069 (0.49)	0.043 (0.41)
I/> (outer shell)	15.1 (2.1)	31.4 (1.98)
Refinement		
R_{work}[2] (%)	23.6	20.6
R_{free}[3] (%)	26.9	24.6
R.m.s.d. bond length	0.009 Å	0.006 Å
R.m.s.d. bond angle	1.18˚	1.03˚
Ramachandran favored (%)	92.8	96.6
Ramachandran outliers (%)	0.2	0.0
Average B factor (Å^2)	76.9	70.6

Table 2-1. SPAK Data Collection and Refinement Statistics.

SPAK Structural Overview

Both SPAK WT and SPAK T243D structures adopt a canonical two-domain kinase fold, with a small N-terminal domain (residues 63-155) connected to a larger C-terminal domain (residues 156-365) through a hinge (Figure 2-3C). The C-terminal domain resembles that of OSR1, and has the canonical kinase helices D to I, as well as small, C-terminal helices J, K, and L. Both structures also possess an extra helix, αM (residues 355-363) that occupies a groove at the back of the kinase close to helix αD and strands β7 and β8. This helix is in a position similar to docking motif interactions found in MAPKs, which allosterically regulate sites distal to the docking site (Chang, Xu et al. 2002, Zhou, Sun et al. 2006, Goldsmith, Akella et al. 2007, Peti and Page 2013). The constructs used to solve the structures of OSR1 lacked the C-terminal

extension, including residues in αM (Lee, Cobb et al. 2009). Overlay of an individual subunit of both the SPAK WT and OSR1 WT structures reveals a RMSD of 0.99 Å. Apparently, neither the sequence variation between SPAK and OSR1, nor the presence of the PF1 domain in SPAK WT (of which helix αM is visible in the density) give rise to significant conformational differences between the molecules (Figure 2-4A). However, conformational differences between the SPAK T243D and SPAK WT structures do exist. A slight (6^{o}) domain rotation is present, with SPAK T243D in the more open configuration. αC and αAL (in the activation loop) show significant differences, again with αAL adopting the more open configuration in SPAK T243D (Figure 2-4A,B).

The nucleotide positions in SPAK T243D and SPAK WT primarily track with the N-terminal domains, and reflect the difference in domain rotation between the two structures (Figure 2-5). In the open T243D structure, the phosphates are bound to the glycine-rich loop. In the more closed SPAK WT structure the γ-phosphate maintains contact with K206 in the catalytic loop in the C-terminal domain. Neither position is identical to that in PKA because PKA has a closed domain structure and ATP contacts both domains. The position of the ATP in the SPAK T243D structure is more similar to that in PKA.

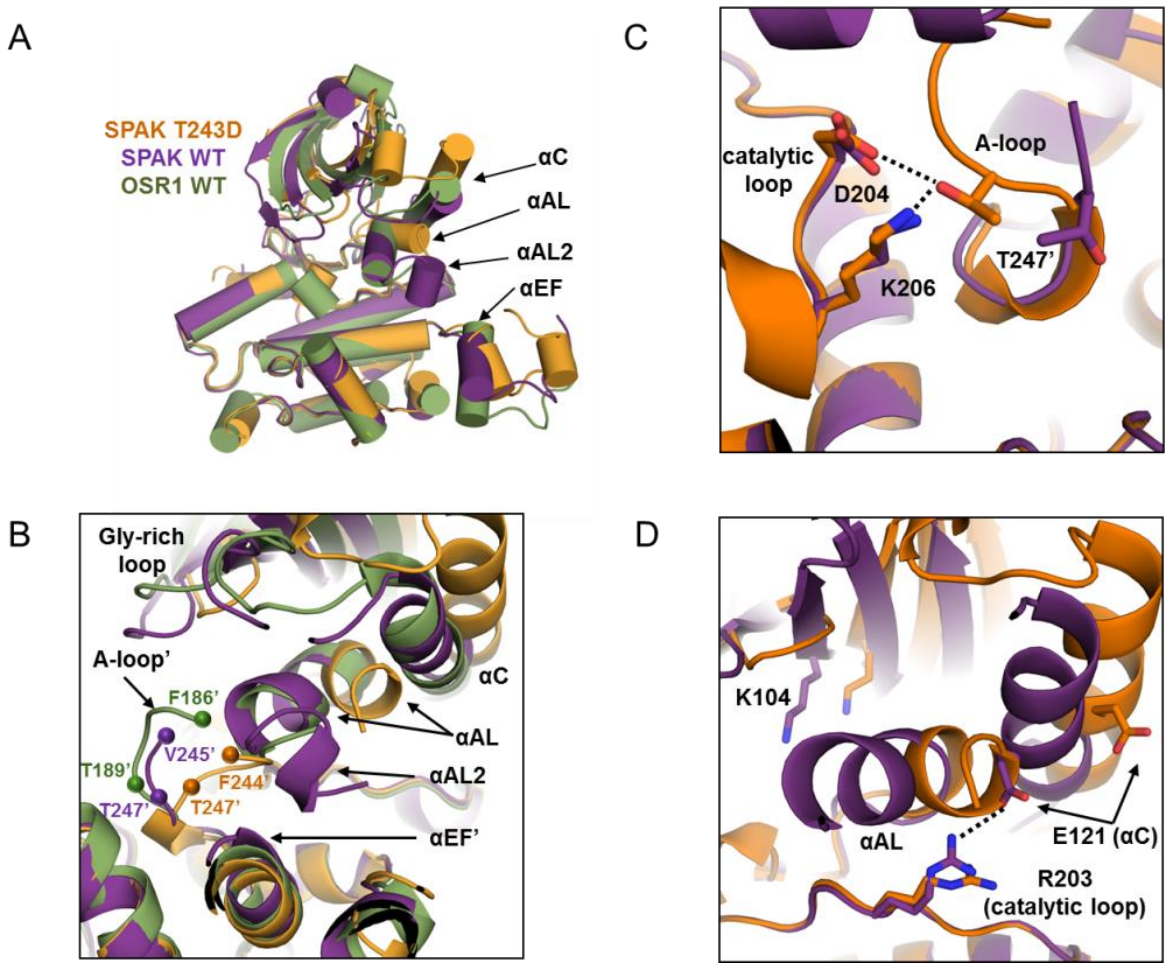

Figure 2-4. Conformational changes occurring in SPAK T243D compared to SPAK WT and OSR1 WT.

(A) Cartoon representation (α-helices represented as cylinders for clarity) of C-terminal domain alignments of SPAK WT (chain A; purple), SPAK T243D (chain A; orange), and OSR1 WT (chain A; green; PDB: 3DAK). Structural elements of particular interest are labeled. (B) Dimer interface near the domain-swapped activation loop and SPAK T243/OSR1 T185 WNK phosphorylation site. Labels marked with a prime (‘) correspond to the second monomer in the dimer. Spheres represent the first residue observed in the activation loop electron density and the SPAK T247'/OSR1 T189' catalytic residue. (C) The D-K-T catalytic triad interaction, formed by catalytic loop residues D204 and K206 and domain-swapped activation loop residue T247', is only present is SPAK T243D. (D) The essential K-E ion pair, between β3 K104 and αC E121, which is a hallmark of active kinases, is not present in SPAK WT or SPAK T243D. An interaction between catalytic loop residue R203 and E121 is present in SPAK WT but lost in SPAK T243D.

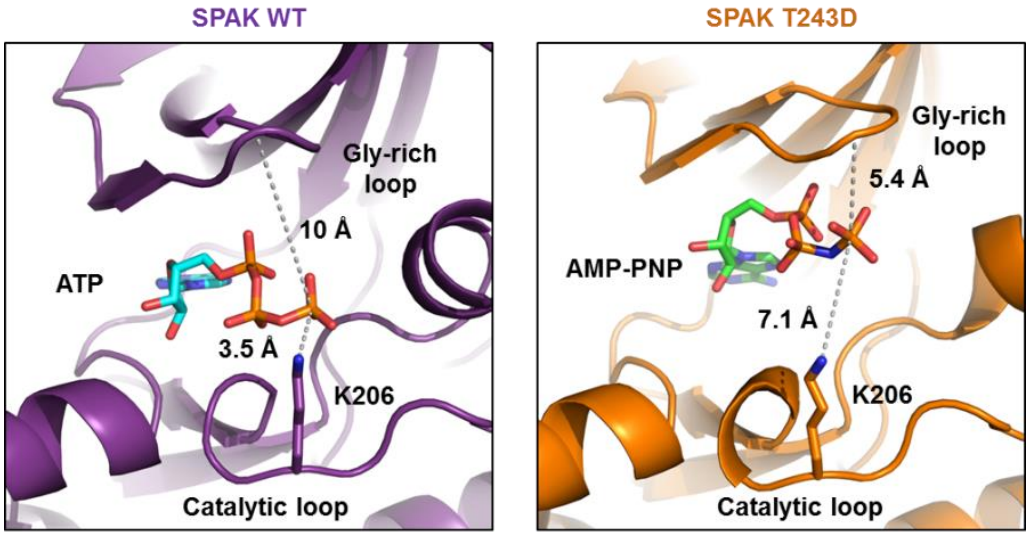

Figure 2-5. Comparison of nucleotide binding modes of SPAK WT and SPAK T243D.

Equivalent views of SPAK WT and SPAK T243D using C-terminal domain alignments. The nucleotide positions primarily track with the N-terminal domains (N-terminal domain above nucleotide; C-terminal domain below). The ATP in SPAK WT is closer to the C-terminal domain, than AMP-PNP in SPAK T243D. In SPAK WT the γ-phosphate of ATP is 3.5 Å from the ε-amino group of K206 and 10.0 Å from the Cα of A85 in the glycine-rich loop. In contrast, in SPAK T243D the γ-phosphate of AMP-PNP is 7.1 Å from the ε-amino group of K206 and 5.4 Å from the Cα of A85 in the glycine-rich loop.

Both SPAK WT and SPAK T243D have similar disordered regions. In the activation loop SPAK T243D only has helix αAL, while SPAK WT has two helices αAL and αAL2. Notably missing from the electron density is the C-terminal part of the PF1 domain (after residue R365 in SPAK T243D). To determine if this C-terminal region of the PF1 box affects activity, Yu-Chi Juang compared wild-type SPAK 63-370 and 63-390, both phosphorylated by WNK1, and found that the longer construct had more activity (Figure 2-6A). SPAK T243D has 10-20 fold more activity than wild-type SPAK 63-390, but only about 10% of the activity of SPAK 63-390 phosphorylated by WNK1 (Figure 2-6B).

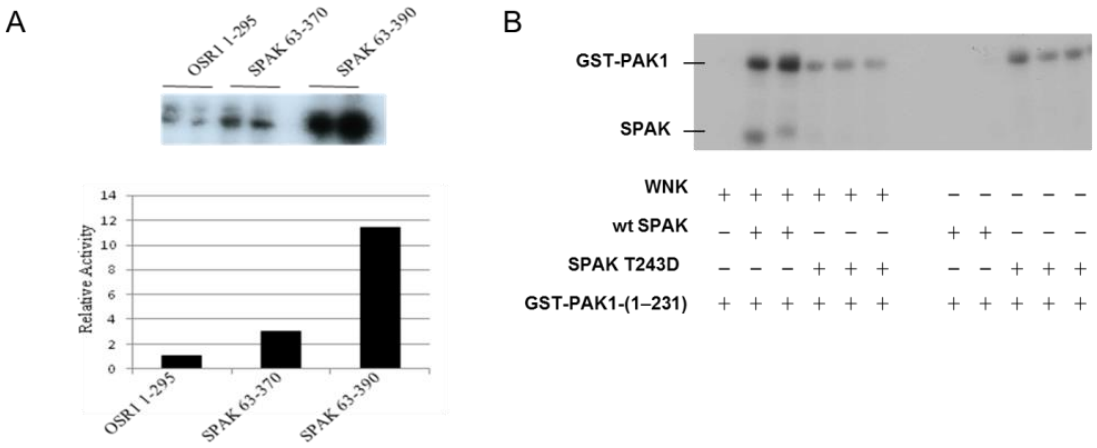

Figure 2-6. PF1 domain truncations and T243D mutation on SPAK kinase activity.

(A) Kinase assay, performed by Yu-Chi Juang, reporting the relative activities of OSR1 kinase domain (1-295), SPAK kinase domain plus first 20 residues of PF1 domain (63-370), and SPAK kinase domain plus 40 residues of PF1 domain including S383 WNK phosphorylation site (63-390, or SPAK WT). (B) Kinase assay, performed by Yu-Chi Juang, with GST PAK1 (1-231) as substrate comparing activities of SPAK (63-390) wild-type, WNK1 activated, and T243D phosphomimetic mutation activated.

SPAK Activation Loop Domain Swapping

The most prominent feature of both the SPAK WT and SPAK T243D structures is that the activation loops are domain-swapped (Figure 2-3B and Figure 2-7A,B). To ensure that the dimers observed in the crystal structures were not artifacts of crystallization, Yu-Chi Juang performed gel filtration experiments. Chromatography on Mono S revealed two peaks. Gel filtration showed that the peaks correspond to monomer and dimer (Figure 2-7C). Rechromatography of proteins from each peak gave rise to both populations (data not shown) indicating SPAK exists in a monomer:dimer equilibrium in solution. In addition, Yu-Chi Juang showed ATP favors dimerization (Figure 2-7D).

Activation loop domain swapping encompasses residues G233-G261: G233-G246 of the activation loop and P+1 specificity pocket (binds P+1 site of substrate), T247 in the active site of the other monomer, helix αE/F (E254-V259), and the following loop leading to helix αF (Figure 2-8A). In SPAK T243D, T247 is hydrogen-bonded to two invariant catalytic residues, D204 and K206, from the opposite monomer (Figure 2-4C, Figure 2-8B). The local structure in this area is similar to that of active canonical non-domain-swapped protein kinases, such as PKA (Figure 2-8B).

The dimer interfaces in SPAK T243D and SPAK WT bury 1906 $Å^2$ and 2003 $Å^2$ of the dimer surface areas, respectively, or approximately 5% of the total surface areas of the dimers as calculated by the PISA server, and are almost entirely hydrophobic (Krissinel and Henrick 2007). Part of the activation loops in both SPAK WT and T243D are disordered; in SPAK T243D these residues encompass T231-D243 in the activation loop of one monomer, and D234-D243 in the activation loop of the other monomer (Figure 2-4B). Similar residues are disordered in SPAK WT, with the exception of the presence of an additional helix αAL2 at the N-terminus of the activation loop. Notably, densities for T243 and the phosphomimetic mutation, T243D, are not present in either structure (Figure 2-4B).

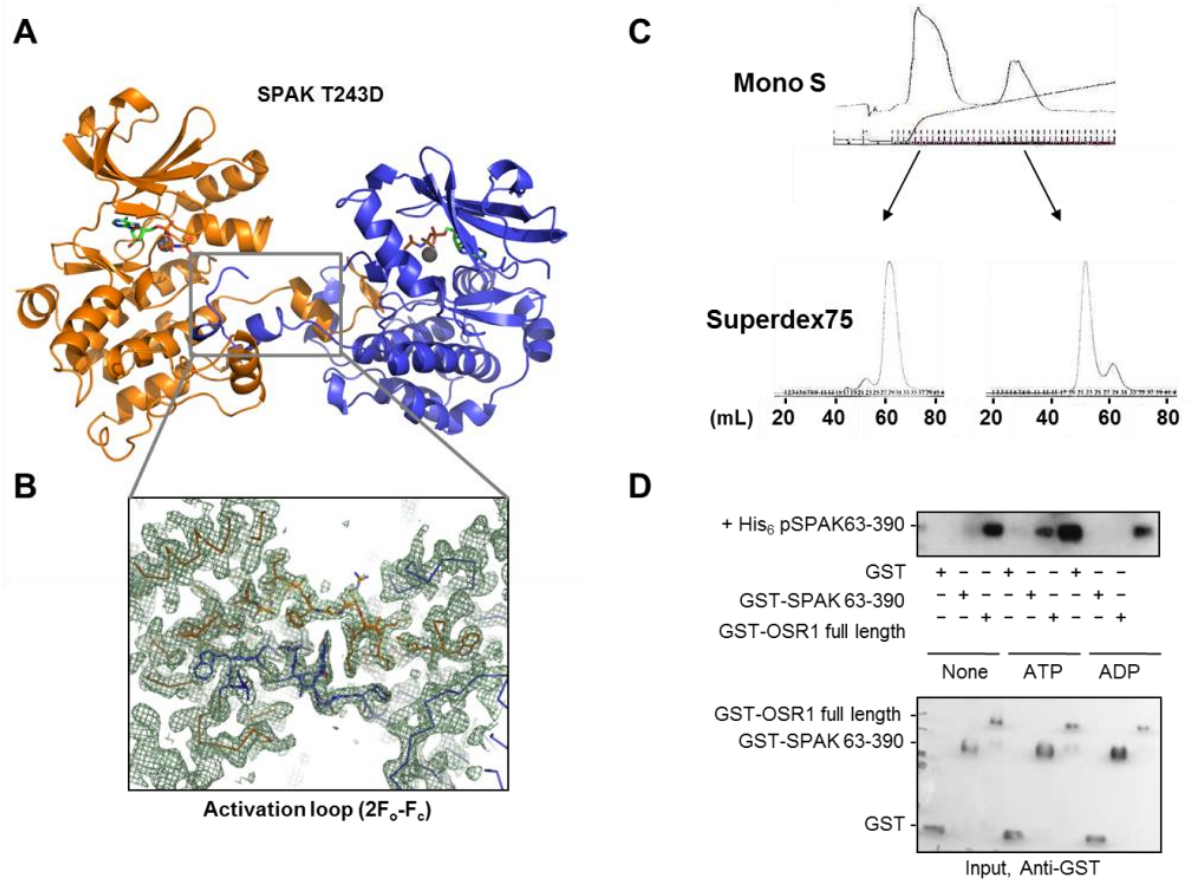

Figure 2-7. Dimerization of SPAK.

(A) Cartoon representation of SPAK T243D dimer with AMP-PNP in green sticks, Mg^{2+} in grey spheres, and domain-swapped activation segments boxed. (B) The interface of the domain-swapped dimer. $2F_o$-Fc electron density map contoured at 1.0σ. (C) SPAK T243D Mono S chromatographic separation yields two peaks containing SPAK. Each peak was subjected to Superdex75 gel filtration. Comparison of SPAK T243D (37.5 kDa) to molecular weight standards (67 kDa: 57.8 ml; 43 kDa: 64.2 ml; 38 kDa: 62.5 ml; 25 kDa: 75 ml) indicates that the first Mono S peak corresponds to SPAK monomer, and the second peak to SPAK dimer. Y-axis reports absorbance at 280 nm wavelength (work performed by Yu-Chi Juang). (D) Effect of ATP and ADP on SPAK protein association, determined by the binding activity of His6-SPAK 63-390 to GST-SPAK 63-390 or GST-OSR1 full-length in a pull-down assay (work performed by Yu-Chi Juang).

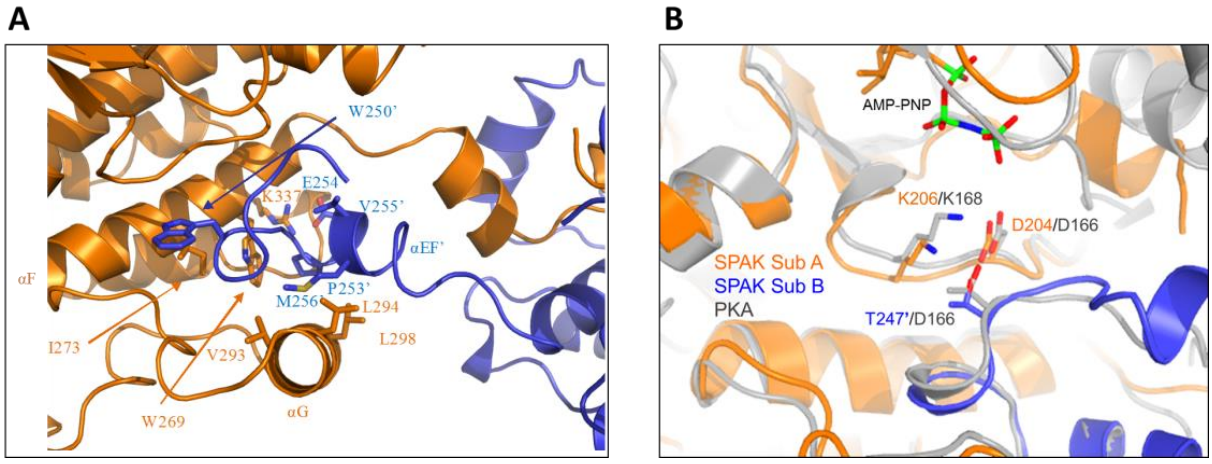

Figure 2-8. SPAK T243D domain-swapped activation loop dimer interface.

(A) Ribbon diagram of SPAK T243D by Yu-Chi Juang indicating interacting residues of one monomer and the domain-swapped activation segment of the second monomer (denoted with prime). Residues within the interface help to form the P+1 substrate pocket. (B) Superposition of SPAK T243D and PKA (PDB 1ATP) reveals formation of D-K-T catalytic triad in SPAK T243D, which is important for proper formation of the P+1 substrate specificity site.

At the quaternary level, the dimeric arrangement of SPAK WT and SPAK T243D differ significantly. Both form two-fold symmetric dimers. However, these dimers are not equivalent due to differences in the orientation of the dimer axes (Figure 2-9A,B). This difference in rotation correlates with tighter dimer packing in SPAK WT, including close contact between the αAL2 helices, which are only ordered in SPAK WT (Figure 2-9C). In SPAK T243D, the two monomers are farther apart by a surprising 5 Å, although the function of this enhanced separation is unclear. Thus, these conformational differences are found not only in specific kinase substructures, but also in the overall organization of the two monomers. These differences might be responsible for alteration of the relative orientation and position of the N- and C-terminal domains, or activation loop accessibility, which are generally associated with kinase activation (Zeqiraj, Filippi et al. 2009, Filippi, de los Heros et al. 2011, Grimm, Taneja et al. 2012, Mehellou, Alessi et al. 2013, Hao, Feng et al. 2014).

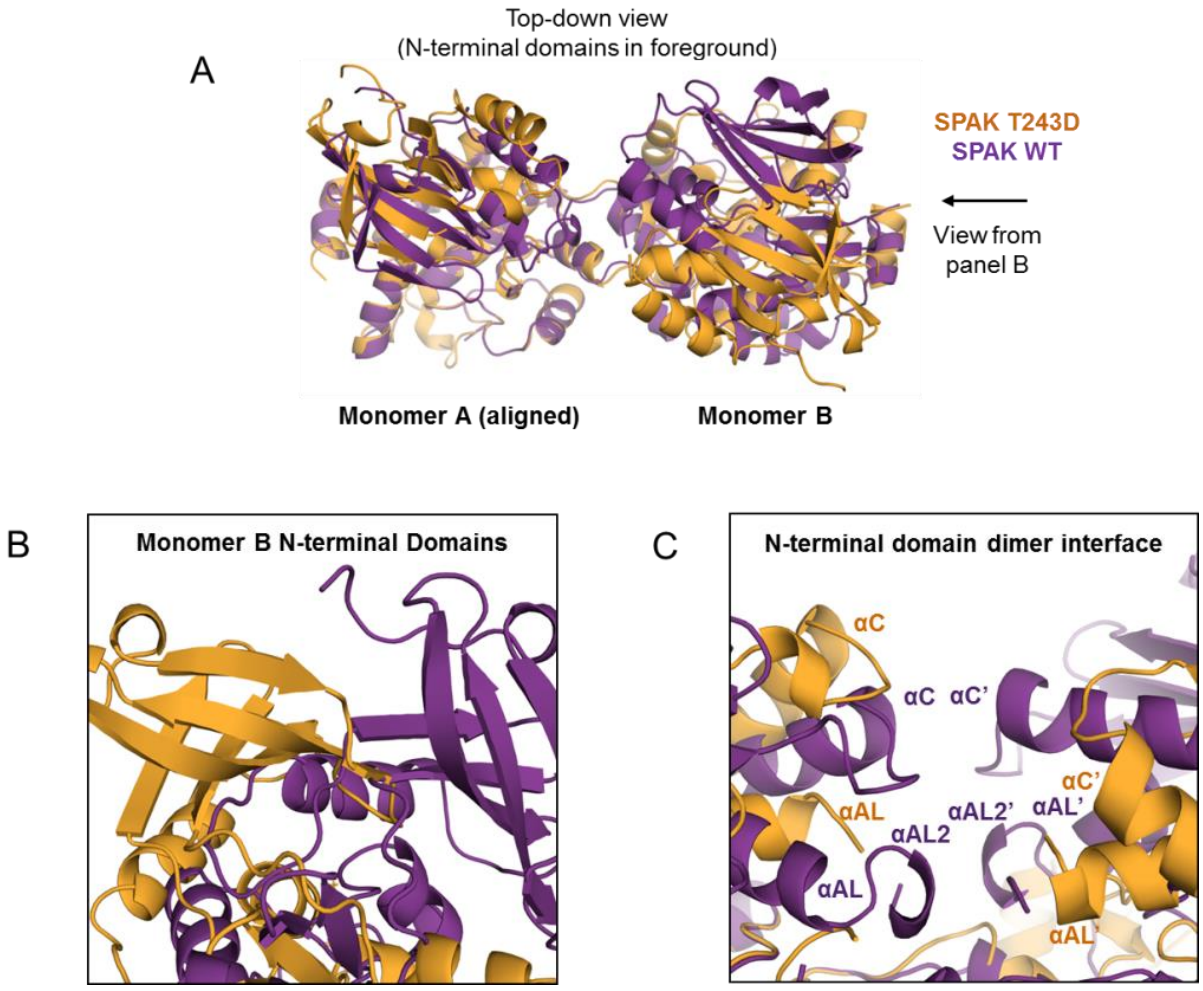

Figure 2-9. Relative monomer orientations in the SPAK WT and SPAK T243D dimers.

(A) Top-down view (N-terminal domain on top) of structural alignment of SPAK WT chain A and SPAK T243D chain A. Arrow denotes view from panel B. (B) Side-view of panel A showing SPAK WT chain B and SPAK T243D chain B with chain A omitted from background for clarity. (C) Close-up of panel A showing N-terminal domain dimer interfaces of SPAK WT and SPAK T243D. Secondary structure elements at interface are labeled. Only SPAK WT has ordered αAL2 helices.

Comparison of the SPAK Structures Suggests a Multistage Activation Mechanism

SPAK WT and SPAK T243D monomers superimpose with a RMSD of ~1.7 Å. The superposition improves considerably using the C-terminal domain alone, with a RMSD of 0.31

Å. The large discrepancy in RMSD is primarily due to the relative positions of the N- and C-terminal domains, with SPAK T243D in the more open configuration, as discussed above (Figure 2-4A). Other specific differences occur in the glycine-rich loop, helix αC, and at both ends of the activation loop. The glycine-rich loop of SPAK T243D falls closer to the ATP binding pocket than it does in both SPAK WT and OSR1 WT, and adopts a closed conformation on the first two β strands. The C-termini of the activation loops adopt different conformations in the SPAK WT and T243D structures (Figure 2-4B). The SPAK T243D configuration is similar to active kinases, as discussed above, with a well-formed P+1 pocket, and T247 from the opposing monomer making standard active site contacts with D204 and K206 in the catalytic loop (Figure 2-4C, Figure 2-8B). In contrast, SPAK WT and OSR1 WT have poorly formed P+1 pockets. In SPAK T243D, the N-terminus of helix αC is shifted about 5 Å relative to SPAK WT. As noted previously in the report on OSR1 WT, SPAK WT R203 from the catalytic loop makes an electrostatic interaction with E121 in αC (Lee, Cobb et al. 2009). This interaction is lost in SPAK T243D, potentially as the result of the movement of helix αAL (Figure 2-4D). However, SPAK T243D still lacks the K104-E121 ion pair, which is a hallmark of active kinases. Thus, SPAK T243D appears more active near the P+1 pocket and T247, but is still in an inactive configuration, because it lacks the K-E ion pair.

Another difference between the SPAK WT and SPAK T243D structures lies in the orientation of the N-termini of the activation loops, and in particular the αAL helix. αAL helices occur in diverse classes of kinases, e.g., EGF receptor (Zhang, Gureasko et al. 2006), and are known to be inhibitory by sterically blocking the inward movement of αC to form the K-E ion pair. Recent work has shown that deletion of the αAL helix in OSR1 leads to enhanced kinase activity(Li, Feng et al. 2014). Interestingly, the positions of SPAK WT and OSR1 WT αAL

helices are incompatible with the position of the SPAK T243D activation loop (Figure 2-4B). I compared the position of αAL using both N and C-terminal domain structural alignments, and found that the movement of αAL was partially independent of the gross movements of the N- and C-terminal domains (Figure 2-10A,B). Several hydrophobic interactions between αAL and αC, are lost in the SPAK T243D structure. In addition, αAL partially unfolds in SPAK T243D, and both αAL and αC exhibit higher B-factors (Figure 2-10C,D,E).

Recent work has shown that the small activating protein MO25, also known as Cab39 (calcium binding protein 39) potently activates SPAK and OSR1 even in the presence of phosphomimetic mutation of the activation loop (Filippi, de los Heros et al. 2011). Structures of MO25 in complex with the related MST kinases reveal that this occurs through stabilization of the K-E ion pair. Therefore, MO25 binding may be required for SPAK and OSR1 to attain fully active conformations (Mehellou, Alessi et al. 2013, Shi, Jiao et al. 2013).

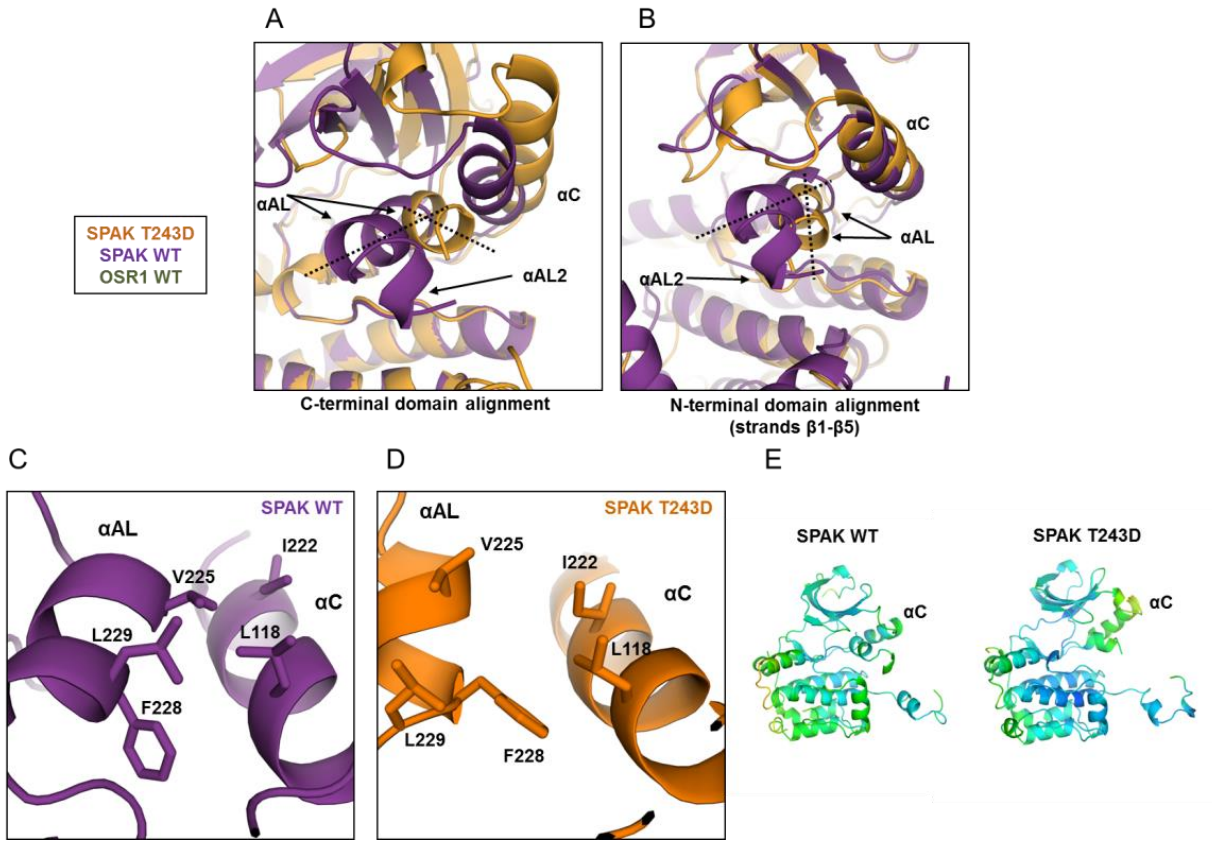

Figure 2-10. Conformational changes in helix αAL.

(A,B) View of helices αC, αAL, andαAL2 in structural alignments of SPAK WT and SPAK T243D using either C-terminal domain alignment (A) or N-terminal domain alignment (B). Dashed lines are used to compare the orientations of αAL in both structures for each alignment. (C,D) Hydrophobic interactions between helices αAL and αC in SPAK WT (A) and SPAK T243D (B). Interactions between αAL V225/L229 and αC I222/L118 are present in SPAK WT but lost in SPAK T243D. An interaction between αAL F228 and αC L118 is only present in SPAK T243D. (E) SPAK WT and SPAK T243D cartoon representation colored by B-factors (blue:lower and orange:higher. Higher B-factors indicate greater mobility in the crystal lattice. A larger increase in αC and αAL Bfactors, relative to the entire molecule, is observed in SPAK T243D.

Residues Permissive for Activation Loop Swapping

The exact N-terminal switch point for the swapping is within the disordered residues D234-T243. The C-terminus of the swapped region ends in the loop that connects helices αEF (short helix following activation loop) and αF (Figure 2-3C, Figure 2-8A). Several other protein kinases exhibit activation loop domain swapping. Ste20-like kinase (SLK), lymphocyte-originated kinase (LOK, also known as STK10), and OSR1 in the Ste group, and in the CaMK group, checkpoint kinase 2 (CHK2) and death-associated protein kinase 3 (DAPK3) show domain swapping (Manning, Whyte et al. 2002, Oliver, Paul et al. 2006, Pike, Rellos et al. 2008, Lee, Cobb et al. 2009). In each case the αE/F helices are intact but bound to the opposite subunit.

Yu-Chi Juang performed a structure-based multiple sequence alignment of SPAK and other kinases in the domain-swapped segment and showed that all the domain-swapped kinases contain either a glycine or a proline at the position corresponding to G261 in SPAK, while the non-swapped kinases (for example, PAK6 and TAO2) have leucine and glutamine instead (Figure 2-11A). Proline is frequently found in the hinge loops of domain-swapped proteins (Rousseau, Schymkowitz et al. 2003).

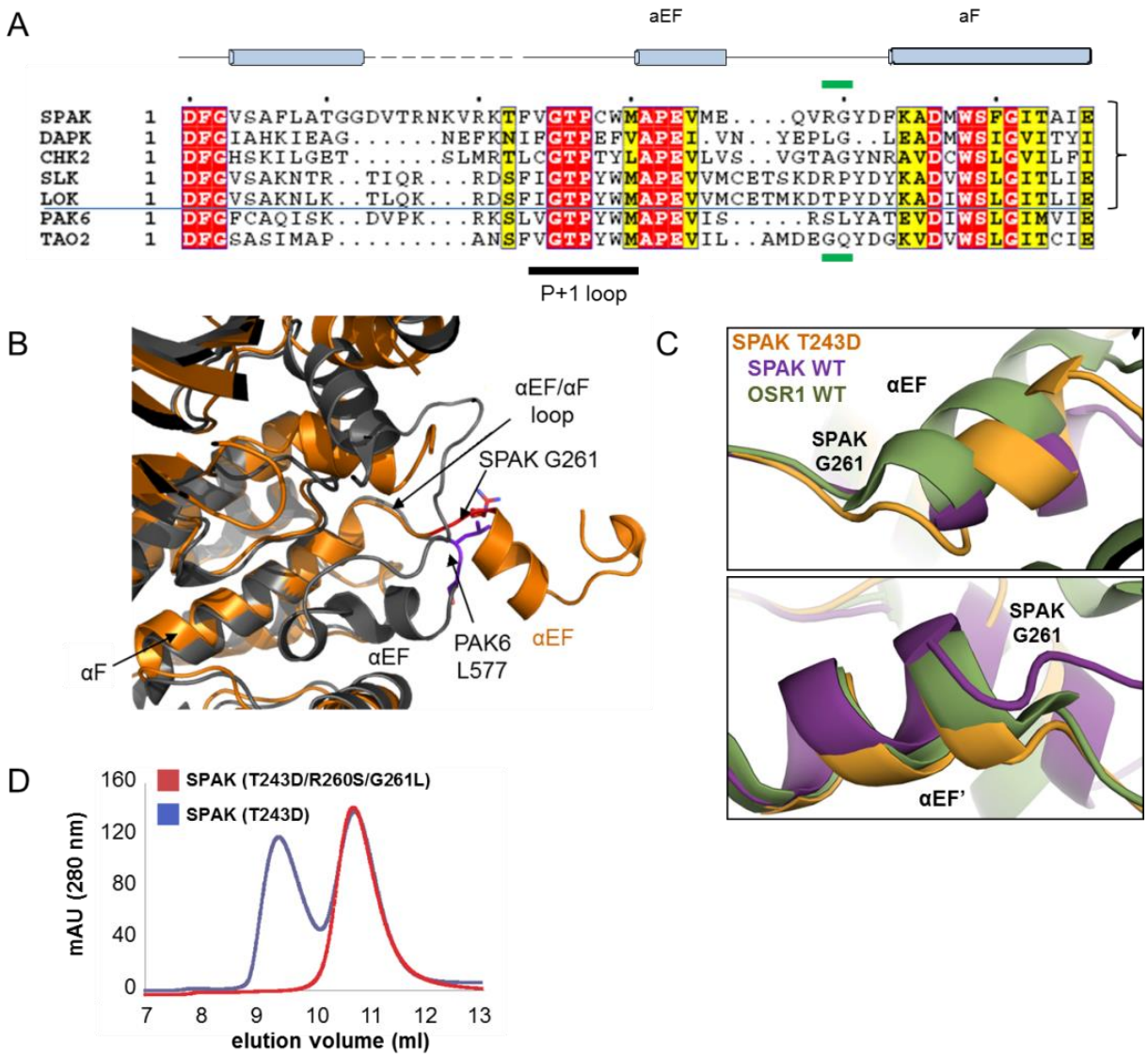

Figure 2-11. Identification and mutation of the domain-swap hinge.

(A) Multiple sequence alignment (Yu-Chi Juang) of representative sequences of domain swapped kinases SPAK, DAPK3, CHK2, SLK, LOK, compared to the non-swapped kinases PAK6 and TAO2. The position corresponding to G261 in SPAK is boxed in green. (B) Superposition of SPAK T243D and the non-swapped kinase PAK6 (PDB 2C30) reveals the difference in the αEF/αF loop. SPAK is colored in orange and PAK6 is in gray. The switch point R260/G261 in SPAK and S576/L577 in PAK6 are represented in sticks and colored in red and purple, respectively. (C) View near αEF and αEF' helices using chain A structural alignments of SPAK WT, SPAK T243D, and OSR1 WT dimers. Positional differences begin to occur near G261 and G261' (G203 in OSR1). (D) Gel filtration profile obtained by Yu-Chi Juang of SPAK T243D and SPAK (T243D/R260S/G261L).

Comparison of domain-swapped and non-swapped kinase structures reveals a major conformational difference in the αEF/αF loop in the backbone conformation between residues R260/G261 in SPAK and S576/L577 in PAK6 (Figure 2-11B). In particular, G261, in SPAK T243D, adopts a left-handed conformation with φ= 83° and ψ= 175°. Additionally, by aligning chain A of the SPAK WT, OSR1 WT, and SPAK T243D dimer structures, the positional differences begin to occur around SPAK G261, or OSR1 G203 (Figure 2-11C). Thus, Yu-Chi Juang suspected that G261 is part of the domain-swap hinge-point (Rousseau, Schymkowitz et al. 2003).

To investigate the role of G261 in activation loop swapping, Yu-Chi Juang mutated R260/G261 of SPAK to S/L as in PAK6. The Superdex75 gel filtration profile of SPAK 63-390 (T243D/R260S/G261L) suggests that it is primarily a monomer in solution, in contrast to SPAK T243D (Figure 2-11D). Thus, apparently R260 and G261 are part of the domain-swap hinge.

I then addressed the question of whether the monomer is active by comparing the activity of SPAK WT and dimerization-blocked mutant. The activity profile was studied in the context of constructs encompassing the entire PF1 domain (SPAK 63-403, and SPAK 63-403 R260S/G261L). In an *in vitro* kinase assay the SPAKs were first preactivated by phosphorylation by WNK1 for 30 min., and both were phosphorylated similarly (Figure 2-12A). The SPAK 63-403 R260S/G261L mutant had ~40% of the activity of SPAK WT towards the substrate GST-NKCC2 1-175 (Figure 2-12B). Data is also presented that SPAK exhibits a small amount of autophosphorylation, and WNK1 exhibits some phosphorylation activity towards GST-NKCC2 1-175 in the absence of SPAK. Similarly, SPAK T243E/R260S/G261L had ~40% activity of SPAK T243E (Figure 2-12C). However, the dimerization blocking mutation has no

effect on the basal activity of SPAK. Taken together we believe these results suggest that the monomeric form of SPAK can be activated by WNK1, and it has kinase activity.

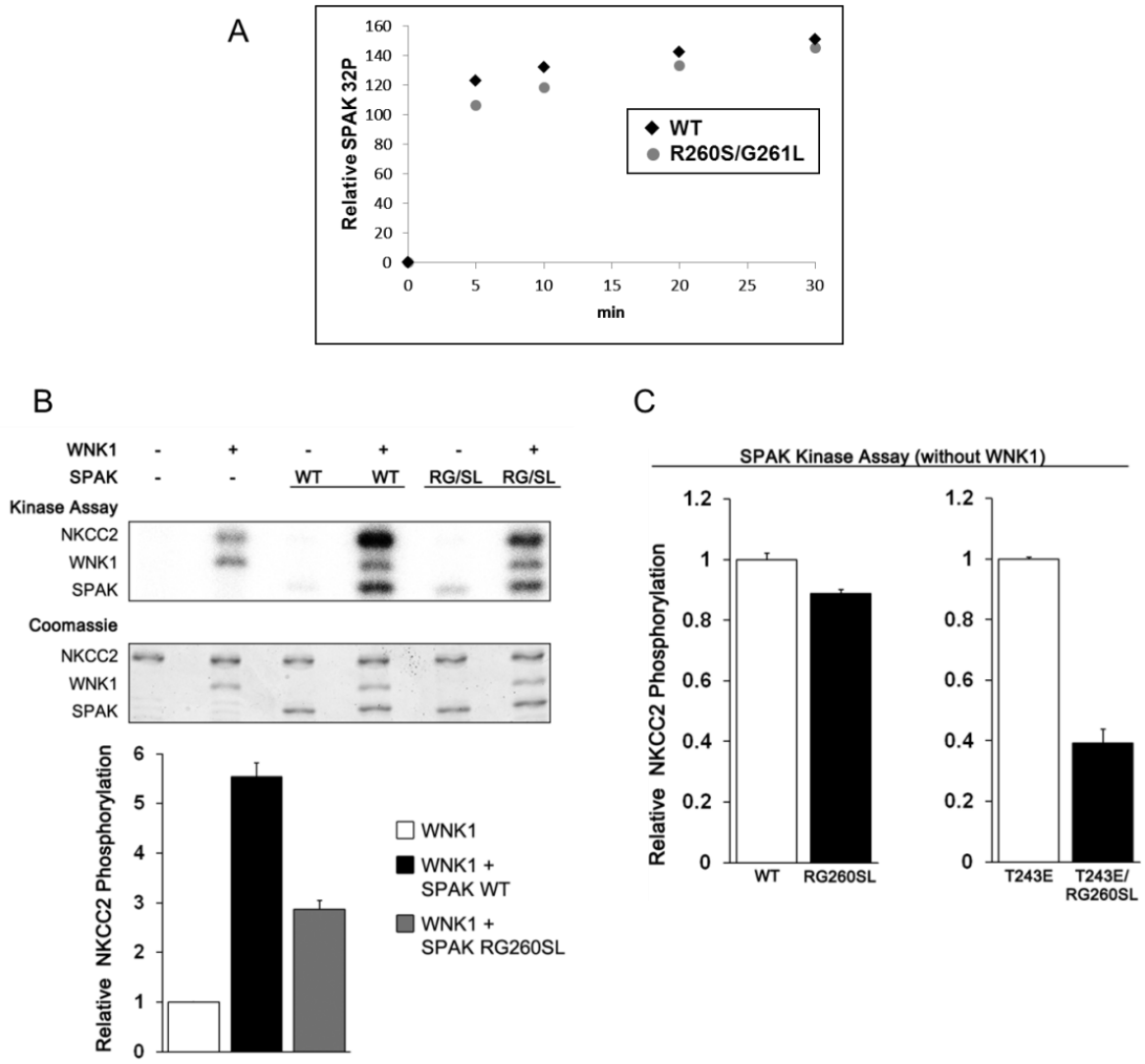

Figure 2-12. Effect of the R260S/G261L mutation on SPAK activity.

(A) Comparison of SPAK 63-403 WT and RG260SL phosphorylation by WNK1 kinase domain (B) Coupled protein kinase assay. SPAK 63-403 WT and R260S/G261L mutant were preincubated with ATP-MgCl2 for 30 minutes with or without WNK1, after which [γ-32P]-ATP was added for radiolabeling, and GST-NKCC2 1-175 was added as substrate. (C) Kinase assays comparing activity of SPAK 63-403 with and without the R260S/G261L mutation. T243E is an activating phosphomimetic mutation in the SPAK activation loop. All results in (B) and (C) are reported as relative activities, and as the mean and standard deviation of triplicate measurements quantified by phosphoimaging.

Discussion

Domain swapping of activation loops is not uncommon among protein kinases. SLK, lymphocyte-originated kinase (LOK, also known as STK10) and OSR1, in the STE group, and checkpoint kinase 2 (CHK2) and death-associated protein kinase (DAPK3), in the CAMK group, are examples of domain-swapped enzymes (Oliver, Paul et al. 2006, Pike, Rellos et al. 2008, Lee, Cobb et al. 2009). Several structures of domain-swapped kinases, some phosphorylated, have been reported. These structures vary considerably in conformation, with some having hallmarks of an active kinase, such as the essential K-E ion pair interaction between helix αC and strand β3, and others appearing inactive. These results show that domain swapping is not a reflection of the state of phosphorylation or activity of the kinase.

Here we report the domain-swapped structures of SPAK WT and SPAK T243D, which mimics the WNK activating phosphorylation site in the SPAK activation loop. SPAK WT adopts an inactive configuration very similar to the previously reported structure of OSR1 WT (Lee, Cobb et al. 2009). SPAK T243D, in contrast, has some features reminiscent of active kinases. Thus, we hypothesize that the present structures reflect two different activity states in a multistage activation process: activation loop phosphorylation, mimicked here with the T243D mutation, induces a partially active conformation that can be further activated. Possible interactions that could lead to a fully active structure are with substrates or with the known activator protein MO25 (Cab39). In support of the multistage activation concept, SPAK and OSR1 harboring the phosphomimetic mutation in the activation loop are still activated by nearly 100-fold in the presence of MO25 (Filippi, de los Heros et al. 2011). We also note that the SPAK T243D active site is much broader compared to SPAK WT and OSR1 WT due both to N-terminal domain rotation and outward movement of helix αAL. The more open SPAK T243D

active site could potentially be more accessible to substrate, but the precise function is unclear from the present study.

By comparing structures and sequences of domain-swapped and non-swapped kinases, we identified a switch point for domain swapping. By mutating switch point residues to ones incompatible with domain swapping, we were able to generate a monomeric mutant form of SPAK, and show that it can be phosphorylated by WNK1 and retains activity, albeit lower than the wild-type kinase. The dimerization blocking mutation should prove valuable in future studies aimed at understanding the role of SPAK and OSR1 domain swapping.

CHAPTER THREE

BINDING SPECIFICITY-BASED PREDICTION OF SPAK/OSR1 DOCKING INTERACTIONS

Abstract

SPAK and OSR1 kinases bind R-F-X-V/I linear sequence motifs through C-terminal protein interactions domains. It is well established that these interactions are required for proper activation by WNK kinases, deactivation by protein phosphatase 1, and phosphorylation of SLC12 cotransporter substrates, all of which are required for proper maintenance of cell volume and ionic composition. Although these interactions have been well characterized within the WNK pathway, little focus has been placed on how these interactions might mediate signaling outside of the canonical pathway. There are over 20,000 unique human proteins that contain approximately 1800 known instances of the sequence R-F-X-V/I. Therefore, I hypothesized that additional specificity determinants must be required to ensure that SPAK and OSR1 only interact with a subset of these potential motifs. Since these motif interactions occur in part through beta-strand addition, the geometric constraints imposed by multiple hydrogen bonds and a linear peptide- bound conformation might minimize the effects of amino acid substitution at one position on adjacent residues within the motif. Therefore, I investigated the effects of single amino acid substitutions by peptide arrays and validated some of the results by fluorescence polarization to generate a binding specificity profile. Affinity purification-mass spectrometry protein ID of pull-downs from HeLa cell lysates was also employed to validate and identify potential interaction partners. An immediate, unexpected result was the discovery of a variant of

the R-F-X-V/I motif, R-X-F-X-V/I. The specificity data was then used to score and rank all of the known motifs in the human proteome. Motifs were then excluded based on conservation, subcellular localization, and structure. All of the characterized interaction motifs clustered near the top of the ranked list and none were excluded, indicating this methodology was successful in identifying known and potentially new interaction partners. A subset of the inward rectifier potassium channels was predicted to interact, and initial experiments have indicated that OSR1 kinase activity can regulate the channels.

Experimental Procedures

Protein expression and purification. Both His_6- and GST-tagged SPAK and OSR1 CCT domains (OSR1432-527, SPAK 459-556) were expressed in RosettaII (DE3) *E.coli* (Novagen). Overnight starter cultures were grown at 30^o C and 180 rpm in the presence of 100 µg/mL ampicillin and 34 µg/mL chloramphenicol, such that they remained in log phase upon inoculation. 5 mL were used to inoculate 1 L of LB. Cells were grown at 37 °C in the presence of 100 µg/mL ampicillin and 34 µg/mL chloramphenicol until OD_{600} reached 0.8, and then grown at 150 rpm and 20^o C for 45 minutes. Cells were then induced with 0.4 mM IPTG and grown overnight. Cells were harvested and resuspended in 20 mL per liter culture 50 mM Tris-HCl, pH 8.0, 0.3 M NaCl, 5% glycerol, 1:1000 PI cocktail (in 62.5 mL of DMSO: 25 mg of pepstatin A, 25 mg of leupeptin, 250 mg of Nα-p-tosyl-L-arginine methyl ester, 250 mg of Nα-p-tosyl-L-lysine chloromethyl ketone hydrochloride, 250 mg of Nα-Benzoyl-L-arginine methyl ester, and 250 mg of soybean trypsin inhibitor), 400 µM PMSF, and reducing agent (2.5 mM BME for His_6 proteins and 5 mM DTT for GST proteins). Resuspended cells were then frozen

slowly at -20^{o} C to aid in lysis. Following freezing, the cells were thawed in a 37^{o} C water bath, 0.5% Triton-X, 400 µM PMSF, and 1 mg/mL lysozyme were added and mixed at 4^{o} C for 30 minutes followed by sonication. Following centrifugation the protocols for His_6- and GST-tagged proteins diverged.

His_6-tagged protein supernatants were applied to nickel-nitrilotriacetic acid-agarose (Ni^{2+}-NTA) with 1 mL bed volume per liter of culture. Beads were washed with 10 column volumes per wash in the following order: 2X with lysis buffer (50 mM Tris-HCl, pH 8.0, 0.3 M NaCl, 5% glycerol), 3X with lysis buffer with 20 mM imidazole, 1X with lysis buffer with 50 mM imidazole. Protein was eluted with lysis buffer with 250 mM imidazole (Figure 3-1A). The eluent was dialyzed overnight with 3K MWCO dialysis tubing in 25 mM Tris-HCl pH 7.75 (pH at room temp), 125 mM NaCl, 2 mM DTT, 1:1000 PMSF. Proteins for peptide arrays and fluorescence polarization were then subjected to gel filtration chromatography on a Superdex200 16/600 column with the same buffer excluding PMSF (Figure 3-1B). Peak 2 from gel filtration was used for experiments.

GST-tagged protein supernatants were applied to glutathione resin with 0.5 mL bed volume per liter of culture. Beads were washed 6X with 10 column volumes per wash lysis buffer with 5 mM DTT. Protein was eluted with lysis buffer with 20 mM glutathione pH 7. The eluent was dialyzed overnight with 10K MWCO dialysis tubing in 25 mM Tris-HCl pH 7.75 (pH at room temp), 125 mM NaCl, 2 mM DTT, 1:1000 PMSF. GST-tagged SPAK and OSR1 CCT domains consisted of a single band on Coomassie stained gel.

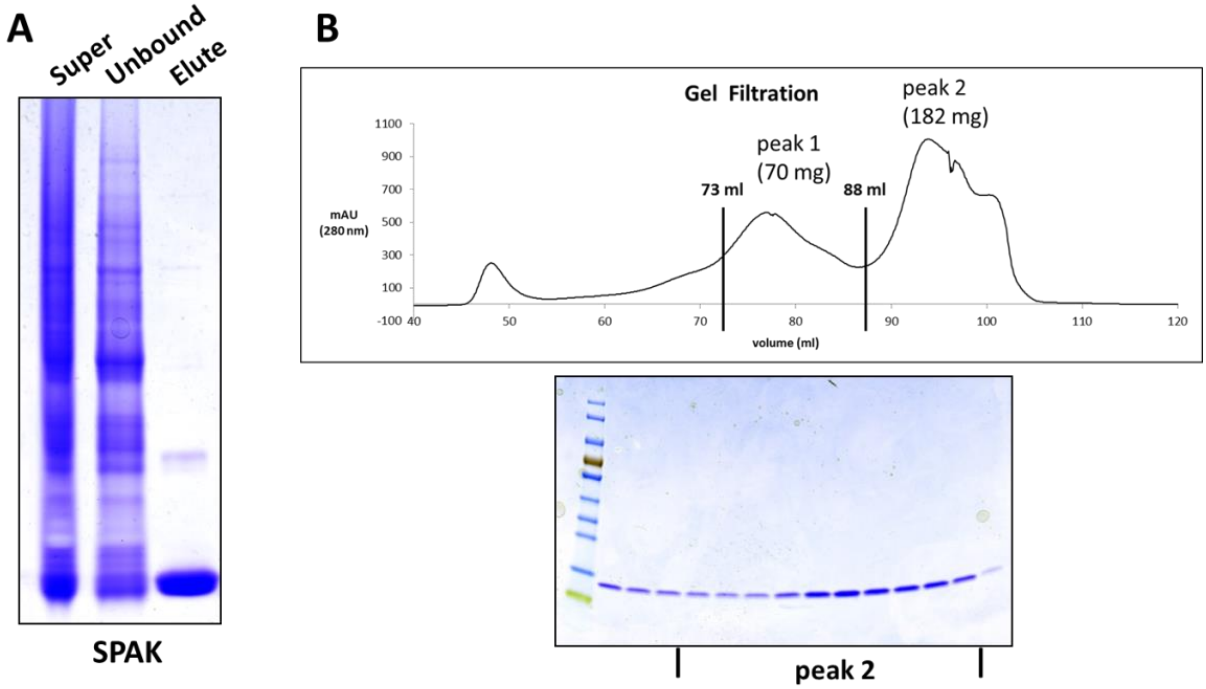

Figure 3-1. His_6-SPAK 459-556 (CCT domain) purification

(A) Ni-NTA purification results for His_6-SPAK CCT domain. (B) Superdex200 16/600 purification results for His_6-SPAK CCT domain. Peaks 1 and 2 were pooled and stored separately. Experiments were performed with peak 2 only. Similar results were obtained for His_6-OSR1 CCT domain. GST-tagged SPAK and OSR1 CCT domains consisted of a single band on Coomassie stained gel.

Peptide arrays. Peptide arrays were custom ordered (Kinexus). Spots were synthesized on a TOTD membrane and N-terminally acetylated. Binding and washing steps were adapted from a preexisting protocol (Briant, Murphy et al. 2009). All wash steps were with 20 ml and for 5 minutes. The membrane was briefly rinsed with ethanol followed by 2 washes with by ddH_2O and 2 washes with TBST (TBS with 0.1% Tween). The membrane was then incubated with 10 mL binding buffer (1:1 TBST to LiCor blocking buffer) for 1 hour at room temperature. This was followed by incubation with 6 mL of 100 µM His_6-SPAK or His_6-OSR1 CCT domain in binding buffer with addition of 1 mM DTT for 1 hour at room temperature. The membrane was

then washed twice with TBST followed by incubation for 15 minutes with 1:1000 mouse monoclonal anti-His_6 antibody (Santa Cruz) in binding buffer. The membrane was then washed twice with TBST followed by incubation for 15 minutes with 1:5000 IRDye 680 anti-mouse antibody. Following three washes the membrane was scanned on LiCor Odyssey imaging system. Spot intensities were quantified using LiCor Odyssey software.

AP-MS Protein ID. 2 mg of tagged SPAK or OSR1 CCT domain was incubated for 1 hour at 4^oC with either 200 µL of Ni-NTA or glutathione agarose. Beads were then washed and incubated for 1 hour with HeLa cell lysates. Following three washes the beads were resuspended in SDS-PAGE loading buffer and boiled. Samples were then run on a gel and submitted for analysis according to the UT Southwestern Proteomics Core Facility guidelines.

Fluorescence anisotropy competition. 3 µM His_6-OSR1 CCT, 100 nM NLVGRF(dap-FAM)VSPVPE peptide probe were combined in binding buffer (25 mM Tris-HCl pH 7.75, 125 mM NaCl, 1 mM DTT). 10 mM stock solutions of peptides (United Biosystems) were then added to a final volume of 200 µL and serially diluted two-fold with binding buffer such that each sample contained 100 µL. 80 µL was then loaded onto a Nunc black 384 well flat bottom plate. Measurements were made on a Synergy BioTek H1 Multimode plate reader using a filter cube designed to measure polarization of fluorescein. Data were analyzed and graphically displayed in GraphPad Prism using a one site K_i binding competition model.

Bioinformatics. Peptide array data were converted to a position-specific scoring matrix and submitted to the Scansite server (scansite3.mit.edu) (Obenauer, Cantley et al. 2003). Search parameters were set to search only *Homo sapiens* in the Uniprot database (Uniprot-Consortium 2015). Outputs were converted to Excel for list maintenance. Proteins were first excluded based

on subcellular localization by comparing to annotations within the Uniprot database. If motifs were not cytosolic, nuclear, or cytosolic facing within membrane proteins, then they were excluded. Proteins were then excluded based on conservation. Uniprot accession numbers were used to search and align to related sequences in the species *Mus musculus, Xenopus laevis,* and *Drosophila melanogaster* using NCBI BLAST(blast.ncbi.nlm.nih.gov/Blast.cgi) (Altschul, Gish et al. 1990). If they were not at least conserved in *Mus musculus*, then they were excluded. Finally, remaining proteins were excluded based on motif solvent accessibility. Uniprot accession numbers were used to search and align to related sequences found in the Protein Data Bank using NCBI BLAST. The result with the highest sequence identity (preferably the protein of interest) or at least a sequence identity of 30% was chosen for comparison (Wilson, Kreychman et al. 2000). The position in the structure that corresponds to the aligned motif in the sequence was analyzed for solvent accessibility. If the protein is part of a complex, then only the chain with the motif or homologous site was analyzed for solvent accessibility. Several criteria were used for exclusion. First, if the motif was part of an α-helix unless at the terminus with at least either R or V/I of the R-F-X-V/I or R-X-F-X-V/I outside of the helix it was excluded. Second, if the motif was part of a β-strand, then it must be part of a terminal β-strand or it was excluded. Third, if the motif was buried within a folded domain or by at least two secondary structure elements it was excluded. If no protein structure with at least 30% sequence identity existed, then the protein was not excluded, but instead if the NCBI BLAST Conserved Domains output indicated the presence of a domain present in the location of the motif that was recorded.

Results

SPAK/OSR1 CCT Domain Specificity Requires Residues Outside the Core Motif

The crystal structure of the OSR1 CCT domain indicates that R-F-X-V/I motifs interact with OSR1and SPAK CCT domains through β-strand addition. The peptide motif binds in an extended conformation where the peptide backbone makes multiple hydrogen bonds with the β2 strand of the CCT domain (Figure 1-8) (Remaut and Waksman 2006, Villa, Goebel et al. 2007). This suggests that probing binding specificity through the use of single amino acid substitutions would be amenable since substitutions at one position would be less likely to affect the orientation of surrounding residues. I used peptide arrays to probe the effects of single amino acid substitutions in and around the core R-F-X-V/I motif of the human WNK4 sequence $_{1012}$QLVGRFQVTSSKE$_{1024}$, and the mutant sequence QLVARFQVTSSKE, to SPAK and OSR1 His_6-tagged CCT domains (Figure 3-2A) (Briant, Murphy et al. 2009, Li and Wu 2009). The motif numbering convention used throughout this text is indicated.

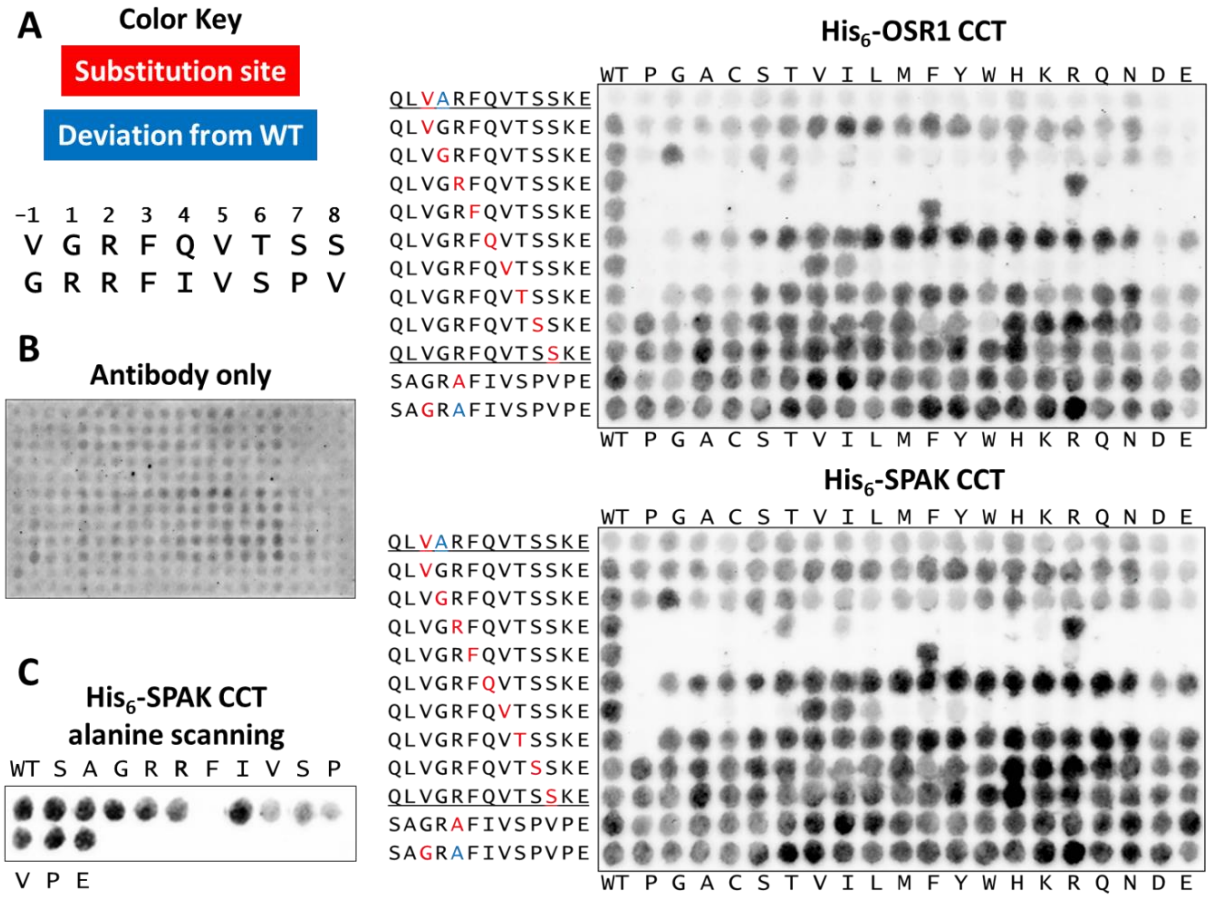

Figure 3-2. Peptide array analysis of SPAK/OSR1 CCT domain binding specificity.

(A) Binding specificity of His_6-SPAK and His_6-OSR1 CCT domains determined by blotting for His_6-tag and visualized by LiCor. Red letters represent the residue within the peptide that is being substituted, and each column represents the residue that is being substituted in place at that position. Blue letters represent an additional mutation within the wild type sequence that is held constant while the position indicated by a red letter is substituted. Positional numbering notation for the motif is also indicated. (B) Control blot with primary and secondary antibody only. (C) Alanine scanning mutagenesis of WNK1 sequence SAGRRFIVSPVPE. Mutation of either arginine does not disrupt binding.

Each residue in and around the motif was substituted to every other amino acid. The mutant sequence was used to probe the effects of substitutions at V1014 in the presence of the mutation G1015A since glycine is inherently more flexible than alanine. In addition, during my initial peptide array experiments performing only alanine scanning mutagenesis on the hWNK4

motif and the hWNK1 motif $_{1505}$SAGRRFIVSPVPE$_{1517}$ my results showed that mutation of R1509 to alanine in the hWNK1 sequence did not prevent interaction suggesting that R-X-F-X-V/I was also a viable motif for CCT domain interaction (Figure 3-2C). Therefore, the effects of substitutions at R1509, and also G1507 in the presence of the mutation R1509A, were also examined (Figure 3-2A)

The array results for SPAK and OSR1 CCT domains are remarkably similar, but some minor differences are present that could further define unique specificities for the two kinases. However, additional work beyond the scope of the present study would be required to fully understand these differences. In the case of the wild type hWNK4 sequence clear preferences for R, F, and V/I at the 2, 3, and 5 positions were observed, with a preference for V over I at the 5 position. T at position 2 also appeared to be tolerated, but was later confirmed to be a false positive, as will be discussed later in the text (Figure 3-3). Preferences for specific residues at all of the other positions tested were also observed for both the wild type and mutant hWNK4 and hWNK1 peptides. These results clearly demonstrate that binding specificity is not only determined by the core R-F-X-V/I and R-X-F-X-V/I motifs, but also by flanking residues.

Although peptide arrays are a powerful tool for probing specificity, they are prone to false positives due to impurities in the peptides and non-specific binding. Therefore, fluorescence anisotropy was used to further validate the results, and provide quantitative binding constant information on the effects of the substitutions at specific positions within the motif sequences for the His_6-OSR1 CCT domain (Figure 3-3).

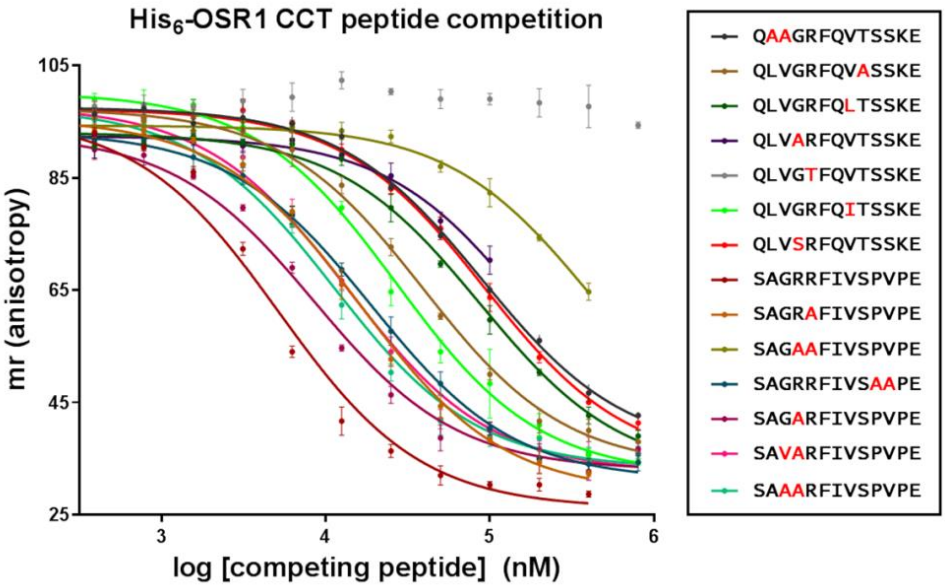

Sequence (red: mutation)	K_i +/- Std. Dev. (µM)
QLVGRF(dap-FITC)VTSSKE (wt probe)	K_D = 3.8
NLVGRF(dap-FAM)SPVPE (comp. probe)	K_D = 1.6
QAAGRFQVTSSKE	88.4 +/- 5.1
QLVGRFQVASSKE	38.4 +/- 2.1
QLVGRFQLTSSKE	85.5 +/- 5.4
QLVARFQVTSSKE	174.5 +/- 108.6
QLVGTFQVTSSKE	No binding
QLVGRFQITSSKE	26.7 +/- 1.9
QLVSRFQVTSSKE	90.8 +/- 5.2
SAGRRFIVSPVPE (wt)	≤ 5.1 +/- 0.4
SAGRAFIVSPVPE	16.1 +/- 0.8
SAGAAFIVSPVPE	407.8 +/- 72.8
SAGRRFIVSAAPE	18.8 +/- 0.8
SAGARFIVSPVPE	8.4 +/- 0.6
SAVARFIVSPVPE	13.4 +/- 0.9
SAAARFIVSPVPE	11.1 +/- 0.8

Figure 3-3. Effects of amino acid substitution on binding constants for His_6-OSR1 CCT.

Unlabeled peptides with amino acid substitutions (red letters) were used to compete for binding with labeled peptide probe (comp. probe) in order to determine inhibitory constants (K_i). Peptide 'SAGRRFIVSPVPE (wt)' likely has a K_i that is lower than the calculated value due to limitations in measuring peptide affinities where the K_i is lower than the K_D of the probe used in the experiment.

Perhaps the most striking result that came from this analysis was the fact that the peptide SAGRAFIVSPVPE had a K_i of 16.1 µM, which verifies that R-X-F-X-V/I is a viable alternative motif that can be utilized to bind CCT domains. Also not expected was the finding that replacement of G with A at position 1 of the hWNK4 peptide nearly abolished binding. However, in the case of the hWNK1 peptide replacement of G with A at position 1 only resulted in a modest decrease in affinity. To test whether this difference was due to the absence or presence of a bulkier, less flexible sidechain, the residues G-R at the -1 and 1 positions in the hWNK1 peptide were replaced with V-A, but this only led to a modest decrease in affinity as well. This result suggests that either the -2 position may need to be a bulky sidechain to prevent binding in the presence of a non-glycine residue at position 1, or that the peptide binds in a slightly different orientation overall. Other substitutions significantly impacted binding, and in some cases affinity decreased by over an order of magnitude, further supporting the finding that residues outside the core motifs further define specificity for the SPAK and OSR1 CCT domains.

A Methodology to Predict SPAK/OSR1 CCT Domain Interactions

Peptide arrays are useful in providing quantitative information for both positive and negative effects on interactions, and more so when combined with binding constant data that helps to validate and further define binding specificity. The results of the OSR1 CCT peptide array spot intensities were translated into position-specific scoring matrices (PSSM). Three matrices were created depending on the identity of the residues at positions 1 and 2 of the motif. The three matrices were (positions 1-3) G-R-F, R-X-F, and $X_{\text{-gly}}$-R-F where $X_{\text{-gly}}$ corresponds to any amino acid except glycine. The three separate sets of spot intensities for positions -1 through

2 were applied to each corresponding set and the common data for positions 3 through 8 were applied to all sets. R and F in each set were weighted at 100 percent, while V and I were weighted according to the fluorescence anisotropy data. All remaining weights came from the peptide array data

The individual PSSMs for the OSR1 CCT were then uploaded to the Scansite3 server (scansite3.mit.edu) and all known motifs found within the Uniprot database under *Home sapiens* were compiled and ranked by the server (Obenauer, Cantley et al. 2003, Uniprot-Consortium 2015). From all three searches the server found and ranked 3,673 motif matches: 149 for G-R-F, 1,976 for R-X-F, and 1,548 for X_{-gly}-R-F. In order to try to exclude false positives a filtering scheme was implemented (Figure 3-4). Potential motifs were filtered based on subcellular localization, conservation, and solvent accessibility. Full details on the filtering methodology can be found in Experimental Procedures.

OSR1 CTT Domain Motif Prediction and Filtering Methodology Analysis

Since motifs were only previously identified for the G-R-F and X_{-gly}-R-F classes there is no way to analyze the results of the R-X-F motif prediction. All of the known motifs for the X_{-gly}-R-F search clustered within the top ~10% of ranked list, except for a single outlier that was ranked at 16%. For the G-R-F search, except for two outliers, the remaining known motifs all clustered within the top ~15% of the ranked list, while the two outliers were ranked at ~40%. The highest ranked results of the G-R-F ranking and filtering are found in Table 3-1 as an example to illustrate that most of the known motifs cluster at the very top of the list, and none of the previously characterized motifs were excluded.

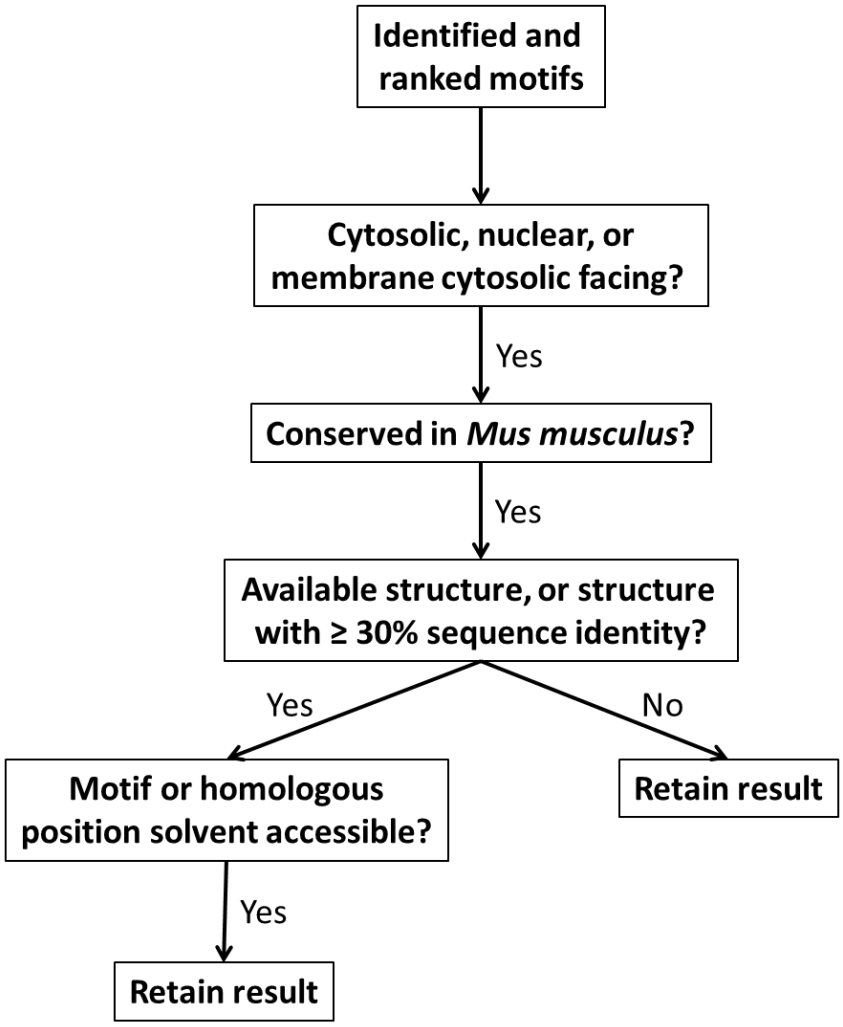

Figure 3-4. Scheme for filtering predicted SPAK/OSR1 CCT binding motifs.

In order to rule out false positives, identified motifs were excluded on the basis of localization, conservation, and motif solvent accessibility according to the following flowchart.

Rank	Protein Annotations	Site	Sequence	Accession	Identifier
1	Heat shock protein 105 kDa	F462	PEAKIGRfVVQNVSA	HS105_HU	Q92598
2	RELT-like protein 1	F228	TVLSVGRfRVTKVEH	RELL1_HU	Q8IUW5
3	RELT-like protein 2	F169	TVFSVGRfRVTHIEK	RELL2_HU	Q8NC24
4	Serine/threonine-protein kinase WNK1	F1946	QPTKVGRfQVTTTAN	WNK1_HU	Q9H4A3
5	Full=Tumor necrosis factor receptor superfamily member 19L	F350	TILSVGRfRVARIPE	TR19L_HU	Q969Z4
6	Solute carrier family 22 member 12	F16	LVGGLGRfQVLQTMA	S22AC_HU	Q96S37
7	Serine/threonine-protein kinase WNK1	F1958	TANKVGRfSVSKTED	WNK1_HU	Q9H4A3
8	Serine/threonine-protein kinase WNK4	F1017	KPQLVGRfQVTSSKE	WNK4_HU	Q96J92
9	Serine/threonine-protein kinase WNK1	F1860	GVFKMGRfQVSVAAD	WNK1_HU	Q9H4A3
10	Serine/threonine-protein kinase WNK2	F1785	PAKTVGRfSVVSTQD	WNK2_HU	Q9Y3S1
11	Endonuclease/exonuclease/phosphatase family domain-containing protein 1	F391	PSPYLGRfKVGSHDL	EEPD1_HU	Q7L9B9
12	TBC domain-containing protein kinase-like protein	F42	SIKILGRfQILKTIT	TBCK_HUM	Q8TEA7
13	Serine/threonine-protein kinase WNK3	F1337	GSFQRGRfQVITIPQ	WNK3_HU	Q9BYP7
14	Alkaline ceramidase 2	F125	FRNDRGRfKVVVSVL	ACER2_HU	Q5QJU3
15	Solute carrier family 22 member 13	F17	EIGDFGRfQIQLLIL	S22AD_HU	Q9Y226
16	Acetylcholine receptor subunit epsilon	F307	SVPLLGRfLIFVMVV	ACHE_HU	Q04844
17	Tyrosine-protein phosphatase non-receptor type 21	F1026	NTVTYGRfKITTRFR	PTN21_HU	Q16825
18	40S ribosomal protein S4	F109	IYDTKGRfAVHRITP	RS4X_HUM	P62701
19	40S ribosomal protein S4	F109	VYDTKGRfAVHRITV	RS4Y1_HU	P22090
20	Obscurin	F7683	TQIQRGRfSVVRQCW	OBSCN_HU	Q5VST9
21	Protein disulfide-isomerase-like protein of the testis	F215	IGNVIGRfHVTLDSV	PDILT_HU	Q8N807
22	Solute carrier family 22 member 25	F16	QVGGLGRfQILQMVF	S22AP_HU	Q6T423
23	Thioredoxin-related transmembrane protein 4	F103	EPGLSGRfFVTTLPA	TMX4_HU	Q9H1E5
24	Sortilin	F787	KYVCGGRfLVHRYSV	SORT_HUM	O99523
25	Ig heavy chain V-III region LAY	F68	ADSVNGRfTISRNDS	HV314_HU	P01775
26	Ig heavy chain V-III region POM	F68	ADSVNGRfTISRNDS	HV313_HU	P01774
27	Ig heavy chain V-III region NIE	F68	ADSVNGRfTISRNDS	HV309_HU	P01770
28	Ig heavy chain V-III region JON	F68	ANSVNGRfTISRNDS	HV319_HU	P01780
29	Ig heavy chain V-III region WAS	F68	ADTVNGRfTISRNDS	HV315_HU	P01776
30	Ig heavy chain V-III region WEA	F68	ADSVKGRfTISRNBS	HV302_HU	P01763
31	Ig heavy chain V-III region BRO	F67	ADSVKGRfTISRNDS	HV305_HU	P01766
32	Collagen alpha-5(VI) chain	F1918	GFDNTGTfQVIPVPP	CO6A5_HU	A8TX70
33	Solute carrier family 2, facilitated glucose transporter member 4	F143	EMLILGRfLIGAYSG	GTR4_HUM	P14672
34	Disintegrin and metalloproteinase domain-containing protein 30	F276	LAEVLGRfVIYKKSV	ADA30_HU	Q9UKF2
35	Bardet-Biedl syndrome 5 protein	F180	DQGNLGTfFITNVRI	BBS5_HUM	Q8N3I7
36	TBC1 domain family member 4	F364	MLFQVGRfEINLISP	TBCD4_HU	O60343
37	43 kDa receptor-associated protein of the synapse	F43	SSDLMGRfRVLGCLV	RAPSN_HU	Q13702
38	Plasma membrane calcium-transporting ATPase 1	F1017	CTIVLGTfVVQIIIV	AT2B1_HU	P20020
39	Thrombospondin-3	F804	SYQDSGRfYVVMWKQ	TSP3_HUM	P49746
40	Solute carrier family 12 member 2	F139	SEEAKGRfRVNFVDP	S12A2_HU	P55011
41	UPF0672 protein CXorf36	F244	YLGSCGRfLVSTSTR	CX036_HU	Q9H7Y0
42	Gelsolin	F679	CSNKIGRfVIEEVPG	GELS_HUM	P06396

Table 3-1. Ranked and filtered list of the G-R-F class motif search for the OSR1 CCT domain.

The top ranked 42 out of 149 sites identified for the G-R-F class motif search for the OSR1 CCT domain are indicated. Brown shading indicates known interactions. Grey shading indicates the motif was excluded based on the criteria in Figure 3-4. Unshaded indicates previously unidentified motifs that were not excluded. Similar results were observed for the $X_{\text{-gly}}$-R-F class search (data not shown). None of the previously characterized motifs were excluded.

In order to validate my analysis and potentially discover other novel CCT domain interaction partners I performed affinity purification-mass spec protein ID (AP-MS) with the assistance of Svetlana Earnest. GST-tagged SPAK and OSR1 CCT domains and GST were used as bait to pull down proteins from HeLa cell lysates. The samples were then run on a gel and mass spectrometry was performed by the UT Southwestern Proteomics Core facility. Only a small number of interaction partners were determined (Figure 3-5). The low number of interactions was expected since my fluorescence anisotropy data suggested that most interactions would be in the range of low to mid micromolar affinity. The proteins identified by AP-MS were then cross-referenced with the ranked lists (not filtered) for the three classes of motif searches to determine if they were also present. The top five AP-MS hits all had predicted motifs that were ranked near the top of the lists, and this included several from the R-X-F class of motif. The remaining hits either did not have a predicted motif or the motif was ranked relatively poorly, which could either indicate that the ranking generated some false negatives or that due to the large number of predicted motifs some AP-MS contaminants had predicted motifs by chance.

Uniprot identifier / Protein name	Normalized spectral counts				Highest motif ranking		
	GST-OSR1 1	GST-OSR1 2	GST 1	GST 2	G-R-F out of 149	X_{-gly}-R-F out of 1548	R-X-F out of 1976
ACACA_HUMAN Acetyl-CoA carboxylase 1	74	76				243	433
F5GWT4_HUMAN Serine/threonine-protein kinase WNK1	24	19	1	2	4	46	80
S12A2_HUMAN Solute carrier family 12 member 2	22	20			22	93	
PTRF_HUMAN Polymerase I and transcript release factor	20	23					15
S12A7_HUMAN Solute carrier family 12 member 7	16	16					70
EF2_HUMAN Elongation factor 2	14	8	4	2		1017	
VDAC1_HUMAN Voltage-dependent anion-selective channel protein 1	11	8	2			1038	
CAV1_HUMAN Caveolin-1	8	7					
BASP1_HUMAN Brain acid soluble protein 1	8	5	2	1			
CLH1_HUMAN Clathrin heavy chain 1	7	10	2				789
NUCL_HUMAN Nucleolin	7	4	1				
PRDBP_HUMAN Protein kinase C delta-binding protein	6	4					
TCPB_HUMAN T-complex protein 1 subunit beta	5	7	1	1			

Figure 3-5. Comparison of OSR1 CCT domain interactions identified by AP-MS to motif predictions and rankings.

GST-tagged OSR1 CCT domain and GST only (control) were used to pull down proteins from HeLa cell lysates. Proteins with spectral counts ≥ 4 and GST-OSR1 CCT/GST spectral counts ≥ 3 were considered hits. AP-MS hits were cross-referenced against the three motif class ranked lists (not filtered) and the highest ranking for that motif class is indicated if one was present.

Validation of the Predicted Interaction Between OSR1 and the Inward Rectifier K^+ Channel Kir 2.1

One of the most immediately interesting predictions that came from my analysis was the identification of 8 of 16 inward rectifier potassium (IRK) channels as having R-X-F class motifs. All 8 of the channels were ranked within the top 2% of the R-X-F list. A channel within this family, although not identified as having an interaction motif in this analysis, is ROMK. ROMK has been shown to be regulated by WNK1 (Lazrak, Liu et al. 2006, Liu, Wang et al. 2009). This further suggests that this family of channels may be regulated by the WNK pathway, although potentially by different mechanisms, since ROMK does not have a predicted motif.

IRK channels, also designated by the naming system KirX.Y, where X refers to their functional grouping and Y refers to the specific member, help mediate potassium flux across cell membranes of many different cell types (Cheng, Sung et al. 2015). In mammalian cells the channels allow more potassium into the cell when open, but under resting membrane potential are generally closed and mediate primarily outward flux of potassium. The channels are active as tetramers, and are generally considered to be constitutive tetramers (Pegan, Arrabit et al. 2005, Tao, Avalos et al. 2009).

In order to determine whether this prediction was physiologically relevant I began a collaboration with the lab of Dr. Chou-Long Huang, whose lab has focused on the regulation of ROMK by the WNK pathway. His lab was set up to immediately begin testing the effects of OSR1 expression and activity on the channel Kir2.1. The crystal structure of the tetramer of the cytoplasmic regulatory domains of the Kir2.1 channel indicates that the motif is buried in the interface between domains, and not solvent accessible in the Kir 2.1 tetramer (Figure 3-6A,B). However, my filtering methodology only takes into account solvent accessibility of the motif as it is in the specific chain of the crystal structure within which it is located. Kir2.1 channel current was found to be increased significantly in the presence of OSR1 kinase activity. Inactive OSR1 had no effect on channel current, but constitutively active OSR1 T185E/S325E and OSR1 in the presence of activating kinase WNIK1 both increased channel activity. These results suggest that in this case my motif ranking and filtering methodology was successful in identifying a new substrate for OSR1. The results also imply that the entire subset of IRK channels with the R-X-F motif type may also be regulated by OSR1, and likely SPAK.

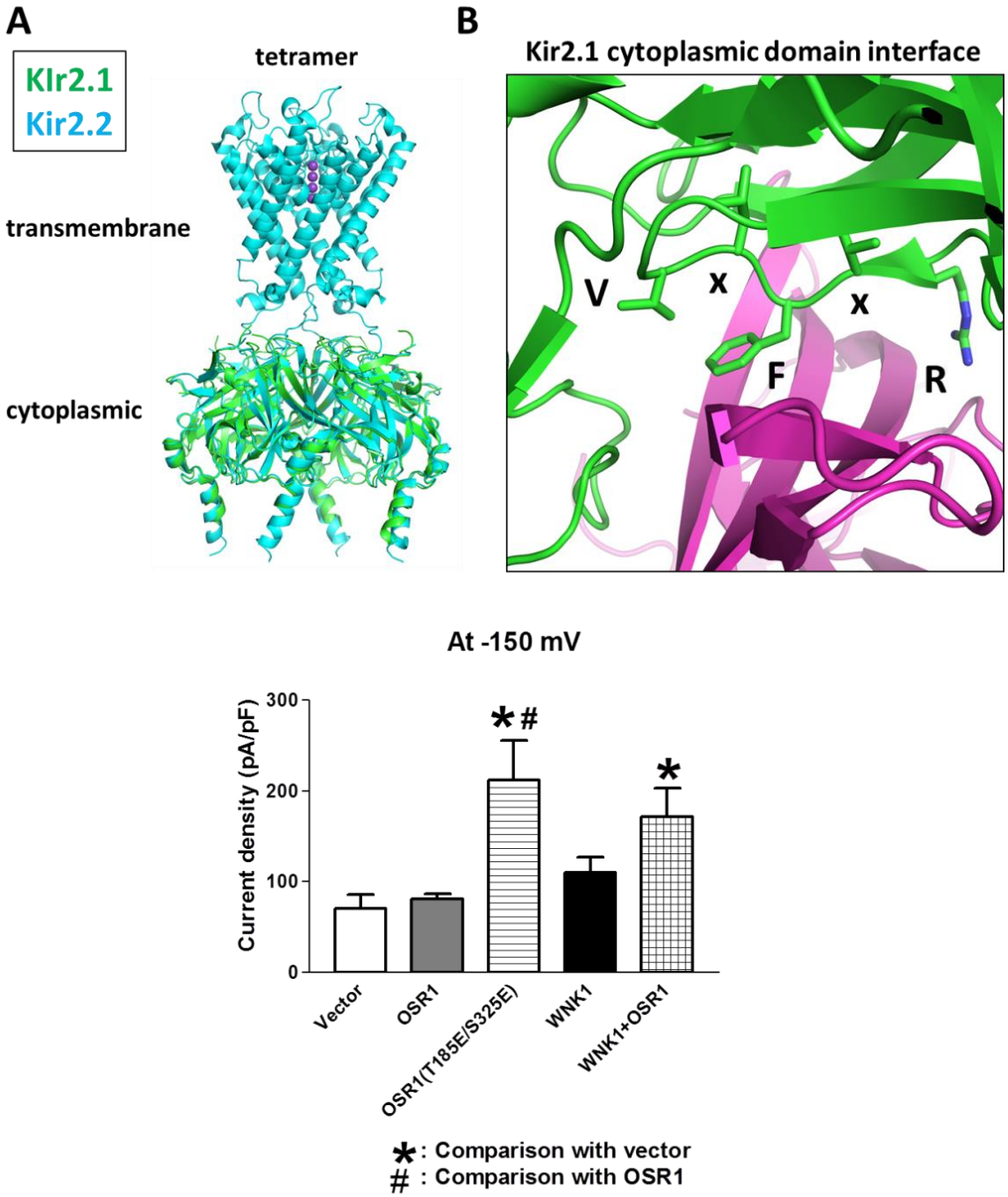

Figure 3-6. Kir2.1 channel current is dependent on OSR1 kinase activity.

(A) Alignments of the crystal structures of the Kir2.1 cytoplasmic regulatory domain tetramer (PDB 1U4F) and the full-length Kir 2.2 tetramer (PDB 3JYC) indicates the regulatory domains both adopt the same tetrameric configuration. (B) The R-X-F-X-V motif in Kir2.1 and the other IRKs with the motif is located at the cytoplasmic domain interface. (C) In collaboration with Chou-Long Haung's lab we determined that OSR1 kinase activity enhanced flux through the Kir2.1 channel.

Discussion

As a result of my work on this project I have shown that SPAK and OSR1 CCT domains utilize interactions outside of the core interaction motif in order to achieve additional binding specificity. Interactions are likely to occur with only small subsets of the approximately 1,800 R-F-X-V/I motifs, and 2,000 of the newly defined R-X-F-X-V/I motifs described in this work. In addition, I developed a methodology to filter out predicted interactions based on localization, conservation, and solvent accessibility. Although I developed this methodology independently, similar methodologies have been implemented in recent years to predict interaction partners with protein interaction domains, such as SH3 domains (Jain and Bader 2016). These filtering methods have proven to be powerful tools to decrease the false-positive rate of traditional experiments utilizing binding specificity data alone (Teyra, Sidhu et al. 2012). A unique feature of the filtering method I have developed is the utilization of homologous structural data, rather than structural data of the protein identified as containing the motif combined with intrinsically disordered region prediction (Teyra, Sidhu et al. 2012, Jain and Bader 2016).

Through identifying and ranking potential SPAK/OSR1 CCT domain binding motif interactions based on the identity of the residues at the 1 and 2 positions (Figure 3-2) followed by application of the filtering method I developed, I determined that all of the known CCT domain interaction partners were clustered near the top of the ranked lists. In addition, none of the known interactions were filtered out as false positives.

Other studies have also attempted to define CCT domain binding specificity and predict interactions. A study by Gagnon and Delpire utilized preexisting information about known SPAK/OSR1 interactions to perform a genome-wide scan for additional motifs (Delpire and

Gagnon 2007). Although informative, their analysis only used sequence alignment information for residues at positions 1 through 3, 5, and 8 with no weighting based on residue identity, and so a list was obtained but not with ranking information. Their results were also likely biased due to the limited sequence information used in the anlysis. More recently, *in silico* analysis of CCT domain binding specificity by Delpire's group suggested, among other things, that histidine could replace arginine at position 2 and tyrosine could replace phenylalanine at position 3, and these results were validated by yeast two-hybrid (Austin, Nannemann et al. 2014). However, my results directly contradict these findings and suggest that the validation of interaction predictions may reflect interactions that are strong enough to be captured by yeast two-hybrid under their experimental setup, but likely not physiologically relevant.

Initial experiments aimed at validating some of the predicted interactions have shown that OSR1 kinase activity regulates flux through the IRK channel, Kir2.1. Since 8 channels within this family of 16 contain similar motifs, all with diverse physiological functions (Cheng, Sung et al. 2015), my findings have the potential to significantly expand the role of the WNK signaling pathway in the regulation of ion flux and cell volume regulation. However, this interaction was only the first to be tested, and it is likely that my findings have the potential to define new relationships between the WNK pathway and other signaling pathways and cellular processes.

CHAPTER FOUR

STRUCTURAL AND FUNCTIONAL CHARACTERIZATION OF THE ERK2 E322K MUTATION

Abstract

ERK2 E322K (rat ERK2 E320K) is the most enriched somatic missense mutation in the MAPK1 gene. The mutation introduces a buried charge reversal at the ERK2 common docking site that is required for proper interaction with multiple signaling partners, including activating MEK1/2, deactivating DUSP6, and substrates. I solved the crystal structure and found that the charge reversal in ERK2 E320K causes substantial disorder in the common docking site, and this was shown to translate to near complete loss of interaction with KIMs. However, the mutation also causes structural changes at sites distal to the mutation, such as activation loop conformation, and likely enhances interdomain mobility. The structure also suggested that the function of additional sites of protein-protein interactions might be affected and I confirmed this to be the case. Kevin Cormier also determined that ERK2 E320K is activated by MEK1 indistinguishably from wild type protein, and can be slowly inactivated by DUSP6 but fails to activate the phosphatase towards other substrates. This decreased ability of ERK2 E320K to be dephosphorylated translates to enhanced activation, and ultimately increased nuclear accumulation of active ppERK2 E320K, and enhanced transcription factor phosphorylation. This implies that although the E320K mutation prevents interaction with KIM-containing substrates both the enhanced activation and nuclear signaling likely contribute to the enrichment of the E322K mutation in human cancers.

Experimental Procedures

X-ray Crystallography. Crystals were obtained by Lisa Ko using hanging drop vapor diffusion. 165 μM ERK2 E320K in 25 mM Tris-Cl, pH 7.5, 100 mM NaCl, 1 mM EDTA, 5 mM DTT was mixed with an equal volume of reservoir solution containing 28% (w/v) PEG1500, 100 mM Tris-Cl, pH 8.0. Crystals were incubated at 20º C, and harvested at one week. Diffraction data were collected at beamline 19-ID at the Advanced Photon Source (Argonne National Laboratory, Argonne, IL). Data were indexed, integrated, and scaled in HKL3000 (Otwinowski and Minor 1997). The structure of ERK2 E320K was determined using molecular replacement in PHASER in Phenix (McCoy, Grosse-Kunstleve et al. 2005, McCoy, Grosse-Kunstleve et al. 2007, Adams, Afonine et al. 2010). The N and C-terminal domains (residues 6-169 and 170-358) of the active ERK2 structure (PDB 2ERK) were used as search models (Canagarajah, Khokhlatchev et al. 1997). The structure contains one molecule per asymmetric unit. Iterative rounds of refinement (TLS, rigid body, individual ADPs, and N-terminal domain atomic positions) were carried out in phenix.refine and model building in Coot (Emsley and Cowtan 2004, Adams, Afonine et al. 2010, Afonine, Grosse-Kunstleve et al. 2012). Secondary structure restraints were used early in model building. Model validation was conducted in phenix.refine, which uses analyses derived, in part, from the MolProbity web server (Davis, Murray et al. 2004, Adams, Afonine et al. 2010, Afonine, Grosse-Kunstleve et al. 2012).

GST pulldowns. The specified amount (4 or 16 μg) of GST bait protein was incubated for 1 hour with 20 μl glutathione agar resin (Pierce) in binding buffer: 25 mM Tris pH 7.75, 125 mM NaCl, 1 mM DTT, 1:1000 protease inhibitor cocktail (in 62.5 mL of DMSO: 25 mg of pepstatin A, 25 mg of leupeptin, 250 mg of Nα-p-tosyl-L-arginine methyl ester, 250 mg of Nα-p-tosyl-L-lysine chloromethyl ketone hydrochloride, 250 mg of Nα-Benzoyl-L-arginine methyl ester, and

250 mg of soybean trypsin inhibitor), and 400 uM PMSF. After 2 x 1 ml washes with binding buffer beads were incubated with 50 nM (GST-PEA15 or 100 nM (GST-ERF 257-425) His_6-ERK2 or His_6-ERK2 E320K. Beads were washed with 2 x 1 ml binding buffer and resuspended in 50 µl 1X SDS-PAGE loading buffer.

Expression of ERK2 and ELK1 in HeLa cells. Dishes of HeLa cells (12-well dish, 2.2 cm diameter well) were transfected with pCMV constructs containing the protein of interest (0.5 µg ELK1, 1.2 µg ERK2 and ERK2 E320K) using FuGene GH transfection reagent. After 18 hours cells were starved in DMEM for 3 hours followed by stimulation with 20% FBS for the indicated amounts of time. Cells were lysed and centrifuged at 13,000 x g for 10 minutes. The supernatant was resuspended in SDS-PAGE buffer and ~50 µg/lane was loaded on a gel.

Fluorescence anisotropy. 25 nM ERKtide-FAM (NH_3^+-IPTTPITTTYFFFK-5FAM-COO^-) was combined with 20 µM ERK2 or ERK2 E320K and 2-fold serial dilutions with buffer containing 25 mM Tris pH 7.75, 125 mM NaCl, 1 mM DTT, 25 nM ERKtide-FAM were performed. Anisotropy measurements were made on a BioTek Synergy H1 plate reader with FP-green filter cube. Data were fit using GraphPad prism.

SCH772984 ERK2 inhibitor titrations. ppERK2 activity was measured using the IMAP-FP kinase assay kit (Molecular Devices) according to the manufacturer's instructions with 100 nM ERKtide-FAM probe and 1 nM ppERK2. ppERK2 E320K activity was measured by monitoring ^{32}P incorporation. 1 nM ppERK2 E320K was incubated with 1 µM MBP in 10 mM Tris, pH 7.5, 10 mM $MgCl_2$, 50 µM ATP, 0.01 mCi/µL [γ-32P]ATP at room temperature.

Results

E320K Disrupts DUSP6-mediated ERK2 Deactivation and ERK2-mediated DUSP6 Allosteric Activation

To begin to understand the effects that the ERK2 E320K mutation has on ERK MAPK signaling we first asked how the mutation would affect the activity of its cognate signaling partner, DUSP6. DUSP6, like some other DUSPs (Figure 1-13D), has the unique property of both having activity towards ERK2 (dephosphorylation of pT183/pY185) and being allosterically activated through interactions with ERK2 (Camps, Nichols et al. 1998).

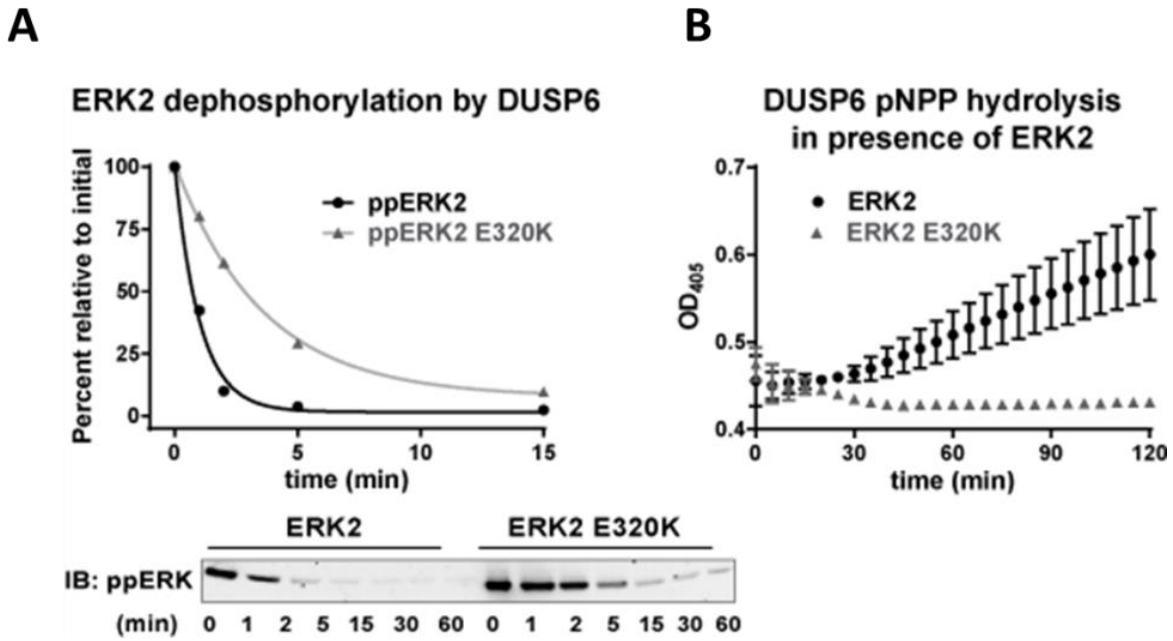

Figure 4-1. E320K effects on DUSP6-mediated ERK2 deactivation and ERK2-mediated DUSP6 activation.

(A) Kevin Cormier measured ppERK2 (black) and ppERK2 E320K (grey) dephosphorylation by DUSP6 by Western blot with ppERK2 antibody (pT183/pY185). (B) Kevin Cormier also measured the activity of DUSP6 towards generic substrate pnitrophenyl phosphate (pNPP) as monitored by change in absorbance at 405 nm in the presence of inactive ERK2 (black) and ERK2 E320K (grey).

In the case of DUSP6, Kevin Cormier determined ppERK2 E320K is deactivated, as monitored by dephosphorylation of pT183/pY185, at a much lower rate than wild type ppERK2 (Figure 4-1A). This is somewhat to be expected since the ERK2 CD site interaction with the DUSP6 KIM is required for efficient dephosphorylation of ERK2(Tanoue, Adachi et al. 2000, Zhou, Wu et al. 2001). In order to determine the mutation's effect on ERK2-mediated allosteric activation of DUSP6 activity Kevin Cormier monitored p-nitrophenyl phosphate (pNPP) hydrolysis in the presence of inactive ERK2 and ERK2 E320K. Interestingly, the E320K mutation caused a complete lack of DUSP6 activity towards pNPP indicating that ERK2 E320K could no longer allosterically activate DUSP6 (Figure 4-1B).

Structure Determination of Rat ERK2 E320K

Since the E320K mutation clearly disrupts the CD site, I next wanted to know what the structural consequences of introduction of a buried charge reversal at the CD site within the L16 loop had on ERK2 (Figure 1-13A. Complete details on crystallization and structure determination can be found in Chapter 5 Experimental Procedures. Briefly, crystals of unphosphorylated rat ERK2 E320K, belonging to space group C121, diffracted to 2.1 Å (Table 4-1). Phases were obtained by molecular replacement using the N- and C-terminal domains of rat ppERK2 (PDB: 2ERK) as separate search models. The final refined model has a R_{work}/R_{free} of 0.22/0.26.

Although the N-terminal domain had well defined electron density, most of the C-terminal domain density was present, but poorly defined (Figure 4-2A), and associated with

increased B-factors relative to the N-terminal domain (Figure 4-2A,B). High mobility of the C-terminal domain made refinement of certain regions of ERK2 E320K difficult.

Data Collection	
Resolution (Å)	50 – 2.1 (2.14-2.10)
Space group	C2
Unit cell: *a,b,c* (Å) α,β,γ (°)	182.3, 41.9, 50.3 90, 105.9, 90
Unique Reflections	17665 (372)
Redundancy	4.0 (3.3)
Completeness (%)	88.5 (53.1)
$\langle I/\sigma_I \rangle$	23.3 (1.7)
R_{merge}	0.055 (0.605)
Refinement	
R_{work} / R_{free} (%)	22.2 / 25.7
Bond rmsd	0.013
Angle rmsd	1.54
Ramachandran favored (%)	90.5
Ramachandran outliers (%)	0.6
Mean B-factor	79.6

Table 4-1. Rat ERK2 E320K data collection and refinement statistics.

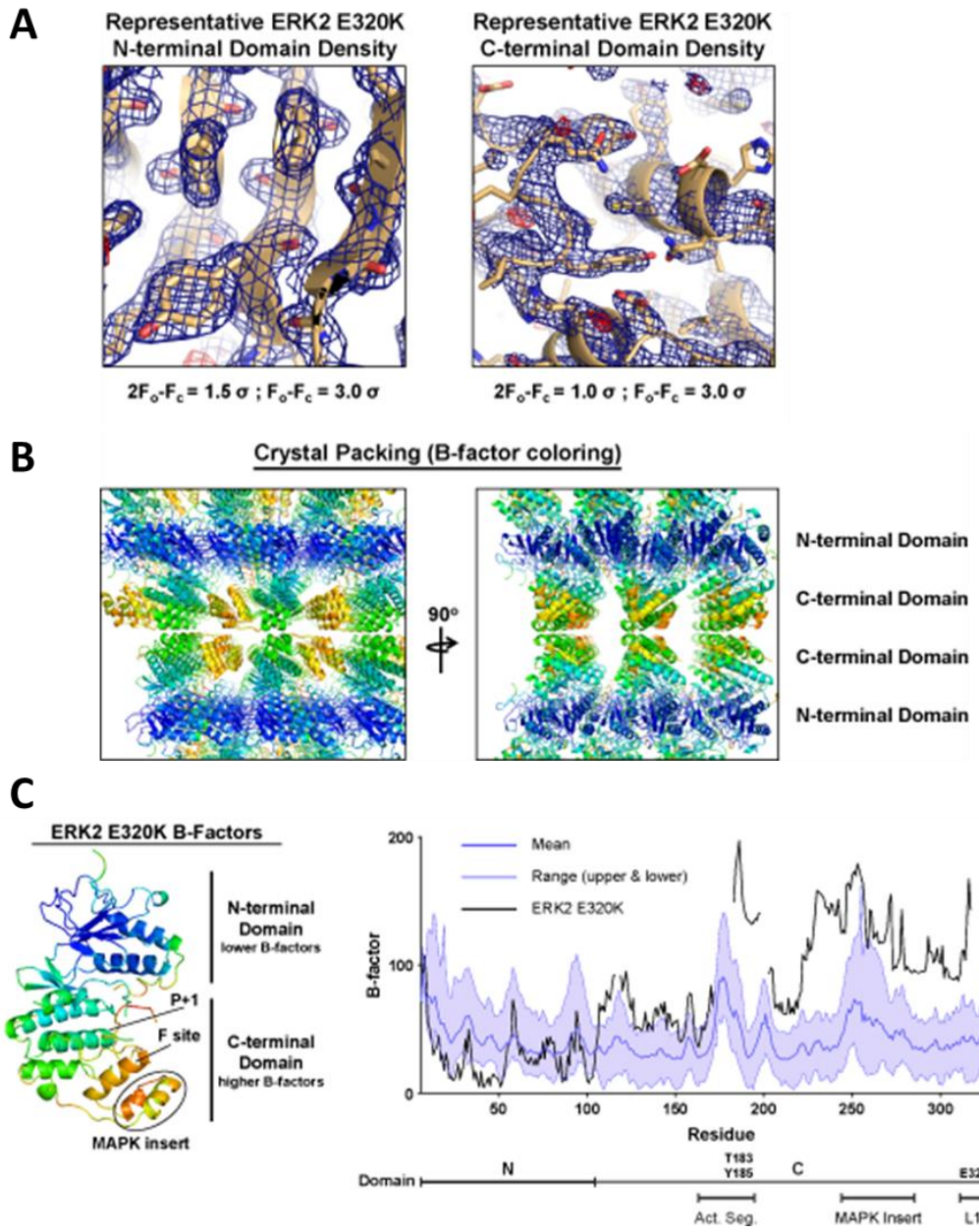

Figure 4-2. ERK2 E320K C-terminal domain mobility is enhanced in the crystal lattice.

(A) $2F_o$-F_c and F_o-F_c maps depicting representative examples of N-terminal domain and C-terminal domain densities. (B) ERK2 E320K crystal lattice. Molecules of ERK2 E320K are colored by B-factor. Most lattice contacts are within the N-terminal domain (blue B-factor colors) while fewer exist for the C-terminal domain (green, yellow, and orange B-factor colors). (C) Structure of ERK2 E320K colored by B-factors and B-factors plot comparing B-factors of nine structures with similar resolutions (1.9 – 2.6 Å) and different crystal lattices (PDBs: 2FYS, 2GPH, 3C9W, 3O71, 3TEI, 4H3P, 4NIF, 4XJ0, 5BUE). The MAPK insert, F site (FxF motif interactions), and P+1 substrate binding pocket (ser/thr-proline specificity) are indicated.

It is unclear from the structure whether the poorly defined C-terminal density was a result of crystal packing, the E320K mutation, or a combination of the two. More crystal lattice contacts are present in the ERK2 E320K N-terminal domain (Figure 4-2A). However, the E320K mutation lies on the L16 loop connecting the N- and C-terminal domains of ERK2 (Figure 1-12). This loop is known to allosterically modulate distal regions of ERK2. Therefore, the introduction of a buried charge reversal could potentially affect the stability of the entire C-terminal domain or interdomain mobility.

Structure of Rat ERK2 E320K

The overall structure of rat ERK2 E320K is similar to other structures of ERK2 (Figure 4-3), based on alignments (all C_α r.m.s.d.) to ERK2 (2.55 Å), ppERK2 (1.83 Å), ERK2:DUSP6 KIM (1.88 Å, chain A), ERK2:HePTP KIM (1.39 Å, PDB: 2GPH). ERK2 E320K has several features in common with ppERK2 and the KIM-bound structures compared to inactive ERK2 that give rise to lower r.m.s.d. values, such as refolding of the N-terminal insert and position of the glycine-rich loop.

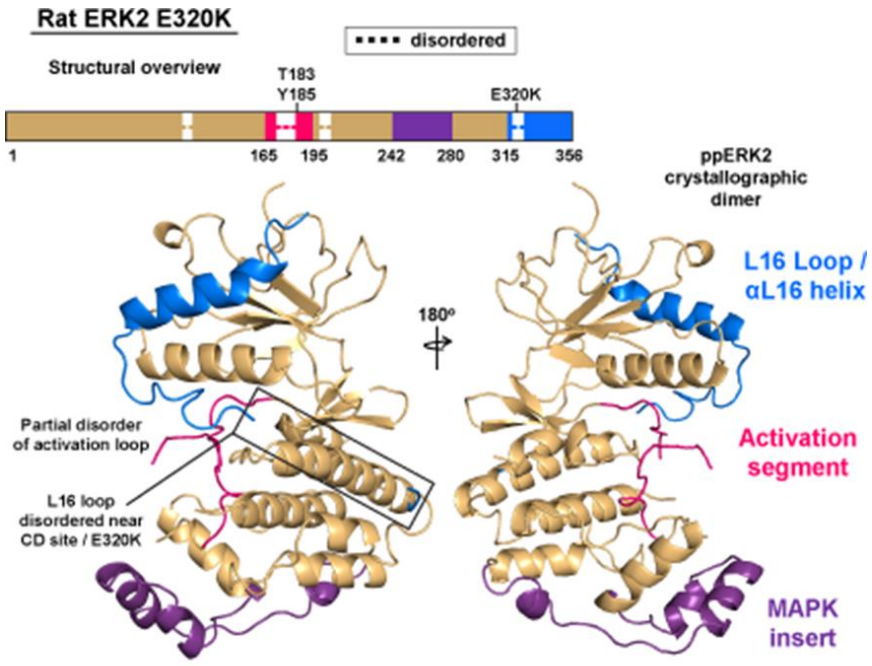

Figure 4-3. Overall structure of rat ERK2 E320K.

Structural overview of rat ERK2 E320K (orange). Schematic indicates positions of relevant structural elements and residues, and regions of disorder in the crystal structure (dashed lines).

Several regions of ERK2 E320K are disordered (Figure 4-3), including activation loop residues 173-182, and residues 318-325 encompassing the E320K mutation in the L16 loop/CD site (Figure 4-4A,B,C,D). The structure provides further evidence that the CD site and activation loop are allosterically coupled. Both regions have higher B-factors (Figure 4-2C) and are partially disordered in ERK2 E320K, whereas both regions are well defined in many other structures of ERK2. Also, the activation loop around T183/Y185 assumes a nearly identical solvent-exposed conformation that is also observed in structures of ERK2 with KIM peptides (DUSP6 and HePTP) bound at the CD site (Figure 4-4A,D), as well as a number of other structures (Liu, Sun et al. 2006, Zhou, Sun et al. 2006, Peti and Page 2013). Since this

conformation is observed in multiple structures with different space groups and unit cell dimensions it is unlikely the result of crystal contacts.

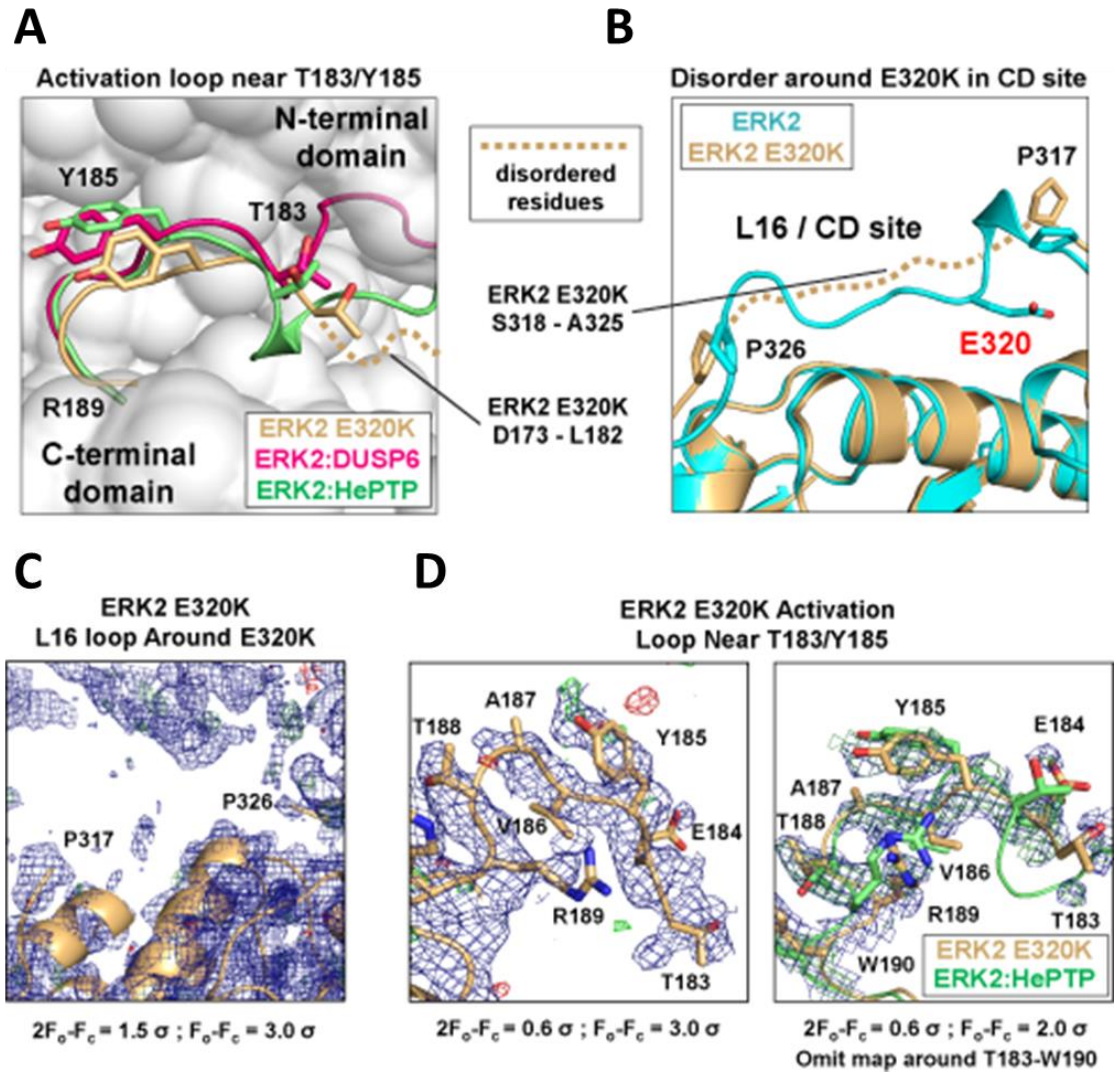

Figure 4-4. E320K disrupts the ERK2 CD site and alters the activation loop conformation.

(A) Comparison of ERK2 E320K activation loop (orange) conformation near T183/Y185 to structures of ERK2 bound to KIM peptides derived from DUSP6 (magenta) and HePTP (PDB: 2GPH, green). (B) Comparison of the L16 loops (part of CD site) of inactive ERK2 (cyan) and ERK2 E320K (orange). The region around E320K (residues 318-325) is disordered in the crystal structure of ERK2 E320K. (C) $2F_o$-F_c and F_o-F_c maps indicating absence of electron density around E320K in the L16 loop from residues 318-325 of ERK2 E320K. Important CD site residues are located within this span of the loop. (D) $2F_o$-F_c and F_o-F_c maps indicating electron density around the activation loop near T183 and Y185 activating ERK2 phosphorylation sites.

The ERK2 E320K structure also suggests that the mutation may affect ERK2 homodimerization. Our lab previously showed that ERK2 dimerizes through an interface composed of the L16 loop around L336 and activation loop around H176 (Khokhlatchev, Canagarajah et al. 1998). In the structure of ppERK2, the crystal lattice utilizes this dimerization interface, but a corresponding interface is not found in the crystal lattice for ERK2 E320K (Figure 4-5A). Additionally, the regions of ERK2 that comprise the dimer interface either have heightened B-factors or are completely absent from the electron density (Figure 4-5B,C, Figure 4-2C).

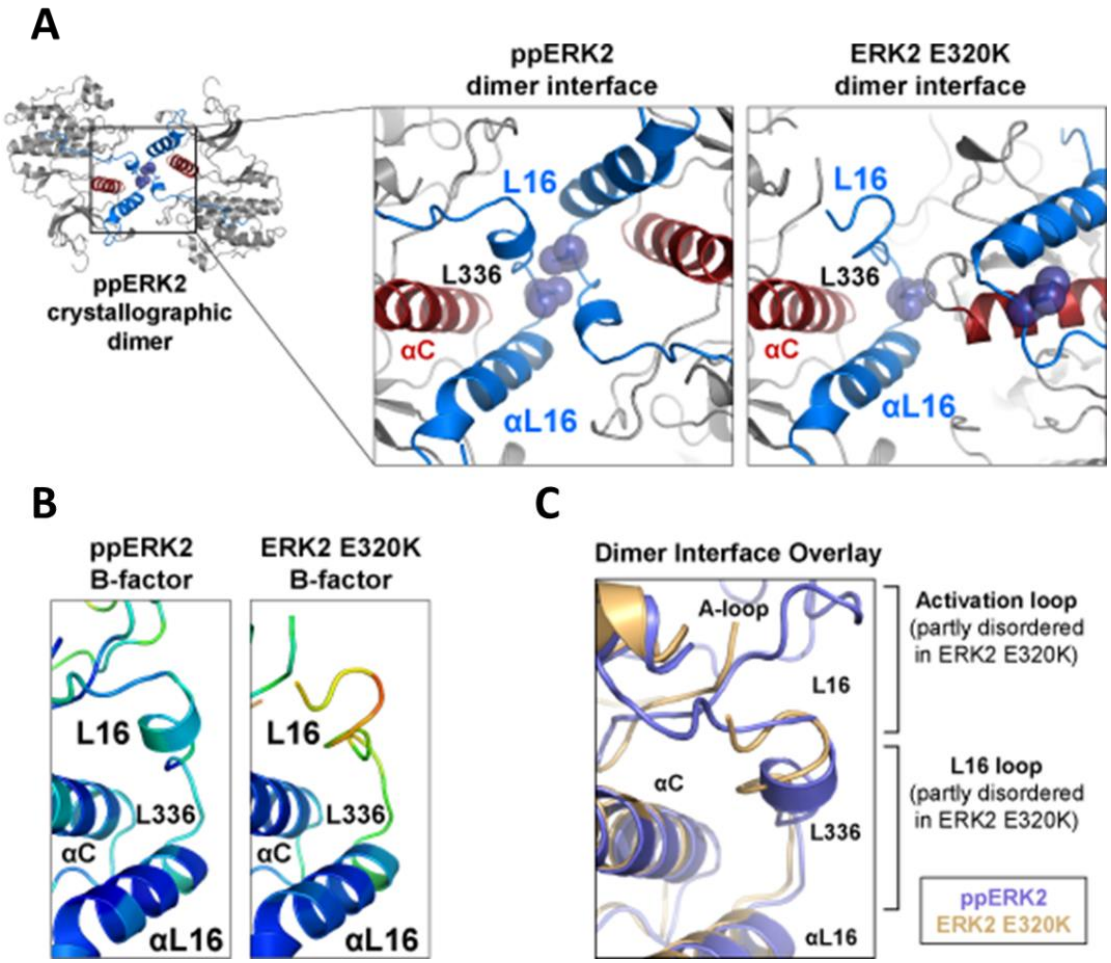

Figure 4-5. ERK2 E3320K dimerization interface.

A) Comparison of the crystallographic dimer interfaces (previously identified and characterized *in vitro* and *in vivo* for ppERK2) of ppERK2 and ERK2 E320K. ppERK2 exists as a two-fold symmetric dimer in the crystal lattice with axis of symmetry about the dimer interface, and ERK2 E20K does not. Essential residue for dimerization, L336, is indicated by grey spheres. (B) Comparison of B-factors about the dimer interfaces of ppERK2 and ERK2 E320K. (C) Overlay comparing the dimerization interfaces of ppERK2 and ERK2 E320K crystal structures.

E320K Disrupts CD Site Signaling

Since the ERK2 E320K mutation causes severe structural disruption of the CD site, and this appears to affect parts of the kinase distal to the CD site, such as the activation loop, we next examined the impact of the mutation on various ERK2 molecular interactions.

Kevin Cormier employed yeast two-hybrid to assay interactions with upstream kinases MEK1 and MEK2, and various fragments and mutants (Figure 4-6A). Comparatively, wild type MEK2 interacted more strongly with ERK2 than wild type MEK1. In the case of MEK1, the E320K mutation did lead to disruption of the interaction with ERK2. Neither the MEK1 N-terminal fragment containing the KIM (1-32), nor the C-terminal fragment containing the kinase domain (33-393) interacted with either ERK2 or ERK2 E320K suggesting the entire molecule is required to interact effectively with ERK2. The constitutively active mutant, MEK1 R4F interacted weakly with both (Mansour, Matten et al. 1994). Interestingly, deletion of the MEK1 proline-rich insert, which has been shown to be required for efficient activation of ERK2 (Dang, Frost et al. 1998), enhanced the interaction with ERK2, and the interaction was diminished for ERK2 E320K. Kinase-dead MEK1 K97M strongly interacted with both ERK2 and ERK2 E320K, likely due to disruption of negative feedback from MEK1→ERK2 signaling. Perhaps most interesting is that the kinase-dead kinase domain fragment of MEK1, MEK1 33—393 K97M, interacted strongly with ERK2 E320K, but weakly with ERK2. In the case of MEK2, and kinase-dead MEK2 K101A, the interactions with ERK2 are stronger than with MEK1, but the E320K mutation has a more dramatic effect, as a significant loss of interaction with ERK2 E320K was observed in both cases. However, constitutively active MEK2 R4F did not bind ERK2 or ERK2 E320K.

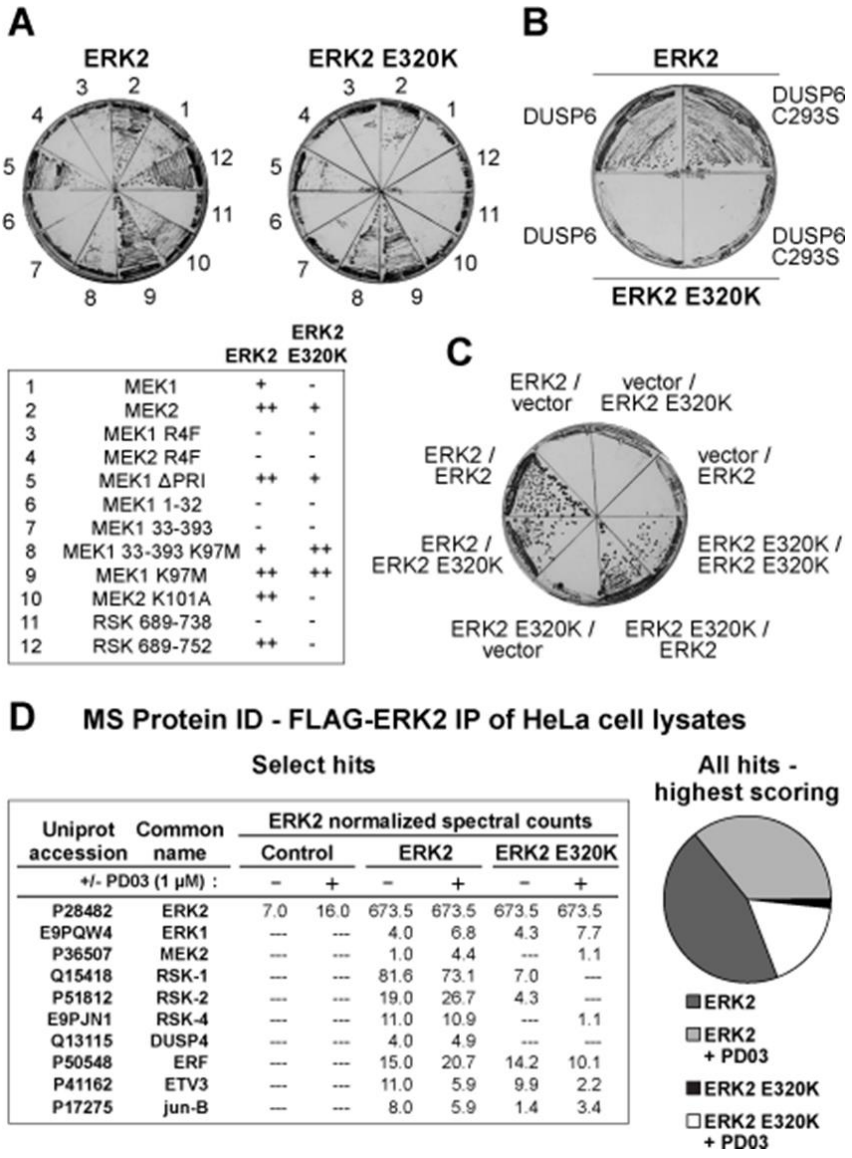

		ERK2	ERK2 E320K
1	MEK1	+	-
2	MEK2	++	+
3	MEK1 R4F	-	-
4	MEK2 R4F	-	-
5	MEK1 ΔPRI	++	+
6	MEK1 1-32	-	-
7	MEK1 33-393	-	-
8	MEK1 33-393 K97M	+	++
9	MEK1 K97M	++	++
10	MEK2 K101A	++	-
11	RSK 689-738	-	-
12	RSK 689-752	++	-

D **MS Protein ID - FLAG-ERK2 IP of HeLa cell lysates**

Select hits

Uniprot accession	Common name	ERK2 normalized spectral counts					
		Control		ERK2		ERK2 E320K	
+/- PD03 (1 μM) :		-	+	-	+	-	+
P28482	ERK2	7.0	16.0	673.5	673.5	673.5	673.5
E9PQW4	ERK1	---	---	4.0	6.8	4.3	7.7
P36507	MEK2	---	---	1.0	4.4	---	1.1
Q15418	RSK-1	---	---	81.6	73.1	7.0	---
P51812	RSK-2	---	---	19.0	26.7	4.3	---
E9PJN1	RSK-4	---	---	11.0	10.9	---	1.1
Q13115	DUSP4	---	---	4.0	4.9	---	---
P50548	ERF	---	---	15.0	20.7	14.2	10.1
P41162	ETV3	---	---	11.0	5.9	9.9	2.2
P17275	jun-B	---	---	8.0	5.9	1.4	3.4

Figure 4-6. The E320K mutation disrupts KIM interactions and ERK2 dimerization.

(A-C) Kevin Cormier performed yeast two-hybrid comparing ERK2 and ERK2 E320K interactions to: (A) Upstream kinases MEK1/2, constitutively active MEK1/2 (R4F), MEK1 lacking the proline-rich insert (ΔPRI), N-terminal KIM of MEK1 (residues 1-32), kinase domain of MEK1 (residues 33-393), kinase-dead MEK1 kinase domain (K97), full-length kinase-dead MEK1, kinase-dead MEK2 (K101A), C-terminal RSK fragment with (residues 689-752) and without (residues 689-738) KIM motif. A table summarizes the results. (B) DUSP6 and DUSP6 C293S (catalytically inactive) (C) ERK2 and ERK2 E320K (dimerization). (D) Mass spectrometry protein ID of immuneprecipitated proteins from HeLa cell lysates using FLAG-ERK2 and ERK2 E320K with or without 1 μM PD03 (MEK inhibitor) treatment. 'Hits' are defined as having at least one sample with spectral counts ≥ 4 and sample/control ratio ≥ 3. All hits (Table 4-2) were normalized to ERK2 samples. Select hits were chosen for relevance to this study. Pie chart represents the overall percentage for each sample where that sample has the highest number of normalized spectral counts compared to the other samples.

As an alternative means of assessing protein interactions with ERK2 and ERK2 E320K we employed protein ID by mass spectrometry (Figure 4-6D, Table 4-2). FLAG-tagged ERK2 and ERK2 E320K were used to pull-down proteins from HeLa cell lysates with or without treatment with MEK inhibitor PD03. PD03 was employed to analyze binding independent of ERK2 phosphorylation, since it has been shown that ERK2 E322K (human numbering) has higher levels of basal activation (Arvind, Shimamoto et al. 2005). Of the 60 hits (hit is defined in Figure 4-6 legend) less than 25 percent of the highest scoring (the most normalized spectral counts) were obtained with ERK2 E320K as the bait implying a substantial decrease in the ability of ERK2 E320K to interact with its signaling partners across the spectrum of protein-protein interaction partners (Figure 4-6D, Table 4-2). Specifically for MEK1/2 results were similar to what was observed by Y2H, MEK2 interacted preferentially with ERK2 in PD03 treated cells, but the interaction with MEK1 was too weak to produce an observable signal.

Table 5-2: MS Protein ID – FLAG-ERK2 IP of HeLa Cell Lysates		Normalized spect. counts (+/- 1 μM MEK inhibitor PDO3)					
Uniprot Accession	Description	control	control +PD03	ERK2 WT	ERK2 WT +PD03	ERK2 E320K	ERK2 E320K +PD03
P28482	MAPK1 (ERK2) *used for normalization*	7.0	16.0	673.5	673.5	673.5	673.5
***Q15418	Ribosomal protein S6 kinase alpha-1			81.6	73.1	7.0	0.0
P49366	Deoxyhypusine synthase			47.1	44.6	60.0	58.3
Q92576	PHD finger protein 3			34.8	42.2	36.7	80.0
Q16543	Hsp90 co-chaperone Cdc37	2.0	2.0	27.8	32.3	11.4	32.3
P47712	Cytosolic phospholipase A2	3.0	1.0	27.0	24.7	1.4	2.2
B4DGT8	MKL/myocardin-like 2			23.8	25.4	1.4	1.1
E7ER32	MKL/myocardin-like protein 1			23.0	22.7	2.8	0.0
J3KNL6	Protein transport protein Sec16A	4.0	1.0	21.8	15.7	14.1	14.5
***P51812	Ribosomal protein S6 kinase alpha-3			19.0	26.7	4.3	0.0
F6RU81	ELM2 and SANT domain-containing protein 1			19.0	13.8	0.0	1.1
O75330	Hyaluronan mediated motility receptor	2.0		17.8	16.6	0.0	1.1
***P50548	ETS domain-containing transcription factor ERF			15.0	20.7	14.2	10.1
P13797	Plastin-3	7.9	4.9	14.7	23.2	5.5	11.0
Q9H4H8	Protein FAM83D		1.0	13.0	11.8	1.4	0.0
Q9UHF7	Zinc finger transcription factor Trps1			12.8	14.6	0.0	0.0
Q92922	SWI/SNF complex subunit SMARCC1	2.4	2.4	12.0	18.5	0.0	15.4
***P41162	ETS translocation variant 3 (ETV3)			11.0	5.9	9.9	2.2
***O75676	Ribosomal protein S6 kinase alpha-4			11.0	10.9	0.0	1.1
Q14160	Protein scribble homolog OS	3.0	3.0	10.9	13.7	4.3	14.5
Q14980	Nuclear mitotic apparatus protein 1	7.9	5.9	10.9	22.5	4.3	25.6
F5GZS0	Probable ATP-dependent RNA helicase DHX36	2.5	0.5	10.9	10.3	0.0	6.2
Q14444	Caprin-1		1.0	10.8	9.8	0.0	12.2
Q13451	Peptidyl-prolyl cis-trans isomerase FKBP5			10.0	7.9	4.3	13.5
Q7Z7A3	Cytoplasmic tRNA 2-thiolation protein 1		1.0	9.0	5.9	1.4	0.0
B9ZVX0	Diaphanous homolog 1	3.0	3.0	9.0	11.8	1.4	4.5
Q8N8S7	Protein enabled homolog	3.0	1.0	8.0	5.9	1.4	5.6
***P17275	Transcription factor jun-B			8.0	5.9	1.4	3.4
P50552	Vasodilator-stimulated phosphoprotein	2.0	2.0	8.0	5.9	1.4	5.6
P15822	Zinc finger protein 40			8.0	4.9	0.0	0.0
J3KMW7	E3 ubiquitin-protein ligase UBR5	4.0	2.0	8.0	11.8	1.4	4.5
Q93008	Ubiquitin carboxyl-terminal hydrolase FAFX	3.0	2.0	8.0	11.8	4.3	10.1
H3BSW6	Cytoplasmic tRNA 2-thiolation protein 2			7.0	6.9	0.0	0.0
Q13643	Four and a half LIM domains protein 3			7.0	2.0	0.0	2.2
Q14195-2	Dihydropyrimidinase-related protein 3	1.0	3.0	7.0	9.8	1.4	6.7
G8JLA8	TGF-β-induced protein ig-h3			6.9	2.0	0.0	2.2
Q5TGY3	AT-hook DNA-binding motif-containing protein 1			6.0	3.9	1.4	1.1
P67870	Casein kinase II subunit beta			6.0	3.0	0.0	0.0
Q14683	Struct. maint. of chromosomes protein 1A		1.0	6.0	2.0	1.4	3.4
O15357	PIP_3 5-phosphatase 2		1.0	6.0	3.0	4.3	6.7
Q7L576	Cytoplasmic FMR1-interacting protein 1	2.0	1.0	5.9	12.7	1.4	7.7
H0YGW7	ATP-binding cassette sub-family F member 1	4.0	3.0	5.0	9.9	2.8	4.5
Q96CW5	Gamma-tubulin complex component 3	3.0	2.0	5.0	8.9	0.0	3.4
Q92619	Minor histocompatibility protein HA-1			5.0	4.9	0.0	0.0
E9PHK9	Treacle protein	1.0		4.9	5.8	1.4	3.4
***Q13115	Dual specificity protein phosphatase 4 (MKP2)			4.0	4.9	0.0	0.0
Q7Z6K3	Prenyltransferase α subunit repeat protein 1	1.0		4.0	3.9	0.0	1.1
Q5RKV6	Exosome complex component MTR3	1.0	1.0	4.0	3.0	0.0	1.1
Q15654	Thyroid receptor-interacting protein 6	1.0	1.0	4.0	2.0	2.8	2.2
Q7Z319	MAP kinase-interacting S/T-protein kinase 1			4.0	2.0	0.0	0.0
H9KV46	Kinesin-like protein KIF18B			4.0	1.0	0.0	0.0
B3KRS5	Histone deacetylase	1.0	1.0	4.0	6.9	0.0	3.4
Q9NR12	PDZ and LIM domain protein 7		1.0	4.0	4.9	2.8	2.2
***E9PQW4	Mitogen-activated protein kinase 3 (ERK1)			4.0	6.8	4.3	7.7
Q8IWJ2	GRIP & coiled-coil domain-containing protein 2		1.0	3.0	7.9	0.0	0.0
Q96RR5	Hepatocellular carcinoma-associated antigen 90			2.0	1.0	1.4	4.5
O94822	E3 ubiquitin-protein ligase listerin			2.0	2.0	0.0	5.6
Q9UPU5	Ubiquitin carboxyl-terminal hydrolase 24			2.0	1.0	2.8	9.0
Q9Y295	Developmentally-reg. GTP-binding protein 1	1.0	1.0	1.0	4.9	2.8	2.2
***P36507	MAP2K2 (MEK2)			1.0	4.4	0.0	1.1
O43592	Exportin-T	1.0	1.0	1.0	6.9	1.4	1.1

Table 4-2. Complete listing of MS hits.

Color corresponds to sample with highest number of spectral counts for that interaction. Hits defined in Figure 4-6 legend.

We next analyzed ERK2 interactions with downstream substrate, RSK. Previously it has been shown that phosphorylation of RSK by human ERK2 E322K is impaired compared to ERK2 (Mahalingam, Arvind et al. 2008). In line with these results, Kevin Cormier found by Y2H that the C-terminal fragment of RSK containing the KIM (689-752) bound strongly to ERK2 but this interaction was completely lost with ERK2 E320K (Figure 4-6B). Neither ERK2 nor ERK2 E320K bound the truncated RSK C-terminal fragment (689-738) lacking the KIM sequence. By mass spec, we found that RSK-1 (RPS6KA1), RSK-2 (RPS6KA3), and RSK-4 (RPS6KA4, MSK2, RSKB) bound almost exclusively to ERK2 with and without PD03 treatment, but not ERK2 E320K (Figure 4-6D, Table 4-2). RSK-3 (RPS6KA2), a putative tumor suppressor, was not observed. RSK5 (RPS6KA5, MSK1, RSKL) was present at low spectral counts only bound to ERK2 with PD03 treatment (data not shown).

We next examined the interaction between ERK2 and ERK2 E320K with DUSP6, and the catalytically inactive mutant DUSP6 C293S. By Y2H, Kevin Cormier observed a strong interaction between ERK2 and both DUSP6 and catalytically inactive DUSP6 C293S. However, this interaction was completely disrupted in the case of ERK2 E320K (Figure 4-6B). An interaction between DUSP6 and ERK2 or ERK2 E320K was not observed by mass spec. However, DUSP4 (MKP2), another MAPK-specific phosphatase with an ERK-interacting KIM, bound ERK2 with and without PD03 treatment, but no binding to ERK2 E320K was detected (Figure 4-6D, Table 4-2).

E320K Signaling Disruption is not Limited to the ERK2 CD Site

We next questioned whether other interactions that occur outside of the CD site might be affected by the E320K mutation. An obvious candidate interaction that could be affected by the E320K mutation is ERK2 dimerization (Figure 4-5). We again turned to Y2H and Kevin Cormier found a strong *in situ* interaction between ERK2 and ERK2 (Figure 4-6C). This interaction was marginally reduced when ERK2 interacted with ERK2 E320K. However, the most pronounced effect was seen between ERK2 E320K and ERK2 E320K, where a significant disruption of the interaction occurred implying that the E320K mutation also affects the stability of the dimerization interface. Again turning to mass spec results, for ERK1 (MAPK3) there were no obvious difference between ERK2 and ERK2 E320K (Figure 4-6D, Table 4-2), but lower spectral counts were observed for cells that were not treated with PD03, which is the opposite of what is to be expected since ERK2 dimerizes upon phosphorylation. However, since ERK1 dimerization with ERK2 has not been thoroughly characterized the explanation for this observation remains unknown.

I then asked whether the other major ERK2 docking site, the F site, was affected by the E320K mutation. The F site has been shown to be made up from elements of the MAPK insert and the ERK2 activation loop (Figure 4-2C), and F-site functionality is modulated by activation loop phosphorylation (Lee, Hoofnagle et al. 2004, Burkhard, Chen et al. 2011). In the crystal structure of ERK2 E320K I observed no electron density for the activation loop near the residues of the MAPK insert that make up part of the F site, and helix αG and MAPK insert helices have exceptionally high B-factors (Figure 4-2C). This suggests that the F site could be more accessible than that of inactive ERK2, but yet, that it may be destabilized.

Since the ERK2 F site is modulated by phosphorylation and yeast may phosphorylate ERK2 versus ERK2 E320K differently, I took an *in vitro* biochemical approach, as opposed to Y2H, to test the ability of ERK2 and ERK2 E320K to interact with proteins that utilize the F site interaction. I examined the interactions with GST-ERF 257-425, GST-PEA-15, and ERKtide-FAM (NH_3^+-IPTTPITTTY**F**<u>F</u>**F**<u>F</u>K-5FAM-COO^-) that contains YxF (bold) and FxF (underlined) motifs.

ERF (Ets2 repressor factor) is an ETS domain-containing transcription factor that represses c-Myc transcription (Verykokakis, Papadaki et al. 2007). ERF interacts with, and is phosphorylated by ERK2, and this leads to ERF nuclear export and inactivation (le Gallic, Sgouras et al. 1999). The ERF fragment 257-425 has been shown to contain two FxF motifs that are both utilized in ERK2 F-site binding to either active or inactive ERK2. Mutations to alanine at either of these sites severely disrupts ERK2 binding depending on the activation state of ERK2 (Polychronopoulos, Verykokakis et al. 2006). PEA-15, is a small protein that interacts with both inactive ERK2 and active ppERK2 at both the CD and F sites. The crystal structure of PEA-15 bound to ERK2 indicates that PEA-15 interacts with the F-site through a large interface and not a canonical linear FxF motif (Mace, Wallez et al. 2013). ERK2 interaction with PEA-15 has been shown to lead to inactive ERK2 cytosolic retention, inhibition of activation by MEK1, and inhibition of kinase activity and dephosphorylation of active ppERK2 (Whitehurst, Robinson et al. 2004).

The ERK2 E320K mutation caused a complete disruption of the interaction with GST-ERF 257-425 (Figure 4-7A). Decreased spectral counts for the ERF interaction with ERK2 E320K were also observed by mass spec. ETV3 and jun-B, two other transcription factors regulated by the ERK MAPK pathway also bound preferentially to ERK2 (Figure 4-6D, Table 4-

2). Interestingly, both ERK2 and ERK2 E320K still phosphorylate GST ERF 257-425 to similar extents (Figure 4-7B), suggesting that the interaction is not required for ERK2 activity toward the ERF fragment, at least in the case of the inactive kinases. In the case of ERKtide-FAM, a peptide substrate that also contains linear FxF motifs both ERK2 and ERK2 E320K appear to have nearly identical affinities (Figure 4-7C). These results suggest that the E320K mutation exerts varying effects on F-site function, although the possibility exists that ERK2 interacts with the ERF fragment in a manner that has yet to be characterized.

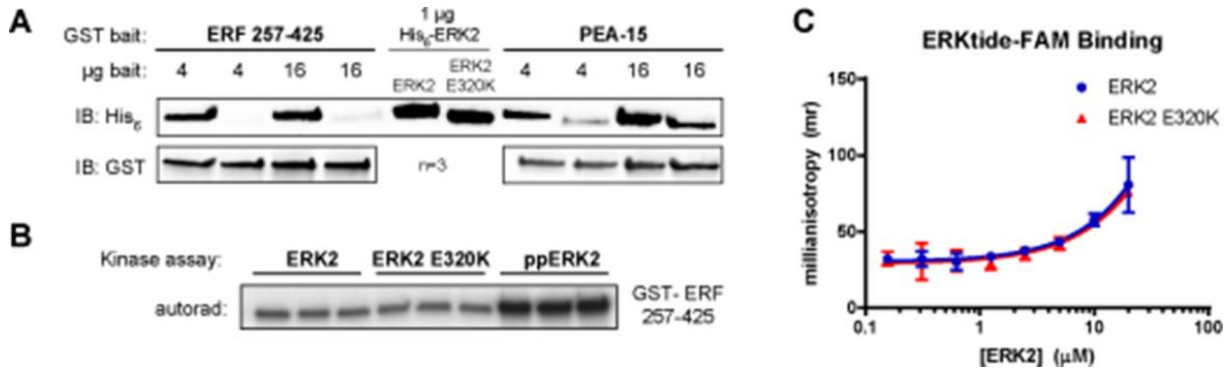

Figure 4-7. F site interactions are disrupted by the ERK2 E320K mutation.

(A) *In vitro* GST pull-downs of His_6-ERK2/ERK2 E320K with GST-ERF 257-425 and GST-PEA15. (B) ERK2 E320K, and ppERK2 kinase activities towards GST-ERF 257-425. 16 hour reaction was required to obtain sufficient phosphorylation by inactive kinases. (C) Binding of ERKtide-FAM (IPTTPITTTYFFFK-5FAM-COO^-) to ERK2 and ERK2 E320K assessed by fluorescence polarization.

As opposed to the linear FxF motifs, GST-PEA-15, which interacts through a broad surface with the ERK2 F-site, also was found to have substantial decrease in affinity for ERK2 E320K (Figure 4-7A). Since PEA-15 is a known inhibitor or ERK signaling, this result implies that at least in this instance changes in ERK2 protein-protein interactions caused by the E320K mutation can potentially enhance ERK2 signaling by relieving inhibition through means other

than loss of interaction with KIM-containing phosphatases.

These combined results suggest that not only does the E320K mutation ablate CD site function and allosterically affect activation loop solvent accessibility, but changes also occur throughout the kinase domain affecting other ERK2 functions such as dimerization and F-site interactions. Therefore, I believe this supports the notion that the structural disruption observed in the crystal structure of ERK2 E320K is at least partially a result of the E320K buried-charge reversal in the L16 loop/CD site (Figure 4-2, 4-3, 4-4, 4-5).

MEK Activation and ppERK2 Activity are Unaffected by the E320K Mutation

Based on the observations that the E320K mutation negatively impacts ERK2 interactions with upstream kinases MEK1/2, and that the ERK2 E320K activation loop assumes a unique, solvent exposed conformation, we next asked what effects the mutation had on ERK2 kinase activation and activity.

First Kevin Cormier determined that recombinant MEK1 R4F *in vitro* kinase activity towards both ERK2 and ERK2 E320K was similar (Figure 4-8A). We next wanted to know what effect the E320K mutation had on active ppERK2 kinase activity (Figure 4-9B). Previously our lab showed that ERK2 E320K has approximately 20-fold higher basal activity towards the generic substrate MBP than ERK2 (Yazicioglu, Goad et al. 2007). MBP is an ideal substrate to test kinase activity since it does not contain any known ERK2 protein interaction motifs that could impact comparison of catalytic activity between ppERK2 and ppERK2 E320K. Using an *in vitro* kinase assay, we assessed the ability of ppERK2 and ppERK2 E320K to phosphorylate MBP. Kevin Cormier and Steve Stippec found that the E320K mutation did not significantly

impact the ability of ppERK2 to phosphorylate MBP (Figure 4-8B). Taken together, these results imply that the ability of ERK2 E320K to be activated by upstream kinases MEK1/2 and kinase activity are relatively unaffected by the mutation. Furthermore, the results suggest that following phosphorylation, the activation loop adopts a configuration seen in the active ppERK2 structure (Figure 1-13C), since this configuration is required to achieve the several orders of magnitude enhancement in ERK2 catalytic activity compared to inactive ERK2 (Robbins, Zhen et al. 1993, Canagarajah, Khokhlatchev et al. 1997).

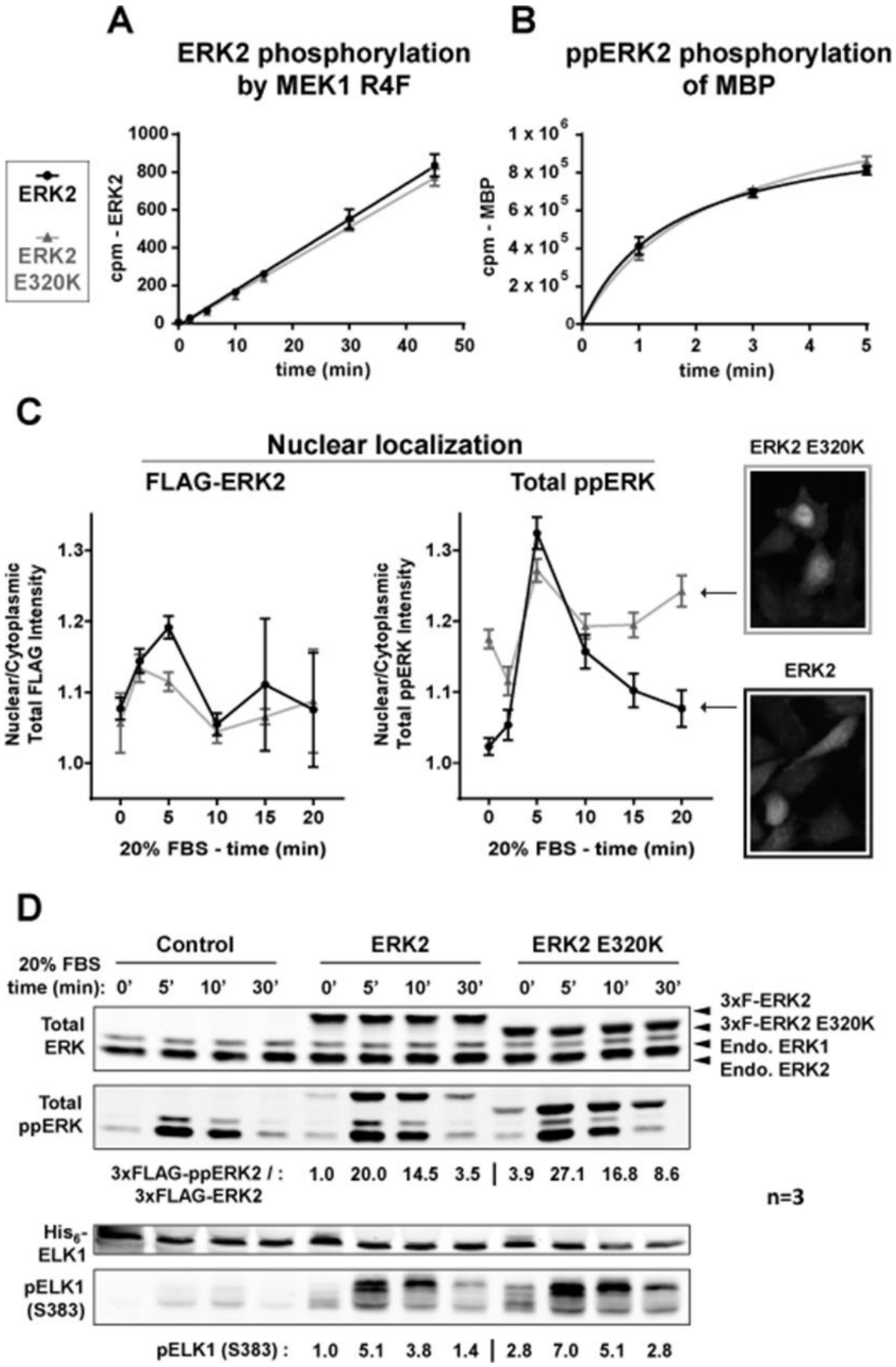
A
ERK2 phosphorylation by MEK1 R4F
ERK2
ERK2 E320K
cpm - ERK2
time (min)
B
ppERK2 phosphorylation of MBP
cpm - MBP
time (min)
C
Nuclear localization
FLAG-ERK2
Total ppERK
Nuclear/Cytoplasmic Total FLAG Intensity
Nuclear/Cytoplasmic Total ppERK Intensity
20% FBS - time (min)
ERK2 E320K
ERK2
D
Control
ERK2
ERK2 E320K
20% FBS
time (min): 0' 5' 10' 30' 0' 5' 10' 30' 0' 5' 10' 30'
Total ERK
Total ppERK
3xF-ERK2
3xF-ERK2 E320K
Endo. ERK1
Endo. ERK2
3xFLAG-ppERK2 / : 3xFLAG-ERK2
1.0 20.0 14.5 3.5 | 3.9 27.1 16.8 8.6
n=3
His6-ELK1
pELK1 (S383)
pELK1 (S383) : 1.0 5.1 3.8 1.4 | 2.8 7.0 5.1 2.8

Figure 4-8. ppERK2 nuclear localization and ELK1 transcription factor phosphorylation are enhanced by the E320K mutation.

(A) *In vitro* kinase assay performed by Kevin Cormier assessing phosphorylation of ERK2 and ERK2 E320K by constitutively active MEK1 R4F. (B) *In vitro* kinase assay performed by Kevin Cormier and Steve Stippec assessing phosphorylation of generic substrate, myelin basic protein (MBP), by ERK2 and ERK2 E320K. (C) Comparison of the nuclear/cytoplasmic ratios of overexpressed FLAG-ERK2 versus FLAG-ERK2 E320K (FLAG immunofluorescence) and total ppERK2 and ppERK2 E320K (pT183/pY185 immunofluorescence) over time following ERK stimulation by 20% FBS. Performed by Chonlarat Wichaidit and Svetlana Earnest (D) Comparison of FLAG-ERK2 and FLAG-ERK2 E320K activation (pT183/pY185), and the effect of approximately 1:1 concentrations (mimicking a single allele) of FLAG-ERK2 and FLAG-ERK2 E320K to endogenous ERK2 on overexpressed transcription factor His_6-ELK1 S383 phosphorylation (ELK1 pS383) over time following ERK stimulation by 20% FBS. Experiment performed with the assistance of Svetlana Earnest. Endogenous ELK1 expression in HeLa cells was too weak to be detected.

ERK2 E320K is Associated with Enhanced Activation, Nuclear Accumulation, and ELK-1 Transcription Factor Phosphorylation

As shown previously in an oral squamous cell carcinoma cell line (HSC6) harboring the E320K mutation, ERK2 E320K has enhanced basal phosphorylation (Arvind, Shimamoto et al. 2005). Based on the differences of active ppERK2 and ppERK2 E320K, we asked whether there were also differences in nuclear accumulation. It is well known that once activated, ERK2 translocates to the nucleus, where it regulates the transcription of target genes (Khokhlatchev, Canagarajah et al. 1998, Yazicioglu, Goad et al. 2007, Wortzel and Seger 2011). Using immunofluorescent labeling (fluorescently-labeled pT183/pY185 and FLAG antibodies) and overexpressed, FLAG-tagged ERK2 and ERK2 E320K in HeLa cells, Chonlarat Wichaidit and Svetlana Earnest compared the nuclear to cytoplasmic ratios of total and active ERK2 and ERK2

E320K up to 20 minutes after stimulation with 20% FBS. Active ppERK2 E320K was elevated in the nucleus prior to stimulation. Five minutes after stimulation both ppERK2 and ppERK2 E320K nuclear accumulation peaked to similar levels, but ERK2 E320K remained elevated in the nucleus while ERK2 returned to the pre-stimulated state (Figure 4-8C). On the other hand, total ERK2 and ERK2 E320K nuclear accumulation showed similar trends, with both becoming elevated following stimulation with a modest increase in ERK2 over ERK2 E320K. The similarity in nuclear accumulation of total ERK2 and ERK2 E320K implies that the docking site mutation does not directly affect nuclear/cytoplasmic shuttling of ERK2 E320K, and any differences likely arise out of differences in the amounts of phosphorylated ERK2 and ERK2 E320K. This data implies that although ERK2 E320K may not interact as well with some proteins that sequester it in the cytosol, such as PEA-15, this does not seem to affect nuclear localization in the absence of stimulation (Figure 4-7A).

Since active ppERK2 E320K was found to be more concentrated in the nucleus, and both docking sites seem to be affected by the mutation, I then asked whether there was a difference in nuclear substrate phosphorylation. ELK1, a well-studied nuclear substrate of ERK2, is phosphorylated by ERK2 at multiple sites, including S383, following ERK2 activation (Gille, Kortenjann et al. 1995, Cruzalegui, Cano et al. 1999). Phosphorylation of ELK1 activates its transcriptional activator activity, which leads to enhanced transcription of target genes, such as FOS, which encodes proto-oncogene c-Fos (Verykokakis, Papadaki et al. 2007). In addition ELK1 also can interact with ERK2 at both the CD and F sites, and mutations at either of these sites leads to a greater than 100-fold decrease in K_D (Burkhard, Chen et al. 2011). With assistance from Svetlana Earnest, and using HeLa cells with overexpressed FLAG ERK2 and

ERK2 E320K, and overexpressed His_6-ELK1 (endogenous ELK1 was undetectable by western blot), we found that phosphorylation of ELK1 at S383 (ELK1 pS383 antibody) was enhanced prior to stimulation, and was consistently elevated to higher levels over 30 minutes following stimulation with 20% FBS in cells overexpressing ERK2 E320K (Figure 4-8D).

In the same experiment ERK2 phosphorylation was also monitored (Figure 4-8D) and was found to follow similar trends in activation of ERK2 and ERK2 E320K as were observed for ELK1 phosphorylation and ppERK2 nuclear accumulation, with enhanced basal activation and higher levels of activating phosphorylation at all time points following FBS stimulation for ERK2 E320K(Figure 4-8D). These combined results demonstrate that enhanced ERK2 E320K phosphorylation leads to both enhanced nuclear accumulation and transcription factor phosphorylation, and imply that ERK2 E320K nuclear signaling is enhanced compared ERK2.

Also surprising is the fact that, even though the CD site is disrupted and the F site appears to also be affected by the mutation, ERK2 E320K is still capable of phosphorylating ELK-1 to a greater extent than ERK2. A previous study has clearly demonstrated that ERK2 D319N is capable of phosphorylating ELK1 to a similar extent as ERK2, but that F-site mutant ERK2 L198A/L235A loses all ability to phosphorylate ELK1, in part due to its inability to be activated by MEK1 (Burkhard, Chen et al. 2011). Therefore, the fact that ERK2 E320K is activated similarly to ERK2 *in vitro* and to a greater extent in cells, and can phosphorylate ELK-1 to a greater extent suggests both that some docking site interactions may be dispensable for ERK2 signaling and that F site interactions are likely disrupted in only some instances (Figure 4-8D).

Discussion

Many cancers employ enhanced signaling through the ERK1/2 MAPK pathway due to the pathway's role in numerous cellular processes such as growth, proliferation, metabolism, etc... (Burotto, Chiou et al. 2014). Although most known oncogenic mutations that lead to aberrant stimulation of the ERK1/2 MAPK pathway are found in the Ras GTPases, and to a lesser Raf kinases, no known oncogenic mutations have been identified within ERK1/2 (Vakiani and Solit 2011, Roskoski 2012). However, within the last ten years a mutation that leads to a buried charge reversal within the ERK2 CD site, E320K (human E322K) has been gaining increased attention (Arvind, Shimamoto et al. 2005, Yazicioglu, Goad et al. 2007, Mahalingam, Arvind et al. 2008, Ojesina, Lichtenstein et al. 2013, Goetz, Ghandi et al. 2014, Van Allen, Lui et al. 2015, Brenan, Andreev et al. 2016, Chang, Asthana et al. 2016).

The ERK2 E320K mutation in human cancers is enriched nearly seven-fold compared to the next most common mutation, D319N (human D321N), which consequently, is also in the ERK2 CD site (Figure 1-11) ((Cerami, Gao et al. 2012, Gao, Aksoy et al. 2013). However, if disruption of CD site signaling, such as loss of interaction with ERK2-inactivating DUSPs, were the only selective advantage that the mutation confers, then the expectation would be that other CD site disrupting mutations should be relatively equally enriched.

The results of this work clearly demonstrate that CD site function is ablated in ERK2 E320K, and that dephosphorylation by DUSP6, and likely all KIM motif-containing DUSPS, is severely compromised. However, this was anticipated, as previously characterized mutations, such as D319N, have such effects (Tanoue, Adachi et al. 2000, Zhou, Wu et al. 2001, Zhang, Zhou et al. 2003). However, unlike D319, which points away from the core kinase domain into

solvent, E320 extends from the L16 loop and faces inward towards the kinase domain making several hydrogen bonds, as well as electrostatic interactions with K136 (Figure 1-13A). I determined the crystal structure of ERK2 E320K to understand the potential structural effects of the mutation. As expected, the CD site and L16 loop around E320K were disrupted. However, what was unanticipated was the degree to which the mutation affected the structure of ERK2. Almost no electron density was even visible above the noise for residues 318 to 325 (Figure 4-4B,C), and this was associated with complete disruption of binding to KIM-containing interaction partners, such as RSKs and DUSP6 (Figure 4-6, Table 5-2. In addition, the adjacent ERK2 dimerization interface was also structurally distorted (Figure 4-5), and ERK2 dimerization *in situ* was diminished (Figure 4-6C). The high B-factors and partial disorder of electron density observed in the C-terminal domain of ERK2 E320K is suggestive of enhanced interdomain mobility, which likely manifested as high C-terminal domain B-factors due to the majority of crystal contacts being present in the N-terminal domain. Perhaps most unexpected was the solvent exposure of activating phosphorylation sites T183 and Y185 (Figure 4-4), and loss of contact between the activation loop and F site. Interactions at the F site were found to be disrupted in some cases (Figure 4-7A,C). The commonly accepted view is that upon activation of ERK2 exposure of the F site enhances interactions, however my results also suggest that contact between the phosphorylated activation loop and elements of the F site may be required for proper interactions with FxF motifs in ERK2 interaction partners.

Although many interactions appear to be affected by the mutation, including those with activating MEKs (Figure 4-6A,D), ERK2 E320K is still activated by MEK1 as well as ERK2, and has similar activity once activated (Figure 4-8). The idea recently put forward by my mentor, Dr. Melanie Cobb, is that MEK1/2 can bypass the normal requirement for docking-induced

activation loop exposure prior to ERK2 activation due to the solvent exposure of the ERK2 E320K activation loop. Once activated ERK2 E320K likely assumes a structure similar to that observed in the structure if active ppERK2, which is supported by both *in vitro* and cellular experiments assessing ERK2 E320K activity (Figure 4-8).

Undoubtedly, the effects of the E320K mutation on ERK2 structure and function can be classified as pleiotropic; affecting protein-protein interactions at multiple sites as well as areas of the kinase distal to the mutation. However, at the core of this significant alteration of signaling inputs and outputs of ERK2 brought about by the E320K mutation, our results suggest that there are two core complementary mechanisms at work (Figure 4-9A). First, the E320K mutation severely diminishes the ability of ERK2 to be deactivated by phosphatases, such as DUSP6. Second, and somewhat unexpected, that the mutation facilitates MEK1/2 activation, even in the presence of diminished interactions. Therefore, activation loop solvent exposure appears to be the most likely candidate for the enrichment of the E320K mutation in cancer as opposed to other docking site mutations that likely do not affect activation loop solvent accessibility. Future studies aimed at understanding the importance of this mutation in cancer will be needed in order to determine if therapies designed to block ERK1/2 MAPK signaling are warranted (Figure 4-9B).

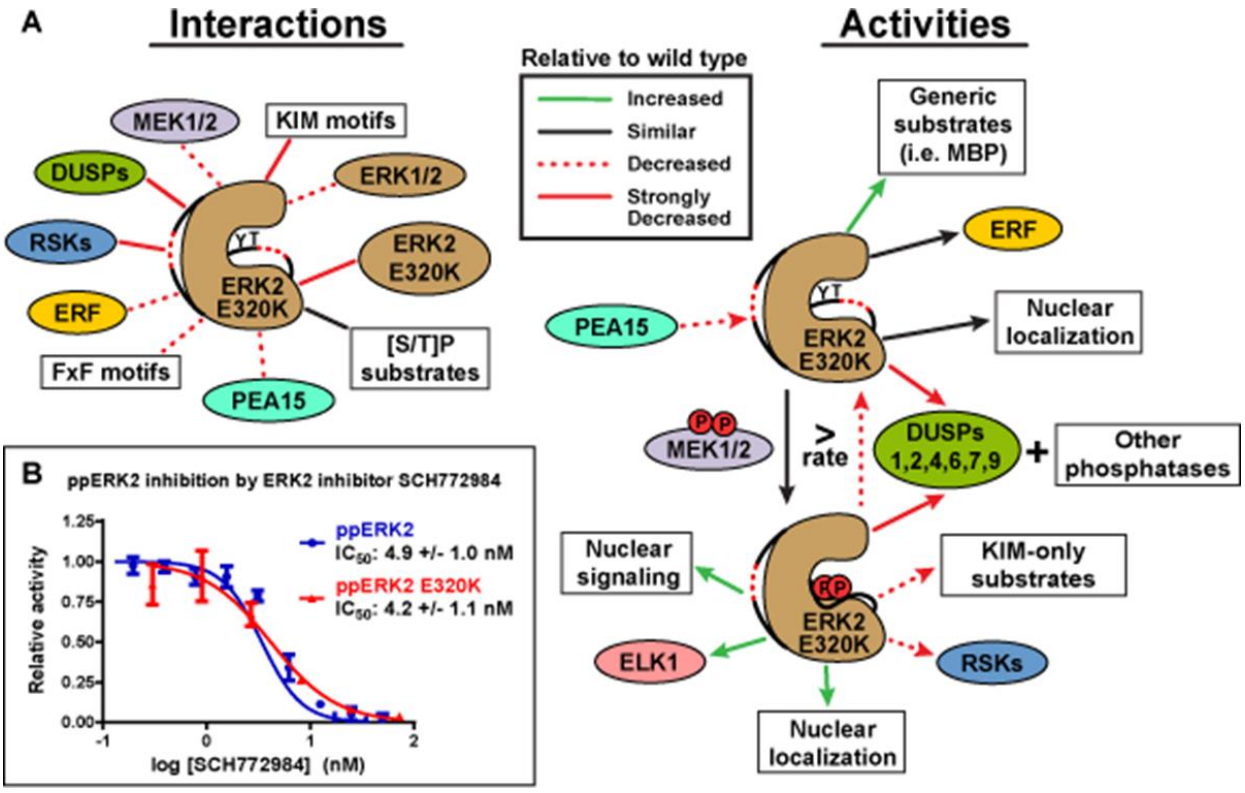

Figure 4-9. A model of signaling by ERK2 E320K.

(A) Models of ERK2 E320K signaling broken down into changes in interactions and activities compared to wild type ERK2. Lines represent protein:protein interactions in the Interactions panel and arrows represent enzymatic activity and functions in the Activities panel. Green solid line: increased; black solid line: similar; red dashed line: decreased; red solid line: strongly decreased or abolished. Cartoon of ERK2 E320K indicates important structural elements as black lines and red dashed lines are disordered residues within those structural elements. (B) IC_{50} determination of an ERK2 inhibitor (SCH772984) towards active ppERK2 and ppERK2 E320K. ppERK2 IC_{50} determined by IMAP FP monitoring phosphorylation of ERKtide-FAM and ppERK2 E320K IC_{50} determined by monitoring ^{32}P incorporation on MBP. Kinase at 1 nM concentration.

CHAPTER FIVE

FUTURE DIRECTIONS

SPAK/OSR1 Activation Loop Domain-Swapping

The results of this project led to a better structural understanding of the activation mechanism of SPAK and OSR1 kinases, identified a novel mutation that could inhibit activation loop-mediated dimerization, and showed that the monomeric form of the kinase is active and can be activated by WNK1. However, the study has left open many questions.

Our results suggest a multistage activation mechanism, and it has been shown that the protein Mo25 can activate constitutively active SPAK and OSR1 mutants by nearly another 100-fold, presumably by stabilizing the αC helix, as has been shown in the related MST3 and MST4 kinases (Zeqiraj, Filippi et al. 2009, Mehellou, Alessi et al. 2013, Shi, Jiao et al. 2013, Hao, Feng et al. 2014). Interestingly, based on alignment between the SPAK dimer and the complex between MST4 and Mo25, it appears that Mo25 binding to one of the subunits of the SPAK dimer is possible, which would generate an asymmetric complex where one of the subunits is further activated by Mo25. Whether this would facilitate asymmetric transactivation is an interesting question that will undoubtedly need to be answered in the future. Additional investigation of the dimerization-deficient mutant in cells will also likely be required to better understand the role of SPAK/OSR1 activation loop domain-swapping.

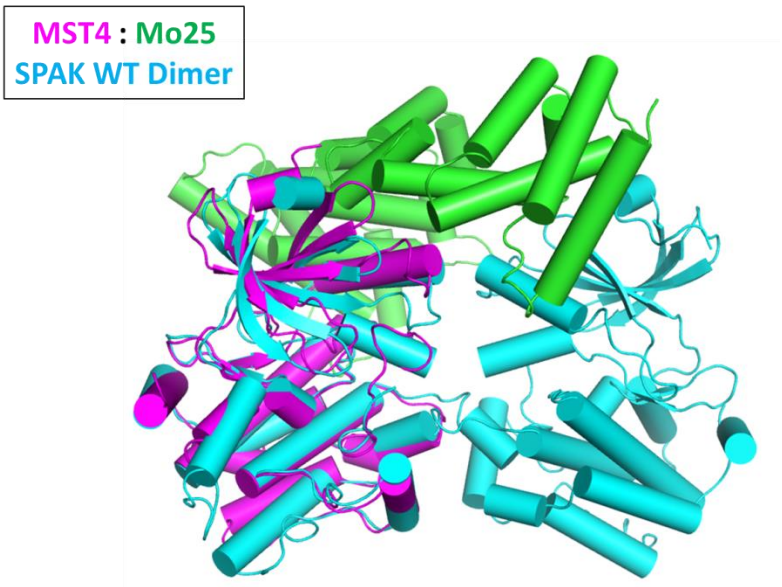

Figure 5-1. Mo25 binding is compatible with the SPAK dimer.

Alignment of the structures of MST4:Mo25 and the SPAK dimer (PDB 4FZA and 5D9H). The alignment implies that the SPAK dimer is compatible with asymmetric binding by Mo25.

New SPAK/OSR1 Interaction Partners

My method for predicting, ranking, and filtering SPAK/OSR1 CCT domain interactions has likely uncovered many new interaction partners, such as the IRK channels. Extensive work will be required to further validate some of these interactions. The initial results of the validation process have potentially uncovered a group of potassium channels that are regulated by the WNK pathway. It is likely that many more interesting new interactions will be validated, further expanding the role of the WNK pathway in multiple cellular processes.

Also of interest is the fact that WNK kinases contain auto-inhibitory (AI) domains adjacent to the kinase domains that have a nearly identical fold and conserved binding site residues as seen in the SPAK/OSR1 CCT domains (Figure 5-2A) (Xu, Min et al. 2002, Villa, Goebel et al. 2007, Moon, Correa et al. 2013). My initial fluorescence anisotropy experiments

using R-F-X-V probes did not detect binding between the domain and the labeled peptides (data not shown). However, the WNK1 AI domain did have a unique specificity profile compared to the CCT domains as determined by peptide array (Figure5-2B). Additional work to find a physiological interaction partner with a defined motif will be required to begin to delineate the similarities and differences in specificity between the CCT domains and AI domains.

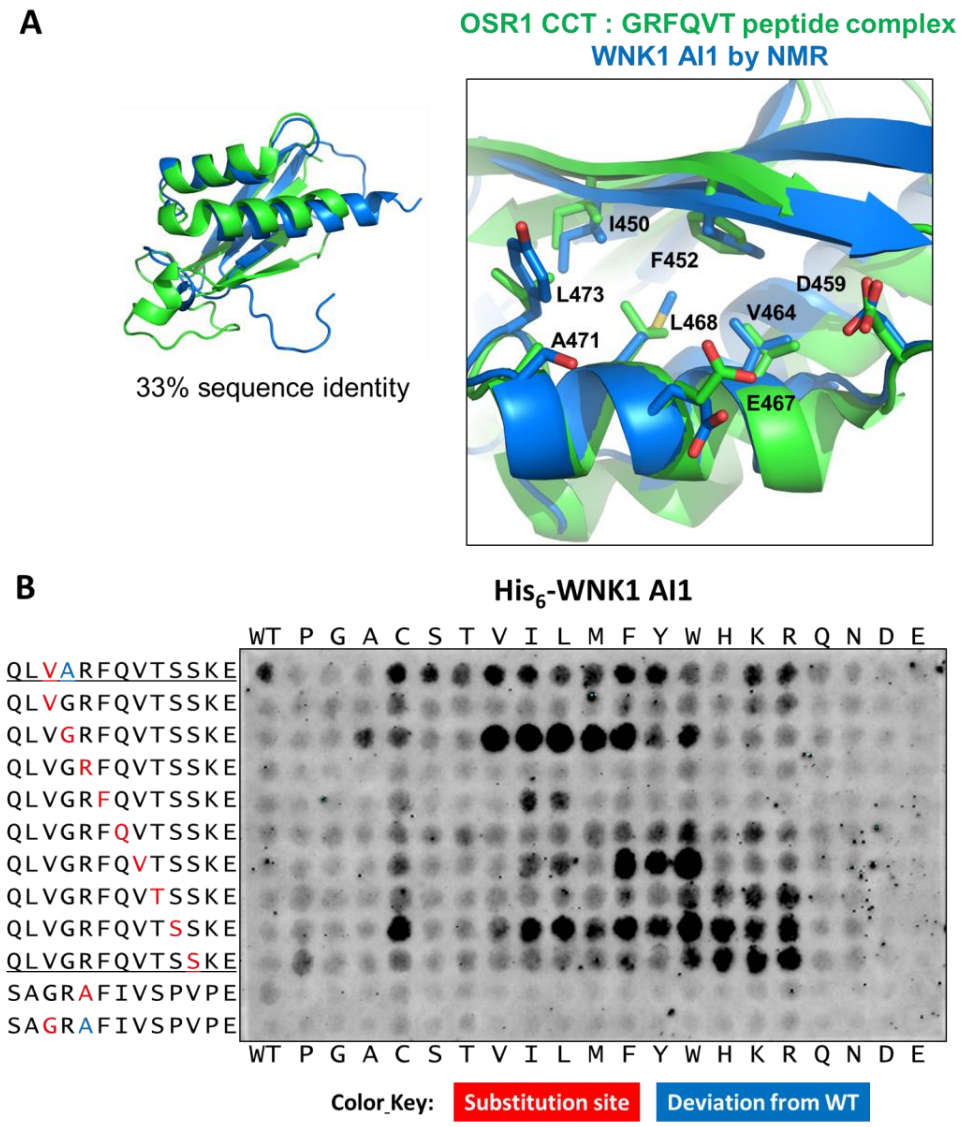

Figure 5-2. WNK1 AI1 has partially overlapping binding specificity compared to SPAK/OSR1 CCT domain.

Alignment of the crystal structure of the OSR1 CCT domain and NMR structure of the WNK1 AI domain (PDB 2V3S and 2LRU). Peptide array blot with His_6-WNK1 AI.

How Relevant is the ERK2 E322K Mutation to Cancer?

We have thoroughly characterized both the structural and functional effects of the E322K mutation in the MAPK1 gene encoding ERK2. The mutation not only prevents normal deactivation by DUSP6, but still permits normal activation by MEK1 R4F. This translates to increased ERK2 activation, nuclear localization, and transcription factor phosphorylation. We showed structurally that this is due to both CD site disruption and a dysregulated activation loop conformation. In addition, we showed that other sites of protein-protein interactions were altered.

The immediate question is whether the E322K mutation is truly an oncogenic mutation. Some evidence, such as a strong patient response to the RTK inhibitor erlotinib in the presence of the E322K mutation, suggests that it is, but more definitive studies will need to be conducted (Van Allen, Lui et al. 2015).

Additional work will also be required in order to further define the implications of disruption of the CD site and the other ERK2 docking sites. Are the other KIM-containing DUSPs also not activated by ERK2 E322K, and does this translate to these DUSPs not being able to dephosphorylate ERK2 and potentially other substrates? What F site interactions are affected by the mutation and what are the resulting phenotypes? How does disruption of dimerization affect signaling? These are all questions that have been generated as a result of the present study, and will likely require many additional studies to fully understand.

Adams, P. D., P. V. Afonine, G. Bunkoczi, V. B. Chen, I. W. Davis, N. Echols, J. J. Headd, L. W. Hung, G. J. Kapral, R. W. Grosse-Kunstleve, A. J. McCoy, N. W. Moriarty, R. Oeffner, R. J. Read, D. C. Richardson, J. S. Richardson, T. C. Terwilliger and P. H. Zwart (2010). "PHENIX: a comprehensive Python-based system for macromolecular structure solution." Acta Crystallogr D Biol Crystallogr **66**(Pt 2): 213-221.

Afonine, P. V., R. W. Grosse-Kunstleve, N. Echols, J. J. Headd, N. W. Moriarty, M. Mustyakimov, T. C. Terwilliger, A. Urzhumtsev, P. H. Zwart and P. D. Adams (2012). "Towards automated crystallographic structure refinement with phenix.refine." Acta Crystallogr D Biol Crystallogr **68**(Pt 4): 352-367.

Akella, R., X. Min, Q. Wu, K. H. Gardner and E. J. Goldsmith (2010). "The third conformation of p38alpha MAP kinase observed in phosphorylated p38alpha and in solution." Structure **18**(12): 1571-1578.

Alessi, D. R., J. Zhang, A. Khanna, T. Hochdörfer, Y. Shang and K. T. Kahle (2014). The WNK-SPAK/OSR1 pathway: Master regulator of cation-chloride cotransporters. Sci. Signal. **7**(334).

Altschul, S. F., W. Gish, W. Miller, E. W. Myers and D. J. Lipman (1990). "Basic local alignment search tool." J Mol Biol **215**(3): 403-410.

Anselmo, A. N., S. Earnest, W. Chen, Y. C. Juang, S. C. Kim, Y. Zhao and M. H. Cobb (2006). "WNK1 and OSR1 regulate the Na+, K+, 2Cl- cotransporter in HeLa cells." Proc Natl Acad Sci U S A **103**(29): 10883-10888.

Arvind, R., H. Shimamoto, F. Momose, T. Amagasa, K. Omura and N. Tsuchida (2005). "A mutation in the common docking domain of ERK2 in a human cancer cell line, which was associated with its constitutive phosphorylation." Int J Oncol **27**(6): 1499-1504.

Austin, T. M., D. P. Nannemann, S. L. Deluca, J. Meiler and E. Delpire (2014). "In silico analysis and experimental verification of OSR1 kinase – Peptide interaction." Journal of Structural Biology **187**(1): 58-65.

Bogan, A. A. and K. S. Thorn (1998). "Anatomy of hot spots in protein interfaces." J Mol Biol **280**(1): 1-9.

Boulton, T. G., G. D. Yancopoulos, J. S. Gregory, C. Slaughter, C. Moomaw, J. Hsu and M. H. Cobb (1990). "An insulin-stimulated protein kinase similar to yeast kinases involved in cell cycle control." Science **249**(4964): 64-67.

Brenan, L., A. Andreev, O. Cohen, S. Pantel, A. Kamburov, D. Cacchiarelli, Nicole S. Persky, C. Zhu, M. Bagul, Eva M. Goetz, Alex B. Burgin, Levi A. Garraway, G. Getz, Tarjei S. Mikkelsen, F. Piccioni, David E. Root and Cory M. Johannessen (2016). "Phenotypic Characterization of a Comprehensive Set of MAPK1/ERK2 Missense Mutants." Cell Reports **17**(4): 1171-1183.

Briant, D. J., J. M. Murphy, G. C. Leung and F. Sicheri (2009). "Rapid identification of linear protein domain binding motifs using peptide SPOT arrays." Methods Mol Biol **570**: 175-185.

Brunner, D., N. Oellers, J. Szabad, W. H. Biggs, 3rd, S. L. Zipursky and E. Hafen (1994). "A gain-of-function mutation in Drosophila MAP kinase activates multiple receptor tyrosine kinase signaling pathways." Cell **76**(5): 875-888.

Burkhard, K. A., F. Chen and P. Shapiro (2011). "Quantitative analysis of ERK2 interactions with substrate proteins: roles for kinase docking domains and activity in determining binding affinity." J Biol Chem **286**(4): 2477-2485.

Burotto, M., V. L. Chiou, J. M. Lee and E. C. Kohn (2014). "The MAPK pathway across different malignancies: a new perspective." Cancer **120**(22): 3446-3456.

Camps, M., A. Nichols, C. Gillieron, B. Antonsson, M. Muda, C. Chabert, U. Boschert and S. Arkinstall (1998). "Catalytic activation of the phosphatase MKP-3 by ERK2 mitogen-activated protein kinase." Science **280**(5367): 1262-1265.

Canagarajah, B. J., A. Khokhlatchev, M. H. Cobb and E. J. Goldsmith (1997). "Activation Mechanism of the MAP Kinase ERK2 by Dual Phosphorylation." Cell **90**(5): 859-869.

Castaneda-Bueno, M. and G. Gamba (2010). "SPAKling insight into blood pressure regulation." EMBO Mol Med **2**(2): 39-41.

Cerami, E., J. Gao, U. Dogrusoz, B. E. Gross, S. O. Sumer, B. A. Aksoy, A. Jacobsen, C. J. Byrne, M. L. Heuer, E. Larsson, Y. Antipin, B. Reva, A. P. Goldberg, C. Sander and N. Schultz (2012). "The cBio Cancer Genomics Portal: An Open Platform for Exploring Multidimensional Cancer Genomics Data." Cancer Discovery **2**(5): 401-404.

Chang, C. I., B. E. Xu, R. Akella, M. H. Cobb and E. J. Goldsmith (2002). "Crystal structures of MAP kinase p38 complexed to the docking sites on its nuclear substrate MEF2A and activator MKK3b." Mol Cell **9**(6): 1241-1249.

Chang, M. T., S. Asthana, S. P. Gao, B. H. Lee, J. S. Chapman, C. Kandoth, J. Gao, N. D. Socci, D. B. Solit, A. B. Olshen, N. Schultz and B. S. Taylor (2016). "Identifying recurrent mutations in cancer reveals widespread lineage diversity and mutational specificity." Nat Biotech **34**(2): 155-163.

Chen, W., M. Yazicioglu and M. H. Cobb (2004). "Characterization of OSR1, a member of the mammalian Ste20p/germinal center kinase subfamily." J Biol Chem **279**(12): 11129-11136.

Cheng, C. J., C. C. Sung, C. L. Huang and S. H. Lin (2015). "Inward-rectifying potassium channelopathies: new insights into disorders of sodium and potassium homeostasis." Pediatr Nephrol **30**(3): 373-383.

Clackson, T. and J. Wells (1995). "A hot spot of binding energy in a hormone-receptor interface." Science **267**(5196): 383-386.

Cruzalegui, F. H., E. Cano and R. Treisman (1999). "ERK activation induces phosphorylation of Elk-1 at multiple S/T-P motifs to high stoichiometry." Oncogene **18**(56): 7948-7957.

Dan, I., N. M. Watanabe and A. Kusumi (2001). "The Ste20 group kinases as regulators of MAP kinase cascades." Trends Cell Biol **11**(5): 220-230.

Dang, A., J. A. Frost and M. H. Cobb (1998). "The MEK1 proline-rich insert is required for efficient activation of the mitogen-activated protein kinases ERK1 and ERK2 in mammalian cells." J Biol Chem **273**(31): 19909-19913.

Darman, R. B. and B. Forbush (2002). "A regulatory locus of phosphorylation in the N terminus of the Na-K-Cl cotransporter, NKCC1." J Biol Chem **277**(40): 37542-37550.

Davis, I. W., L. W. Murray, J. S. Richardson and D. C. Richardson (2004). "MOLPROBITY: structure validation and all-atom contact analysis for nucleic acids and their complexes." Nucleic Acids Res **32**: W615-619.

de Los Heros, P., D. R. Alessi, R. Gourlay, D. G. Campbell, M. Deak, T. J. Macartney, K. T. Kahle and J. Zhang (2014). "The WNK-regulated SPAK/OSR1 kinases directly phosphorylate and inhibit the K+-Cl- co-transporters." Biochem J **458**(3): 559-573.

Delpire, E. and K. B. Gagnon (2007). "Genome-wide analysis of SPAK/OSR1 binding motifs." Physiol Genomics **28**(2): 223-231.

Denton, J., K. Nehrke, X. Yin, R. Morrison and K. Strange (2005). "GCK-3, a newly identified Ste20 kinase, binds to and regulates the activity of a cell cycle-dependent ClC anion channel." J Gen Physiol **125**(2): 113-125.

Dowd, B. F. and B. Forbush (2003). "PASK (proline-alanine-rich STE20-related kinase), a regulatory kinase of the Na-K-Cl cotransporter (NKCC1)." J Biol Chem **278**(30): 27347-27353.

Emsley, P. and K. Cowtan (2004). "Coot: model-building tools for molecular graphics." Acta Crystallogr D Biol Crystallogr **60**(Pt 12 Pt 1): 2126-2132.

Filippi, B. M., P. de los Heros, Y. Mehellou, I. Navratilova, R. Gourlay, M. Deak, L. Plater, R. Toth, E. Zeqiraj and D. R. Alessi (2011). "MO25 is a master regulator of SPAK/OSR1 and MST3/MST4/YSK1 protein kinases." EMBO J **30**(9): 1730-1741.

Gagnon, K. B. and E. Delpire (2010). "Multiple pathways for protein phosphatase 1 (PP1) regulation of Na-K-2Cl cotransporter (NKCC1) function: the N-terminal tail of the Na-K-2Cl cotransporter serves as a regulatory scaffold for Ste20-related proline/alanine-rich kinase (SPAK) AND PP1." J Biol Chem **285**(19): 14115-14121.

Gagnon, K. B. and E. Delpire (2010). "On the substrate recognition and negative regulation of SPAK, a kinase modulating Na+-K+-2Cl- cotransport activity." Am J Physiol Cell Physiol **299**(3): C614-620.

Gagnon, K. B. and E. Delpire (2012). "Molecular physiology of SPAK and OSR1: two Ste20-related protein kinases regulating ion transport." Physiol Rev **92**(4): 1577-1617.

Gagnon, K. B., R. England and E. Delpire (2006). "Characterization of SPAK and OSR1, regulatory kinases of the Na-K-2Cl cotransporter." Mol Cell Biol **26**(2): 689-698.

Gagnon, K. B., R. England and E. Delpire (2006). "Volume sensitivity of cation-Cl- cotransporters is modulated by the interaction of two kinases: Ste20-related proline-alanine-rich kinase and WNK4." Am J Physiol Cell Physiol **290**(1): C134-142.

Gagnon, K. B., R. England and E. Delpire (2007). "A single binding motif is required for SPAK activation of the Na-K-2Cl cotransporter." Cell Physiol Biochem **20**(1-4): 131-142.

Gagnon, K. B., R. England, L. Diehl and E. Delpire (2007). "Apoptosis-associated tyrosine kinase scaffolding of protein phosphatase 1 and SPAK reveals a novel pathway for Na-K-2C1 cotransporter regulation." Am J Physiol Cell Physiol **292**(5): C1809-1815.

Gao, J., B. A. Aksoy, U. Dogrusoz, G. Dresdner, B. Gross, S. O. Sumer, Y. Sun, A. Jacobsen, R. Sinha, E. Larsson, E. Cerami, C. Sander and N. Schultz (2013). "Integrative analysis of complex cancer genomics and clinical profiles using the cBioPortal." Sci Signal **6**(269): pl1.

Gille, H., M. Kortenjann, O. Thomae, C. Moomaw, C. Slaughter, M. H. Cobb and P. E. Shaw (1995). "ERK phosphorylation potentiates Elk-1-mediated ternary complex formation and transactivation." EMBO J **14**(5): 951-962.

Goetz, E. M., M. Ghandi, D. J. Treacy, N. Wagle and L. A. Garraway (2014). "ERK mutations confer resistance to mitogen-activated protein kinase pathway inhibitors." Cancer Res **74**(23): 7079-7089.

Goldsmith, E. J., R. Akella, X. Min, T. Zhou and J. M. Humphreys (2007). "Substrate and docking interactions in serine/threonine protein kinases." Chem Rev **107**(11): 5065-5081.

Grimm, P. R., T. K. Taneja, J. Liu, R. Coleman, Y. Y. Chen, E. Delpire, J. B. Wade and P. A. Welling (2012). "SPAK isoforms and OSR1 regulate sodium-chloride co-transporters in a nephron-specific manner." J Biol Chem **287**(45): 37673-37690.

Hao, Q., M. Feng, Z. Shi, C. Li, M. Chen, W. Wang, M. Zhang, S. Jiao and Z. Zhou (2014). "Structural insights into regulatory mechanisms of MO25-mediated kinase activation." Journal of Structural Biology **186**(2): 224-233.

Heidenreich, P. A., J. G. Trogdon, O. A. Khavjou, J. Butler, K. Dracup, M. D. Ezekowitz, E. A. Finkelstein, Y. Hong, S. C. Johnston, A. Khera, D. M. Lloyd-Jones, S. A. Nelson, G. Nichol, D. Orenstein, P. W. Wilson and Y. J. Woo (2011). "Forecasting the future of cardiovascular disease in the United States: a policy statement from the American Heart Association." Circulation **123**(8): 933-944.

Jain, S. and G. D. Bader (2016). "Predicting physiologically relevant SH3 domain mediated protein-protein interactions in yeast." Bioinformatics **32**(12): 1865-1872.

Jones, S. and J. M. Thornton (1996). "Principles of protein-protein interactions." Proc Natl Acad Sci U S A **93**(1): 13-20.

Keshet, Y. and R. Seger (2010). "The MAP kinase signaling cascades: a system of hundreds of components regulates a diverse array of physiological functions." Methods Mol Biol **661**: 3-38.

Khokhlatchev, A. V., B. Canagarajah, J. Wilsbacher, M. Robinson, M. Atkinson, E. Goldsmith and M. H. Cobb (1998). "Phosphorylation of the MAP kinase ERK2 promotes its homodimerization and nuclear translocation." Cell **93**(4): 605-615.

Knighton, D. R., J. H. Zheng, L. F. Ten Eyck, V. A. Ashford, N. H. Xuong, S. S. Taylor and J. M. Sowadski (1991). "Crystal structure of the catalytic subunit of cyclic adenosine monophosphate-dependent protein kinase." Science **253**(5018): 407-414.

Krissinel, E. and K. Henrick (2007). "Inference of macromolecular assemblies from crystalline state." J Mol Biol **372**(3): 774-797.

Lazrak, A., Z. Liu and C. L. Huang (2006). "Antagonistic regulation of ROMK by long and kidney-specific WNK1 isoforms." Proc Natl Acad Sci U S A **103**(5): 1615-1620.

le Gallic, L., D. Sgouras, G. Beal and G. Mavrothalassitis (1999). "Transcriptional Repressor ERF Is a Ras/Mitogen-Activated Protein Kinase Target That Regulates Cellular Proliferation." Molecular and Cellular Biology **19**(6): 4121-4133.

Lee, S. J., M. H. Cobb and E. J. Goldsmith (2009). "Crystal structure of domain-swapped STE20 OSR1 kinase domain." Protein Sci **18**(2): 304-313.

Lee, T., A. N. Hoofnagle, Y. Kabuyama, J. Stroud, X. Min, E. J. Goldsmith, L. Chen, K. A. Resing and N. G. Ahn (2004). "Docking Motif Interactions in MAP Kinases Revealed by Hydrogen Exchange Mass Spectrometry." Molecular Cell **14**(1): 43-55.

Leiserson, W. M., E. W. Harkins and H. Keshishian (2000). "Fray, a Drosophila serine/threonine kinase homologous to mammalian PASK, is required for axonal ensheathment." Neuron **28**(3): 793-806.

Lemmon, M. A. and J. Schlessinger (2010). "Cell signaling by receptor tyrosine kinases." Cell **141**(7): 1117-1134.

Lenertz, L. Y., B. H. Lee, X. Min, B. E. Xu, K. Wedin, S. Earnest, E. J. Goldsmith and M. H. Cobb (2005). "Properties of WNK1 and implications for other family members." J Biol Chem **280**(29): 26653-26658.

Li, C., M. Feng, Z. Shi, Q. Hao, X. Song, W. Wang, Y. Zhao, S. Jiao and Z. Zhou (2014). "Structural and Biochemical Insights into the Activation Mechanisms of Germinal Center Kinase OSR1." J Biol Chem. **289**(52) 35969-78.

Li, S. C. and C. Wu (2009). Using Peptide Array to Identify Binding Motifs and Interaction Networks for Modular Domains. Peptide Microarrays. M. Cretich and M. Chiari, Humana Press. **570:** 67-76.

Li, Y., Y. Huang, C. P. Swaminathan, S. J. Smith-Gill and R. A. Mariuzza (2005). "Magnitude of the hydrophobic effect at central versus peripheral sites in protein-protein interfaces." Structure **13**(2): 297-307.

Liu, S., J. P. Sun, B. Zhou and Z. Y. Zhang (2006). "Structural basis of docking interactions between ERK2 and MAP kinase phosphatase 3." Proc Natl Acad Sci U S A **103**(14): 5326-5331.

Liu, Z., H. R. Wang and C. L. Huang (2009). "Regulation of ROMK channel and K+ homeostasis by kidney-specific WNK1 kinase." J Biol Chem **284**(18): 12198-12206.

Liu, Z., J. Xie, T. Wu, T. Truong, R. J. Auchus and C. L. Huang (2011). "Downregulation of NCC and NKCC2 cotransporters by kidney-specific WNK1 revealed by gene disruption and transgenic mouse models." Hum Mol Genet **20**(5): 855-866.

London, N., D. Movshovitz-Attias and O. Schueler-Furman (2010). "The Structural Basis of Peptide-Protein Binding Strategies." Structure **18**(2): 188-199.

Mace, P. D., Y. Wallez, M. F. Egger, M. K. Dobaczewska, H. Robinson, E. B. Pasquale and S. J. Riedl (2013). "Structure of ERK2 bound to PEA-15 reveals a mechanism for rapid release of activated MAPK." Nat Commun **4**: 1681.

Mahalingam, M., R. Arvind, H. Ida, A. K. Murugan, M. Yamaguchi and N. Tsuchida (2008). "ERK2 CD domain mutation from a human cancer cell line enhanced anchorage-independent cell growth and abnormality in Drosophila." Oncol Rep **20**(4): 957-962.

Manning, G., D. B. Whyte, R. Martinez, T. Hunter and S. Sudarsanam (2002). "The protein kinase complement of the human genome." Science **298**(5600): 1912-1934.

Mansour, S. J., W. T. Matten, A. S. Hermann, J. M. Candia, S. Rong, K. Fukasawa, G. F. Vande Woude and N. G. Ahn (1994). "Transformation of mammalian cells by constitutively active MAP kinase kinase." Science **265**(5174): 966-970.

Markadieu, N. and E. Delpire (2014). "Physiology and pathophysiology of SLC12A1/2 transporters." Pflugers Arch **466**(1): 91-105.

McCormick, J. A. and D. H. Ellison (2011). "The WNKs: atypical protein kinases with pleiotropic actions." Physiol Rev **91**(1): 177-219.

McCoy, A. J., R. W. Grosse-Kunstleve, P. D. Adams, M. D. Winn, L. C. Storoni and R. J. Read (2007). "Phaser crystallographic software." J Appl Crystallogr **40**(Pt 4): 658-674.

McCoy, A. J., R. W. Grosse-Kunstleve, L. C. Storoni and R. J. Read (2005). "Likelihood-enhanced fast translation functions." Acta Crystallogr D Biol Crystallogr **61**(Pt 4): 458-464.

Mehellou, Y., D. R. Alessi, T. J. Macartney, M. Szklarz, S. Knapp and J. M. Elkins (2013). "Structural insights into the activation of MST3 by MO25." Biochem Biophys Res Commun **431**(3): 604-609.

Moon, T. M., F. Correa, L. N. Kinch, A. T. Piala, K. H. Gardner and E. J. Goldsmith (2013). "Solution structure of the WNK1 autoinhibitory domain, a WNK-specific PF2 domain." J Mol Biol **425**(8): 1245-1252.

Mori, T., E. Kikuchi, Y. Watanabe, S. Fujii, M. Ishigami-Yuasa, H. Kagechika, E. Sohara, T. Rai, S. Sasaki and S. Uchida (2013). "Chemical library screening for WNK signaling inhibitors by using fluorescent correlation spectroscopy." Biochem J. **455**: 339-345.

Moriguchi, T., S. Urushiyama, N. Hisamoto, S. Iemura, S. Uchida, T. Natsume, K. Matsumoto and H. Shibuya (2005). "WNK1 regulates phosphorylation of cation-chloride-coupled cotransporters via the STE20-related kinases, SPAK and OSR1." J Biol Chem **280**(52): 42685-42693.

Murshudov, G. N., A. A. Vagin and E. J. Dodson (1997). "Refinement of macromolecular structures by the maximum-likelihood method." Acta Crystallogr D Biol Crystallogr **53**(Pt 3): 240-255.

Obenauer, J. C., L. C. Cantley and M. B. Yaffe (2003). "Scansite 2.0: Proteome-wide prediction of cell signaling interactions using short sequence motifs." Nucleic Acids Res **31**(13): 3635-3641.

Ojesina, A. I., L. Lichtenstein, S. S. Freeman, C. S. Pedamallu, I. Imaz-Rosshandler, T. J. Pugh, A. D. Cherniack, L. Ambrogio, K. Cibulskis, B. Bertelsen, S. Romero-Cordoba, V. Trevino, K. Vazquez-Santillan, A. S. Guadarrama, A. A. Wright, M. W. Rosenberg, F. Duke, B. Kaplan, R. Wang, E. Nickerson, H. M. Walline, M. S. Lawrence, C. Stewart, S. L. Carter, A. McKenna, I. P. Rodriguez-Sanchez, M. Espinosa-Castilla, K. Woie, L. Bjorge, E. Wik, M. K. Halle, E. A. Hoivik, C. Krakstad, N. B. Gabino, G. S. Gomez-Macias, L. D. Valdez-Chapa, M. L. Garza-Rodriguez, G. Maytorena, J. Vazquez, C. Rodea, A. Cravioto, M. L. Cortes, H. Greulich, C. P. Crum, D. S. Neuberg, A. Hidalgo-Miranda, C. R. Escareno, L. A. Akslen, T. E. Carey, O. K. Vintermyr, S. B. Gabriel, H. A. Barrera-Saldana, J. Melendez-Zajgla, G. Getz, H. B. Salvesen and M. Meyerson (2013). "Landscape of genomic alterations in cervical carcinomas." Nature.

Oliver, A. W., S. Knapp and L. H. Pearl (2007). "Activation segment exchange: a common mechanism of kinase autophosphorylation?" Trends Biochem Sci **32**(8): 351-356.

Oliver, A. W., A. Paul, K. J. Boxall, S. E. Barrie, G. W. Aherne, M. D. Garrett, S. Mittnacht and L. H. Pearl (2006). "Trans-activation of the DNA-damage signalling protein kinase Chk2 by T-loop exchange." EMBO J **25**(13): 3179-3190.

Otwinowski, Z. and W. Minor (1997). Processing of X-ray diffraction data collected in oscillation mode. Methods in Enzymology. Charles W. Carter, Jr., Academic Press. **Volume 276:** 307-326.

Pacheco-Alvarez, D., N. Vazquez, M. Castaneda-Bueno, P. de-Los-Heros, C. Cortes-Gonzalez, E. Moreno, P. Meade, N. A. Bobadilla and G. Gamba (2012). "WNK3-SPAK interaction is required for the modulation of NCC and other members of the SLC12 family." Cell Physiol Biochem **29**(1-2): 291-302.

Painter, J. and E. A. Merritt (2006). "Optimal description of a protein structure in terms of multiple groups undergoing TLS motion." Acta Crystallogr D Biol Crystallogr **62**(Pt 4): 439-450.

Pawson, T. and P. Nash (2003). "Assembly of cell regulatory systems through protein interaction domains." Science **300**(5618): 445-452.

Pegan, S., C. Arrabit, W. Zhou, W. Kwiatkowski, A. Collins, P. A. Slesinger and S. Choe (2005). "Cytoplasmic domain structures of Kir2.1 and Kir3.1 show sites for modulating gating and rectification." Nat Neurosci **8**(3): 279-287.

Peti, W. and R. Page (2013). "Molecular basis of MAP kinase regulation." Protein Sci **22**(12): 1698-1710.

Piala, A. T., T. M. Moon, R. Akella, H. He, M. H. Cobb and E. J. Goldsmith (2014). "Chloride Sensing by WNK1 Involves Inhibition of Autophosphorylation." Sci. Signal. **7**(324): ra41-.

Piechotta, K., J. Lu and E. Delpire (2002). "Cation chloride cotransporters interact with the stress-related kinases Ste20-related proline-alanine-rich kinase (SPAK) and oxidative stress response 1 (OSR1)." J Biol Chem **277**(52): 50812-50819.

Pike, A. C., P. Rellos, F. H. Niesen, A. Turnbull, A. W. Oliver, S. A. Parker, B. E. Turk, L. H. Pearl and S. Knapp (2008). "Activation segment dimerization: a mechanism for kinase autophosphorylation of non-consensus sites." EMBO J **27**(4): 704-714.

Polychronopoulos, S., M. Verykokakis, M. N. Yazicioglu, M. Sakarellos-Daitsiotis, M. H. Cobb and G. Mavrothalassitis (2006). "The Transcriptional ETS2 Repressor Factor Associates with Active and Inactive Erks through Distinct FXF Motifs." J Biol Chem **281**(35): 25601-25611.

Ponce-Coria, J., P. San-Cristobal, K. T. Kahle, N. Vazquez, D. Pacheco-Alvarez, P. de Los Heros, P. Juarez, E. Munoz, G. Michel, N. A. Bobadilla, I. Gimenez, R. P. Lifton, S. C. Hebert and G. Gamba (2008). "Regulation of NKCC2 by a chloride-sensing mechanism involving the WNK3 and SPAK kinases." Proc Natl Acad Sci U S A **105**(24): 8458-8463.

Rafiqi, F. H., A. M. Zuber, M. Glover, C. Richardson, S. Fleming, S. Jovanovic, A. Jovanovic, K. M. O'Shaughnessy and D. R. Alessi (2010). "Role of the WNK-activated SPAK kinase in regulating blood pressure." EMBO Mol Med **2**(2): 63-75.

Remaut, H. and G. Waksman (2006). "Protein–protein interaction through β-strand addition." Trends in Biochemical Sciences **31**(8): 436-444.

Richardson, C. and D. R. Alessi (2008). "The regulation of salt transport and blood pressure by the WNK-SPAK/OSR1 signalling pathway." J Cell Sci **121**(Pt 20): 3293-3304.

Richardson, C., F. H. Rafiqi, H. K. Karlsson, N. Moleleki, A. Vandewalle, D. G. Campbell, N. A. Morrice and D. R. Alessi (2008). "Activation of the thiazide-sensitive Na+-Cl- cotransporter by the WNK-regulated kinases SPAK and OSR1." J Cell Sci **121**(Pt 5): 675-684.

Richardson, C., K. Sakamoto, P. de los Heros, M. Deak, D. G. Campbell, A. R. Prescott and D. R. Alessi (2011). "Regulation of the NKCC2 ion cotransporter by SPAK-OSR1-dependent and -independent pathways." J Cell Sci **124**(Pt 5): 789-800.

Rinehart, J., N. Vazquez, K. T. Kahle, C. A. Hodson, A. M. Ring, E. E. Gulcicek, A. Louvi, N. A. Bobadilla, G. Gamba and R. P. Lifton (2011). "WNK2 kinase is a novel regulator of essential neuronal cation-chloride cotransporters." J Biol Chem **286**(34): 30171-30180.

Robbins, D. J., E. Zhen, H. Owaki, C. A. Vanderbilt, D. Ebert, T. D. Geppert and M. H. Cobb (1993). "Regulation and properties of extracellular signal-regulated protein kinases 1 and 2 in vitro." J Biol Chem **268**(7): 5097-5106.

Roskoski, R., Jr. (2012). "ERK1/2 MAP kinases: structure, function, and regulation." Pharmacol Res **66**(2): 105-143.

Rousseau, F., J. W. Schymkowitz and L. S. Itzhaki (2003). "The unfolding story of three-dimensional domain swapping." Structure **11**(3): 243-251.

Shi, Z., S. Jiao, Z. Zhang, M. Ma, Z. Zhang, C. Chen, K. Wang, H. Wang, W. Wang, L. Zhang, Y. Zhao and Z. Zhou (2013). "Structure of the MST4 in Complex with MO25 Provides Insights into Its Activation Mechanism." Structure **21**(3): 449-461.

Tanoue, T., M. Adachi, T. Moriguchi and E. Nishida (2000). "A conserved docking motif in MAP kinases common to substrates, activators and regulators." Nat Cell Biol **2**(2): 110-116.

Tao, X., J. L. Avalos, J. Chen and R. MacKinnon (2009). "Crystal structure of the eukaryotic strong inward-rectifier K+ channel Kir2.2 at 3.1 A resolution." Science **326**(5960): 1668-1674.

Taylor, C. A. t., Y. C. Juang, S. Earnest, S. Sengupta, E. J. Goldsmith and M. H. Cobb (2015). "Domain-Swapping Switch Point in Ste20 Protein Kinase SPAK." Biochemistry **54**(32): 5063-5071.

Teyra, J., S. S. Sidhu and P. M. Kim (2012). "Elucidation of the binding preferences of peptide recognition modules: SH3 and PDZ domains." FEBS Lett **586**(17): 2631-2637.

Uniprot-Consortium (2015). "UniProt: a hub for protein information." Nucleic Acids Res **43**(Database issue): D204-212.

Vakiani, E. and D. B. Solit (2011). "KRAS and BRAF: drug targets and predictive biomarkers." J Pathol **223**(2): 219-229.

Van Allen, E. M., V. W. Lui, A. M. Egloff, E. M. Goetz, H. Li, J. T. Johnson, U. Duvvuri, J. E. Bauman, N. Stransky, Y. Zeng, B. R. Gilbert, K. P. Pendleton, L. Wang, S. Chiosea, C. Sougnez, N. Wagle, F. Zhang, Y. Du, D. Close, P. A. Johnston, A. McKenna, S. L. Carter, T. R. Golub, G. Getz, G. B. Mills, L. A. Garraway and J. R. Grandis (2015). "Genomic Correlate of Exceptional Erlotinib Response in Head and Neck Squamous Cell Carcinoma." JAMA Oncol **1**(2): 238-244.

Verissimo, F. and P. Jordan (2001). "WNK kinases, a novel protein kinase subfamily in multi-cellular organisms." Oncogene **20**(39): 5562-5569.

Verykokakis, M., C. Papadaki, E. Vorgia, L. Le Gallic and G. Mavrothalassitis (2007). "The RAS-dependent ERF control of cell proliferation and differentiation is mediated by c-Myc repression." J Biol Chem **282**(41): 30285-30294.

Villa, F., M. Deak, D. R. Alessi and D. M. van Aalten (2008). "Structure of the OSR1 kinase, a hypertension drug target." Proteins **73**(4): 1082-1087.

Villa, F., J. Goebel, F. H. Rafiqi, M. Deak, J. Thastrup, D. R. Alessi and D. M. van Aalten (2007). "Structural insights into the recognition of substrates and activators by the OSR1 kinase." EMBO Rep **8**(9): 839-845.

Vitari, A. C., M. Deak, N. A. Morrice and D. R. Alessi (2005). "The WNK1 and WNK4 protein kinases that are mutated in Gordon's hypertension syndrome phosphorylate and activate SPAK and OSR1 protein kinases." Biochem J **391**(Pt 1): 17-24.

Vitari, A. C., J. Thastrup, F. H. Rafiqi, M. Deak, N. A. Morrice, H. K. Karlsson and D. R. Alessi (2006). "Functional interactions of the SPAK/OSR1 kinases with their upstream activator WNK1 and downstream substrate NKCC1." Biochem J **397**(1): 223-231.

Wang, Y., J. R. O'Connell, P. F. McArdle, J. B. Wade, S. E. Dorff, S. J. Shah, X. Shi, L. Pan, E. Rampersaud, H. Shen, J. D. Kim, A. R. Subramanya, N. I. Steinle, A. Parsa, C. C. Ober, P. A. Welling, A. Chakravarti, A. B. Weder, R. S. Cooper, B. D. Mitchell, A. R. Shuldiner and Y. P. Chang (2009). "From the Cover: Whole-genome association study identifies STK39 as a hypertension susceptibility gene." Proc Natl Acad Sci U S A **106**(1): 226-231.

Welling, P. A., Y. P. Chang, E. Delpire and J. B. Wade (2010). "Multigene kinase network, kidney transport, and salt in essential hypertension." Kidney Int **77**(12): 1063-1069.

Whitehurst, A. W., F. L. Robinson, M. S. Moore and M. H. Cobb (2004). "The Death Effector Domain Protein PEA-15 Prevents Nuclear Entry of ERK2 by Inhibiting Required Interactions." Journal of Biological Chemistry **279**(13): 12840-12847.

Wilson, C. A., J. Kreychman and M. Gerstein (2000). "Assessing annotation transfer for genomics: quantifying the relations between protein sequence, structure and function through traditional and probabilistic scores1." Journal of Molecular Biology **297**(1): 233-249.

Wilson, F. H., S. Disse-Nicodeme, K. A. Choate, K. Ishikawa, C. Nelson-Williams, I. Desitter, M. Gunel, D. V. Milford, G. W. Lipkin, J. M. Achard, M. P. Feely, B. Dussol, Y. Berland, R. J. Unwin, H. Mayan, D. B. Simon, Z. Farfel, X. Jeunemaitre and R. P. Lifton (2001). "Human hypertension caused by mutations in WNK kinases." Science **293**(5532): 1107-1112.

Wortzel, I. and R. Seger (2011). "The ERK Cascade: Distinct Functions within Various Subcellular Organelles." Genes Cancer **2**(3): 195-209.

Xie, J., L. Craig, M. H. Cobb and C. L. Huang (2006). "Role of with-no-lysine [K] kinases in the pathogenesis of Gordon's syndrome." Pediatr Nephrol **21**(9): 1231-1236.

Xie, J., T. Wu, K. Xu, I. K. Huang, O. Cleaver and C. L. Huang (2009). "Endothelial-specific expression of WNK1 kinase is essential for angiogenesis and heart development in mice." Am J Pathol **175**(3): 1315-1327.

Xie, J., J. Yoon, S. S. Yang, S. H. Lin and C. L. Huang (2013). "WNK1 protein kinase regulates embryonic cardiovascular development through the OSR1 signaling cascade." J Biol Chem **288**(12): 8566-8574.

Xu, B., J. M. English, J. L. Wilsbacher, S. Stippec, E. J. Goldsmith and M. H. Cobb (2000). "WNK1, a novel mammalian serine/threonine protein kinase lacking the catalytic lysine in subdomain II." J Biol Chem **275**(22): 16795-16801.

Xu, B. E., X. Min, S. Stippec, B. H. Lee, E. J. Goldsmith and M. H. Cobb (2002). "Regulation of WNK1 by an autoinhibitory domain and autophosphorylation." J Biol Chem **277**(50): 48456-48462.

Yarden, Y. and J. Schlessinger (1987). "Self-phosphorylation of epidermal growth factor receptor: evidence for a model of intermolecular allosteric activation." Biochemistry **26**(5): 1434-1442.

Yazicioglu, M. N., D. L. Goad, A. Ranganathan, A. W. Whitehurst, E. J. Goldsmith and M. H. Cobb (2007). "Mutations in ERK2 binding sites affect nuclear entry." J Biol Chem **282**(39): 28759-28767.

Zagorska, A., E. Pozo-Guisado, J. Boudeau, A. C. Vitari, F. H. Rafiqi, J. Thastrup, M. Deak, D. G. Campbell, N. A. Morrice, A. R. Prescott and D. R. Alessi (2007). "Regulation of activity and localization of the WNK1 protein kinase by hyperosmotic stress." J Cell Biol **176**(1): 89-100.

Zeqiraj, E., B. M. Filippi, M. Deak, D. R. Alessi and D. M. van Aalten (2009). "Structure of the LKB1-STRAD-MO25 complex reveals an allosteric mechanism of kinase activation." Science **326**(5960): 1707-1711.

Zhang, F., A. Strand, D. Robbins, M. H. Cobb and E. J. Goldsmith (1994). "Atomic structure of the MAP kinase ERK2 at 2.3 A resolution." Nature **367**(6465): 704-711.

Zhang, J., B. Zhou, C. F. Zheng and Z. Y. Zhang (2003). "A bipartite mechanism for ERK2 recognition by its cognate regulators and substrates." J Biol Chem **278**(32): 29901-29912.

Zhang, X., J. Gureasko, K. Shen, P. A. Cole and J. Kuriyan (2006). "An Allosteric Mechanism for Activation of the Kinase Domain of Epidermal Growth Factor Receptor." Cell **125**(6): 1137-1149.

Zhou, B., L. Wu, K. Shen, J. Zhang, D. S. Lawrence and Z. Y. Zhang (2001). "Multiple regions of MAP kinase phosphatase 3 are involved in its recognition and activation by ERK2." J Biol Chem **276**(9): 6506-6515.

Zhou, T., L. Sun, J. Humphreys and E. J. Goldsmith (2006). "Docking interactions induce exposure of activation loop in the MAP kinase ERK2." Structure **14**(6): 1011-1019.